Master's Degree in Automotive Engineering

Master's Degree Thesis

Impact of Climatic Conditions on Electric Vehicle Range, Battery Degradation, and Economic Performance: A Case Study for Uzbekistan

Supervisors

Prof Stefano Paolo PASTORELLI

Candidate

Lazizkhon Umidov

2025

Acknowledgements

I would like to express my deepest gratitude to my supervisor, Prof. Stefano Paolo Pastorelli, as well as to the committee chair, for their unwavering patience, invaluable guidance, and continuous support throughout the development of this thesis. Their readiness to share their knowledge, provide critical feedback, and encourage independent thinking has played a decisive role in shaping both the scientific quality and direction of this research.

I am equally grateful to my classmates and fellow cohort members, particularly my office colleagues, for their assistance in reviewing drafts and for their constant moral encouragement during demanding phases of the work. Their collaboration and academic exchange greatly enriched my experience.

My sincere appreciation also extends to the university librarians and research staff whose professional assistance and resource support contributed significantly to the completion of this study.

Finally, I would like to acknowledge the unwavering support of my family, especially my parents and my wife. Their patience, understanding, and enduring belief in me have been a continuous source of motivation and strength throughout this academic journey.

Abstract

The performance of battery electric vehicles (BEVs) is significantly affected by ambient temperature, especially in areas with substantial seasonal fluctuations. This thesis examines the influence of Uzbekistan's continental climate on electric vehicle range, battery deterioration, and operational expenses through the creation of a validated MATLAB/Simulink-based electro-thermal vehicle model. We chose three representative BEVs to study: the Nissan Leaf (24 kWh), the Chevrolet Bolt EV (60 kWh), and the 2017 Volkswagen e-Golf (35.8 kWh, DC fast-charging version).

The modeling framework combines longitudinal vehicle dynamics, battery behavior that changes with temperature, HVAC auxiliary loads, and range data that has been tested in controlled laboratory campaigns. The model was calibrated using published test results at different ambient temperatures, and the measured data matched the model very closely (R^2 up to 0.99 and deviation usually below 10%).

Using validated temperature–range relationships, monthly climatic data for major Uzbek regions were applied to estimate annual charging frequency for a representative driving distance of 20,000 km. Results indicate that real climatic operation increases annual charging demand by approximately 24–29% compared to moderate-condition OEM expectations. This increase not only affects electricity expenditure but also accelerates battery cycling intensity. A piecewise multiplicative degradation model was therefore implemented to quantify long-term capacity loss under climate-adjusted cycling conditions.

The findings demonstrate that continental temperature extremes significantly influence both short-term vehicle efficiency and long-term battery health. The proposed framework provides a climate-aware predictive tool for realistic performance estimation and supports evidence-based planning for electric mobility deployment in regions with pronounced seasonal variability.

Table of Contents

List of Tables

List of Figures

Acronyms

AAA – American Automobile Association
Ah – Ampere-hour
ANL – Argonne National Laboratory
AVTA – Advanced Vehicle Testing Activity
BEV – Battery Electric Vehicle
BMS – Battery Management System
BTMS – Battery Thermal Management System
CAN – Controller Area Network
CFD – Computational Fluid Dynamics
COP – Coefficient of Performance
DC – Direct Current
DoD – Depth of Discharge
DOE – U.S. Department of Energy
ECM – Equivalent Circuit Model
ECMWF – European Centre for Medium-Range Weather Forecasts
EPA – Environmental Protection Agency
ERA5 – Fifth Generation ECMWF Atmospheric Reanalysis
EV – Electric Vehicle
FWD – Front-Wheel Drive
GHG – Greenhouse Gas
GIS – Geographic Information System
GWh – Gigawatt-hour
HVAC – Heating, Ventilation and Air Conditioning
IEA – International Energy Agency
INL – Idaho National Laboratory
IPCC – Intergovernmental Panel on Climate Change
JRC – Joint Research Centre (European Commission)
kW – Kilowatt

kWh – Kilowatt-hour
LMO – Lithium Manganese Oxide
LFP – Lithium Iron Phosphate
Li-ion – Lithium-ion
MATLAB – Matrix Laboratory
Mendeley – Reference Management Software
Nm – Newton-meter
NOAA – National Oceanic and Atmospheric Administration
NREL – National Renewable Energy Laboratory
OCV – Open Circuit Voltage
OEM – Original Equipment Manufacturer
PI – Proportional-Integral (Controller)
PPP – Purchasing Power Parity
Rint – Internal Resistance
RWD – Rear-Wheel Drive
Simscape – MATLAB Physical Modeling Environment
SOC – State of Charge
SOH – State of Health
TMS – Thermal Management System
UzHydromet – Uzbekistan Hydrometeorological Service
V – Volt
WLTP – Worldwide Harmonized Light Vehicles Test Procedure
WLTPC – Worldwide Harmonized Light Vehicles Test Cycle

1. Introduction and Theoretical Framework

The global transition toward electric mobility marks a pivotal shift in the transportation and energy sectors, driven by the growing need to reduce greenhouse gas emissions, improve energy efficiency, and decrease dependency on fossil fuels. Electric vehicles (EVs) have emerged as one of the most promising solutions to achieve sustainable transportation, offering zero tailpipe emissions and high drivetrain efficiency compared to conventional internal combustion engine (ICE) vehicles. However, the performance and long-term reliability of EVs are strongly influenced by environmental factors—most notably, climatic conditions such as temperature, humidity, and solar radiation[1].

In this context, Uzbekistan presents a unique and challenging environment for EV operation due to its continental climate, characterized by extremely hot summers exceeding 40 °C and cold winters dropping below –10 °C. These temperature extremes directly affect battery performance, energy consumption, and degradation rates, leading to deviations between laboratory-rated and real-world driving ranges. Understanding these effects is essential for developing reliable predictive models, optimizing energy management, and supporting policy decisions aimed at accelerating electric mobility in Central Asia[2].

This chapter provides a comprehensive foundation for the research, outlining the background and context of EV development, the global transition toward electrified mobility, and the architecture and configuration of modern EV powertrains. It also describes the climatic and environmental conditions of Uzbekistan, emphasizing how temperature variations and regional factors influence EV operation. Furthermore, it identifies current challenges and research gaps related to battery degradation, range estimation, and thermal management under continental climatic conditions[3].

The final sections of the chapter detail the research methodology and objectives, including the use of verified data sources from the Idaho National Laboratory (INL), National Renewable Energy Laboratory (NREL), and Worldwide Harmonized Light Vehicle Test Procedure (WLTP3), as well as the implementation of a MATLAB/Simulink-based simulation model. This model integrates climatic data and vehicle parameters to analyze temperature-dependent variations in energy efficiency, range, and degradation[4].

Overall, Chapter One establishes the conceptual, environmental, and methodological framework necessary for assessing the impact of Uzbekistan's climatic conditions on electric vehicle range, battery degradation, and operational performance, setting the stage for the analytical and simulation-based findings presented in subsequent chapters.

1.1. Background and Context of Electric Vehicle Development

The rapid advancement of electric mobility represents one of the most significant transitions in the history of road transportation. Driven by environmental concerns, technological progress, and policy initiatives, electric vehicles (EVs) have moved from niche applications to mainstream transportation solutions. BEVs, in particular, have become central to decarbonization efforts due to their zero tailpipe emissions and high drivetrain efficiency. Early evaluations of electrified powertrains emphasize that BEVs benefit from simplified energy pathways—high-voltage battery to inverter to electric motor—without the mechanical complexities associated with internal-combustion systems [5], [6].

Global climate targets accelerate this shift, as mobility accounts for a substantial fraction of urban CO_2 emissions. Municipalities, national governments, and industries increasingly acknowledge that deep decarbonization is unattainable without large-scale substitution of internal-combustion vehicles with BEVs. Policies such as zero-emission vehicle mandates, renewable-energy integration strategies, and charging-infrastructure development create an enabling environment for BEV deployment [6].

Economic and technological factors further support the transition. Widespread investment in battery research has led to improvements in energy density, cost reduction, and extended cycle life, making BEVs more competitive. Industry-focused analyses—such as those examining military vehicle fleets—note that electrification offers operational advantages, including reduced operating costs, lower logistical burdens, and enhanced energy security [7]. Together, these factors establish the foundation for global BEV adoption and motivate detailed analysis of their architecture and performance, forming the basis of the modeling work carried out in this thesis.

1.1.1. Global Transition Toward Electrified Mobility

The global transition toward electrified mobility is accelerating as governments, industries, and communities work to reduce greenhouse gas emissions and shift toward low-carbon energy systems. The transport sector accounts for a significant share of total CO_2 emissions, making vehicle electrification a central pillar of climate and energy strategies worldwide [6].

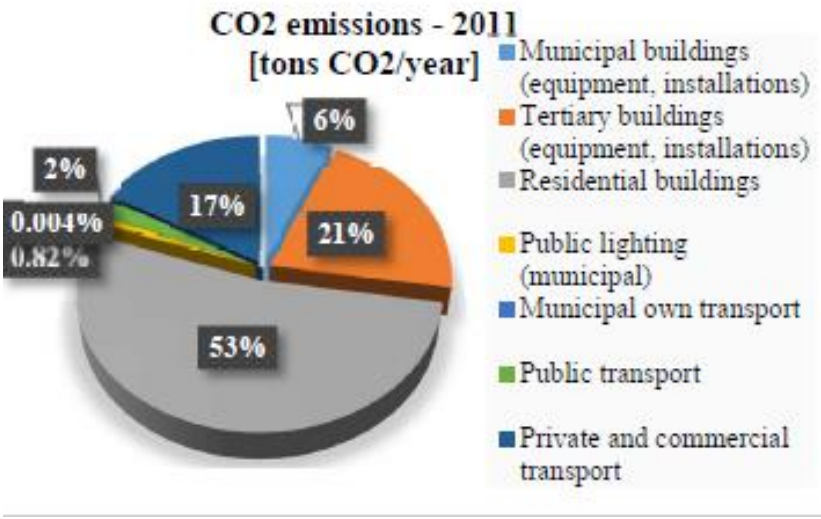

Figure 1.1 *Sectoral CO_2 emissions distribution[6]*

At the global level, mobility electrification is increasingly aligned with broader sustainability agendas and policy frameworks. Multiple regions, including the European Union, California, and China, have established aggressive targets for phasing out internal-combustion vehicle sales. California's Zero-Emission Vehicle (ZEV) mandate aims to eliminate petrol and diesel vehicle sales by 2035, while the European Union's "Fit for 55" package sets a requirement to reduce fleet-wide emissions by 55% by 2030. These policy signals establish clear regulatory pathways that push automotive manufacturers and energy providers toward mass-scale electrification[8].

The strategic momentum toward electrification is also evident in institutional and governmental fleet planning. An assessment of U.S. Army vehicle electrification shows an organizational-level commitment to decarbonization, efficiency improvements, and energy-resilience goals. The U.S. Army Climate Strategy sets a roadmap for full electrification of the non-tactical fleet by 2027 and progressively expands electrification into tactical vehicle classes toward 2050. This shift reflects a recognition of both operational benefits and long-term energy-security advantages of electric propulsion systems, underscoring how electrification is expanding beyond civilian markets into high-demand mission environments.

From an economic perspective, global projections indicate that electric vehicles are expected to reach cost parity with internal-combustion vehicles by the late 2020s. Market analyses referenced in fleet-transition studies show that improvements in battery energy density, cost reductions, and economies of scale in manufacturing are driving the global shift toward electrified mobility. Once cost parity is achieved, EV adoption is projected to accelerate rapidly, with electric vehicles potentially reaching the majority of global

new-vehicle sales by the mid-2030s. These projections are already influencing mobility planning, infrastructure development, and long-term energy strategies across countries and municipalities [7].

Global transition dynamics are further shaped by urban-scale decarbonization efforts. Local communities increasingly integrate mobility electrification with renewable-energy deployment, grid modernization, and sustainable urban planning. Case studies from European climate-neutral city initiatives highlight that transport accounts for roughly 16–21% of municipal CO_2 emissions, making EV adoption an essential mechanism for achieving climate-neutrality commitments. Cities implementing integrated approaches—combining EV charging networks, electrified public transport, and renewable energy systems—demonstrate more resilient and sustainable energy-mobility ecosystems [6].

Electrified mobility also depends on advances in infrastructure, especially in charging systems. Research on electric bus transportation systems underscores those technological barriers—such as limited charging access, long recharging times, and high infrastructure costs—remain among the primary constraints for widespread transition. Wireless power transfer (WPT) and dynamic WPT technologies are being explored to enable continuous energy supply for transit fleets, helping overcome limitations associated with static charging models and reducing range anxiety in high-utilization applications [8].

1.1.2. Electric Vehicle Architectures and Powertrain Energy Flow

Electric vehicle (EV) architectures describe the arrangement of propulsion and energy-management components that convert stored electrochemical energy into mechanical torque at the wheels. Foundational analytical work comparing propulsion-system configurations highlights that drivetrain topology strongly influences efficiency. Early evaluations of series, parallel, and through-the-road hybrid systems showed that architectures with fewer energy-conversion stages—such as battery-electric layouts—experience lower losses, especially during low-speed urban driving where repeated transitions between acceleration and deceleration dominate[9].

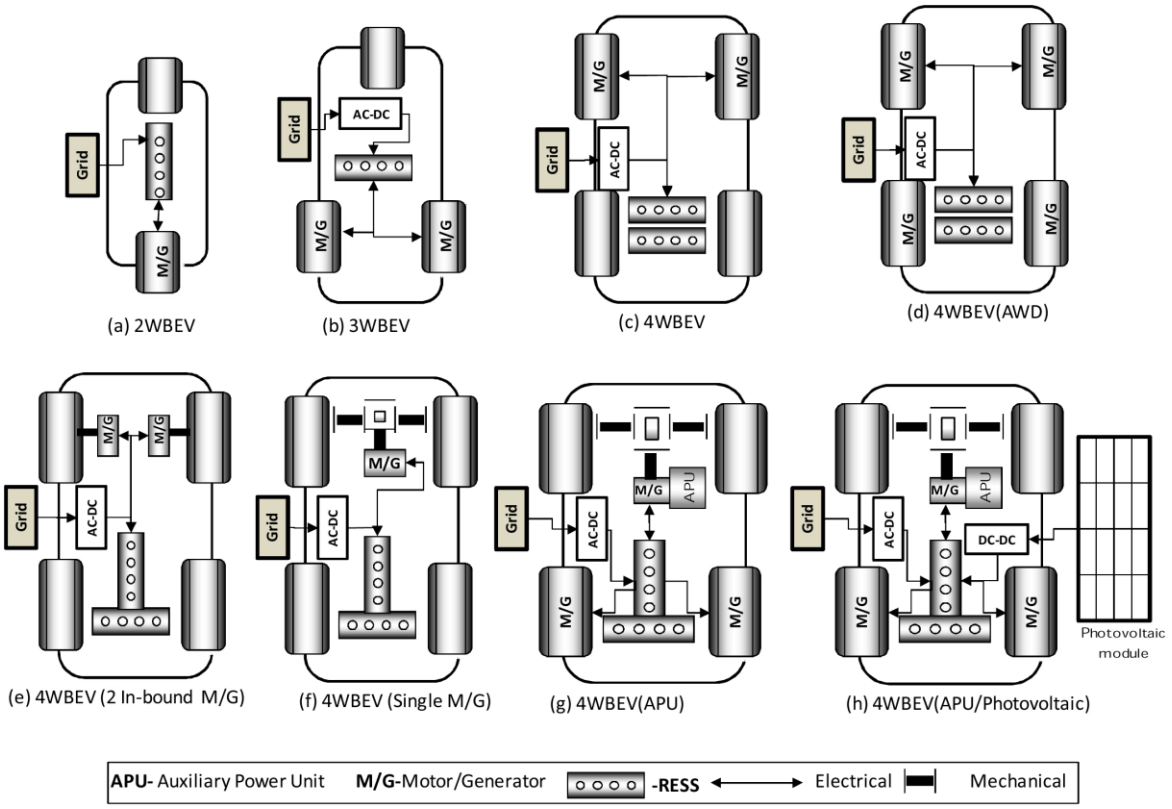

Figure 1.2 *Topology of various propulsion system architectures for USVs[9].*

As EV technology evolved toward mass-production models, the industry shifted toward highly integrated electric drive units designed to minimize parasitic losses and improve packaging. The propulsion system of the Spark EV demonstrates a representative early-generation architecture in which the traction motor, inverter, reduction gearset, accessory power modules, and thermal circuits are closely integrated. This configuration reduces wiring length, improves thermal uniformity, and enhances transient response. The Spark EV energy-flow representation illustrates how electrical energy travels from the high-voltage battery to the inverter and then to the motor during propulsion, and how the process reverses during regenerative braking when mechanical energy is recovered and converted back into electrical energy to recharge the battery[10].

Modern EVs expand beyond single-motor layouts to include architectures with two or more traction machines. Recent analyses compare several key configurations: single-motor rear-wheel-drive (RWD), dual-motor symmetric all-wheel-drive (AWD), and dual-motor asymmetric AWD. These configurations differ not only in physical placement but also in how their power electronics and torque-control strategies distribute power between axles. The architectural schematic presented in recent modeling studies clearly differentiates motor sizes, inverter structures, and power-flow paths for each configuration[11].

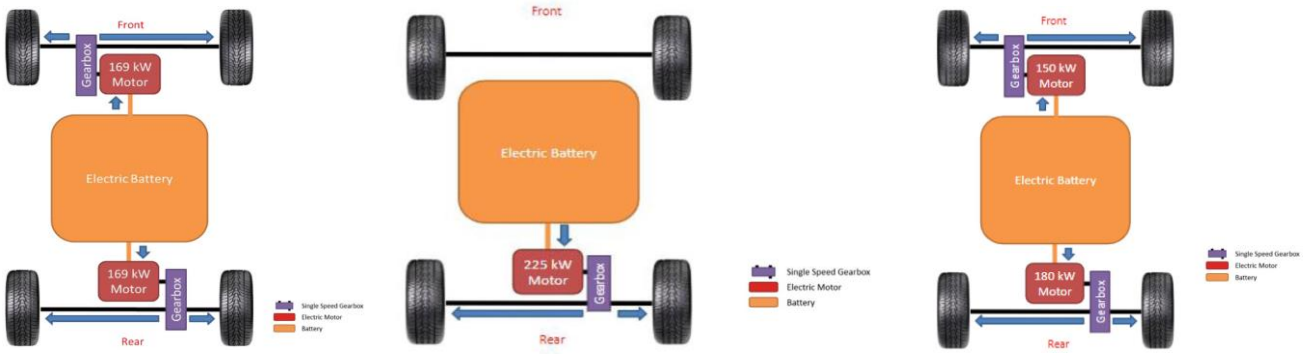

Figure 1.3 *Spark EV power-flow diagram [10].*

Simulation results across standard drive cycles demonstrate that dual-motor AWD systems can achieve higher efficiency than single-motor layouts when torque split is optimized. AWD architectures allow each motor to operate closer to its most efficient operating region, reducing conduction, switching, and magnetic losses. The studies report efficiency improvements in the range of 5.4–37.9% in MPGe depending on drive cycle, motor sizing, and torque-distribution method. This advantage becomes more prominent in conditions requiring rapid torque transitions or high regenerative-braking potential, where both motors can contribute to energy recovery.

Torque-split control is central to the performance of multi-motor systems. Evaluations of several control strategies—including fixed front/rear splits, optimization-based distributions, and user-defined logic—show that a balanced 50/50 torque split often provides a strong compromise between efficiency, stability, and responsiveness. Efficiency-map analyses further indicate that unbalanced torque splits may push one motor into a low-efficiency operating zone, whereas more even distributions maintain both units within higher-efficiency regions, especially during steady-state cruising and moderate acceleration.

Complementary open-access modeling research reinforces the conclusion that optimal energy flow in EVs requires both hardware and software co-design. Control strategies that shape motor torque commands, modulate inverter switching behavior, and coordinate thermal-management responses play a critical role in real-time efficiency. These elements ensure that the architecture's theoretical advantages translate into practical performance improvements. Thermal constraints in particular influence allowable current, inverter duty cycles, and battery discharge rates, meaning that even high-efficiency architectures can experience significant efficiency loss if thermal-management strategies are inadequate [11].

Collectively, these findings demonstrate that EV energy-flow characteristics are defined by the interaction between architecture, component integration, and intelligent control. The progression from single-motor BEV layouts to advanced multi-motor systems

reflects a broader industry shift toward architectures that exploit real-time optimization, motor synergy, and regenerative-braking capability to maximize overall drivetrain performance[9].

EV architectures have evolved from simple single-motor systems to highly optimized multi-motor configurations that leverage sophisticated control strategies and integrated components. Efficient energy flow now depends equally on mechanical layout, electrical subsystem design, and real-time optimization, enabling modern EVs to achieve significantly higher performance and energy-conversion efficiency[11].

1.1.3. Classification of Electric Vehicle Types and Configurations

Battery Electric Vehicles (BEVs) are fully propelled by electric machines using energy stored in high-voltage battery packs. As emphasized in early architecture surveys, BEVs feature the simplest energy pathway—battery → inverter → motor → wheels—without mechanical coupling to combustion engines or auxiliary propulsion systems. This structural clarity distinguishes BEVs from all other electrified powertrains and forms the foundation for their configuration-based classification[12].

Single-Motor Central Drive BEVs

The most common BEV layout uses a single electric traction motor coupled with a reduction gearbox. Depending on the vehicle's design, the drive unit may be positioned on the front or rear axle:

- **Front-wheel-drive (FWD) BEVs**
- **Rear-wheel-drive (RWD) BEVs**

Integrated drive units combine the motor, inverter, and gearbox within a single sealed assembly, improving thermal management, serviceability, and packaging efficiency. This configuration dominates the market because it minimizes drivetrain losses, reduces vehicle mass, and simplifies control logic[1].

Dual-Motor All-Wheel-Drive BEVs

Dual-motor BEVs use an independent electric motor on each axle, allowing enhanced traction, performance, and stability control. In this configuration, torque vectoring is achieved through software rather than mechanical differentials, enabling rapid and precise torque allocation. Although the IEEE paper examines motor configurations in a broader electrified-vehicle context, its architecture figure 1.4 clearly illustrate multi-motor layouts with independent electric machines—topologies directly applicable to dual-motor BEV systems.

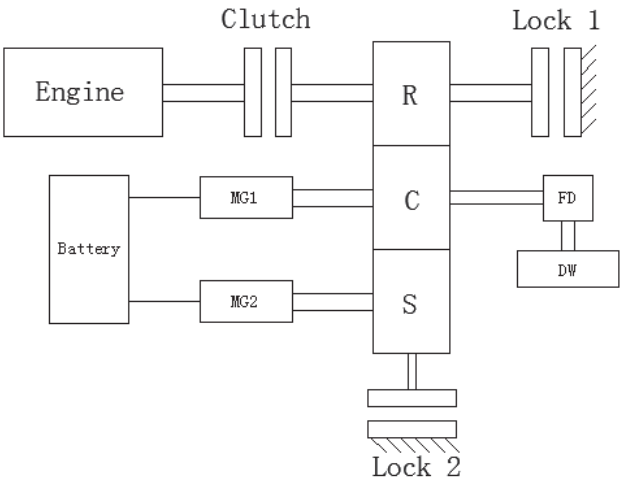

Figure 1.4 *Structure of power split configuration of Toyota prius[12]*

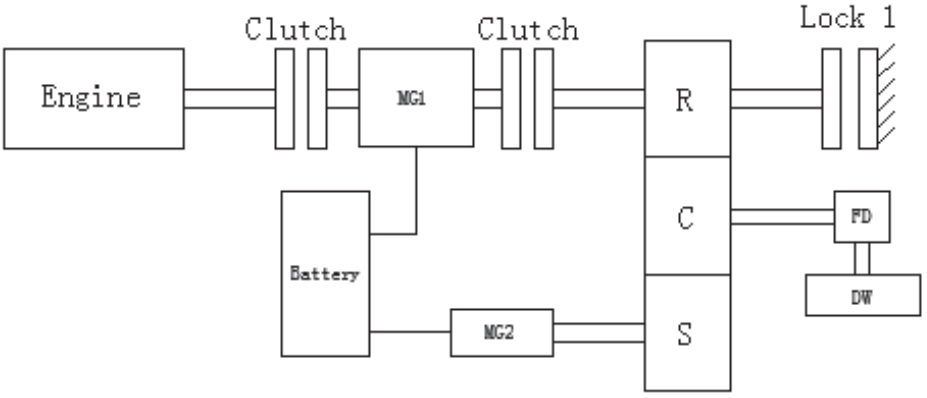

Figure 1.5 *Structure of power split configuration of GM-Volt[12]*

The opening section provides a foundational understanding of Battery Electric Vehicles (BEVs) within the global shift toward sustainable transportation. It highlights how climate policies, emission-reduction targets, and rapid progress in battery and power-electronics technologies are accelerating worldwide BEV adoption. Transport remains a major contributor to urban CO_2 emissions, making electrification an essential element of national and municipal decarbonization strategies. Policy frameworks, cost-parity trends, and infrastructure development further reinforce this transition.

BEV propulsion systems are examined through their core architectural principles, including direct electrical energy flow, integrated drive units, dual-motor all-wheel-drive layouts, and emerging in-wheel motor designs. These configurations reduce mechanical complexity and enhance drivetrain efficiency, making BEVs well suited for advanced control and energy-management strategies. The classification of BEVs by motor placement, system integration, and thermal-battery design provides a structural basis for

performance modeling and supports the MATLAB/Simulink simulations developed later in the thesis[1], [12].

1.2. Climatic and Environmental Conditions in Uzbekistan

The Uzbekistan's climatic and environmental conditions are shaped by its landlocked position in the center of the Eurasian continent and its highly diverse terrain. Much of the country consists of extensive desert and semi-desert landscapes, including the Kyzyl-Kum and the expanding Aralkum, which together account for nearly four-fifths of national territory. These arid lowlands contrast with the southeastern mountain systems—the Tien-Shan and Gissar–Alai ranges—which rise to elevations above 4,000 m and generate substantial spatial variation in humidity, cloud cover, and precipitation. The Climate Risk Country Profile illustrates this contrast, showing annual mean temperature and precipitation gradients that define the country's major ecological zones[2].

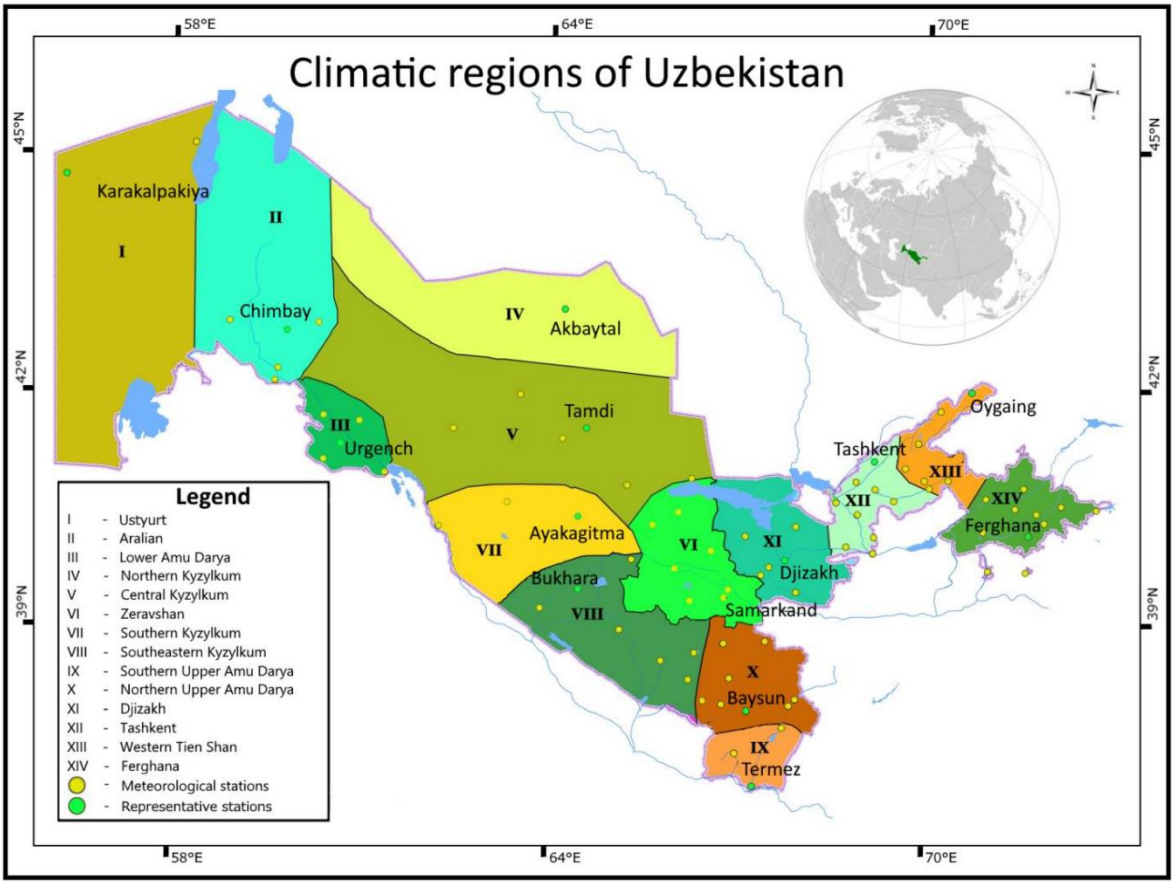

Figure 1.6 *Climatic regions / spatial maps[2]*

According to long-term assessments, Uzbekistan experiences persistent aridity, low

annual precipitation in western regions (<100 mm), and significantly wetter conditions in the mountainous southeast. Recent regional climate analyses further document declining snow cover, increased heat stress, and amplified surface drying—features consistent with broader warming trends across[13]. The WMO State of the Climate 2025 similarly highlights intensified aridification and reduced cryospheric stability, underscoring the vulnerability of Uzbekistan's environmental system to temperature extremes and hydrological imbalance [2], [14].

1.2.1. Geographic and Meteorological Characteristics

Uzbekistan's geographic and meteorological conditions form the fundamental environmental boundary for transportation systems and energy-related activities. The country is entirely landlocked and situated deep within Central Asia, which intensifies its continentality—low atmospheric moisture, strong radiation exposure, and large temperature variability. National assessments indicate that 79% of Uzbekistan's territory consists of flat semi-desert or desert surfaces, most prominently the Kyzyl-Kum and the newly formed Aralkum emerging from the desiccated Aral Sea. Elevation ranges from 12 m below sea level in the Amu Darya delta to over 4,000 m in the western Tien-Shan foothills, creating sharp spatial differences in meteorological conditions[2]

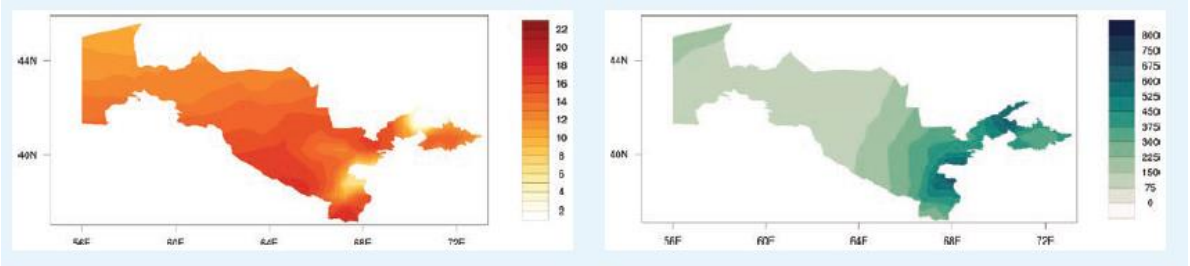

Picture 1.7 *(Left) annual mean temperature (°C), and (right) annual mean precipitation (mm) in Uzbekistan over the period 1991–2020 [2]*

These strong elevation gradients influence humidity, cloud formation, and precipitation distribution across the country. While the western lowlands receive less than 100 mm of annual precipitation, the southeastern foothills of the Tien-Shan and Gissar–Alai ranges receive 800–900 mm/year, including significant snow accumulation in winter months. Snowpack in these mountainous areas plays a critical hydrological role by storing winter precipitation and releasing meltwater in spring, feeding the upper tributaries of the Amu Darya and Syr Darya. By contrast, snow cover in the desert west is thin, irregular, and short-lived, reflecting extreme aridity [2].

Large-scale meteorological analyses from the World Meteorological Organization highlight additional structural features of Uzbekistan's climate system. WMO's 2025

regional assessment notes persistent declines in snow cover, enhanced soil dryness, and expanding lowland aridity across Central Asia. The report also documents a tendency toward stronger climatic extremes over desert basins, where evapotranspiration greatly exceeds precipitation. These findings indicate intensified pressure on water resources and increasing vulnerability of lowland areas to dust-storm activity and land degradation processes [14].

High-resolution observational data refine this picture at the urban scale. Tashkent, located at ~450 m elevation near the western Tien-Shan foothills, receives approximately 380 mm of total annual precipitation, with only a minor share occurring as snow. WeatherSpark's 2025 dataset shows that clear or mostly clear skies dominate over half the year, increasing solar load and surface heating. Wind climatology is characterized by northeasterly flows in winter and westerly–northwesterly winds in summer, with average speeds of 2.5–4 m/s, influencing ventilation, dust transport, and microclimatic comfort. These features reinforce the classification of Uzbekistan as a dry, high-radiation environment with distinct orographic contrasts

Wind statistics from the same dataset reveal prevailing northeasterly winds during winter and westerly–northwesterly patterns in summer, with mean speeds of 2.5–4 m/s, influencing air circulation, thermal comfort, and pollutant dispersion [2]

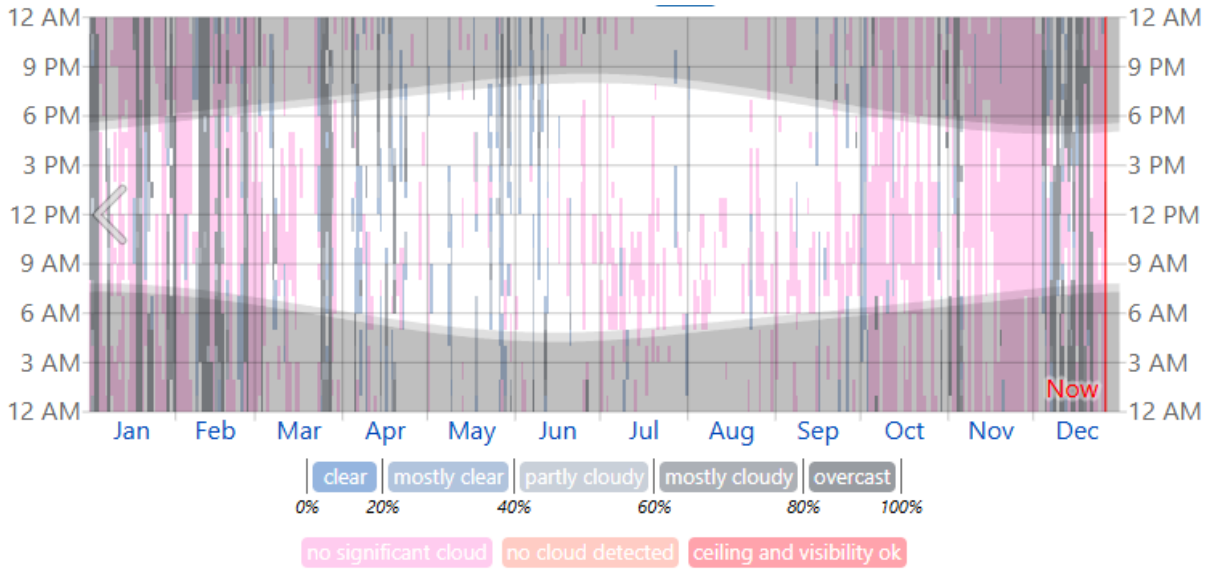

Figure 1.8 The hourly reported cloud coverage, categorized by the percentage of the sky covered by clouds [15]

Taken together, Uzbekistan's environmental system is shaped by continentality, aridity, extensive desert land cover, elevation-driven climatic differentiation, and snow-dependent hydrology. These geographic and meteorological fundamentals directly influence water availability, surface heating, dust generation, and environmental loads on infrastructure. They also establish the baseline climatic context for electric-vehicle

operation, determining thermal loads, HVAC demand, and the operating envelope under which seasonal temperature dynamics are assessed [2], [14].

1.2.2. Seasonal and Regional Temperature Variations, Working-Hour Profiles

From previous chapter we know that Uzbekistan's climate is best described as strongly continental with predominantly arid/semi-arid land cover and complex terrain ranging from lowland deserts to mountain-influenced valleys. For BEV operation, this means two things dominate the annual vehicle energy balance: (i) large seasonal swings (winter cold vs summer heat) and (ii) a strong diurnal cycle, where the temperatures during typical driving hours differ systematically from full-day averages. Therefore, the main output of this subsection is not only a qualitative climate description, but a simulation-ready pair of temperature vectors: monthly national 24-hour mean temperature and monthly national working-hour mean temperature (09:00–17:00) derived from real station sensors across Uzbekistan [16].

Data sources and why they are suitable for a national BEV study

This thesis uses a station-based approach because BEV performance is sensitive to real near-surface air temperature, which is measured directly by national meteorological sensors. Hourly observations are taken from the UzHydromet station network that is archived in the NOAA Integrated Surface Database (ISD); the ISD provides standardized access and long-term continuity suitable for scientific analysis. This ensures the temperature inputs represent measured atmospheric conditions rather than generalized climate narratives [16].

To streamline retrieval and processing of hourly station data, the dataset is accessed through Meteostat, which provides structured station metadata and time series built on internationally available archives. Using Meteostat also enables consistent filtering (e.g., selecting 09:00–17:00) and reproducible aggregation to monthly values for the full study period (2010–2024) across multiple Uzbek stations [17], [18].

Finally, WorldClim v2 is used as a context layer (not the main input) to support spatial interpretation—i.e., to describe how the national average emerges from distinct climatic zones (desert lowlands vs valleys/foothills). WorldClim provides high-resolution climatological surfaces that help explain why regions differ, while the operational monthly vectors in this thesis remain observation-driven [17], [19].

Station network and national representativeness (10-station composite)
To avoid over-reliance on a single city and to represent Uzbekistan as a whole, a 10-station composite is employed, covering north, west, central basins, east valleys, and south hot plains.

***Figure 1.9**. Meteorological stations used for the 10-station Uzbekistan* [17].

The stations used are: Nukus (38353), Urgench (38379), Bukhara (38457), Samarkand (38493), Karshi (38507), Termez (38518), Namangan (38609), Andijan (38611), Fergana (38618), Tashkent (38457). This configuration captures the dominant national gradients caused by latitude and elevation, while still reflecting where population and vehicle activity are concentrated [17], [18].

Method to compute the two monthly temperature vectors
For each station, hourly temperature is aggregated in two parallel ways:
Monthly 24-hour mean temperature: average of all hourly values in the month (captures full day–night cycle).Monthly working-hour mean temperature (09:00–17:00 local time): average of hourly values inside the driving-relevant window (captures daytime operating exposure).Then the station monthly values are combined into a national composite (equal-weight average across the 10 stations, unless a later section applies area-weights). This produces the two monthly vectors required for annual BEV characterization under Uzbekistan conditions[17], [18].

Seasonal pattern at the national scale
The composite results confirm Uzbekistan's classic continental structure: cold winters, rapid spring warming, very hot summers, and rapid autumn cooling. In winter (Dec–Feb) the national mean is near or below freezing in many regions, reflecting frequent cold air intrusions and strong radiative cooling under dry skies. In summer (Jun–Aug) sustained heat dominates, with working-hour temperatures around 30–32 °C nationally and regional extremes far above that in southern and central lowlands. These patterns are consistent with continental interior climates where the absence of oceanic moderation amplifies seasonal amplitude[20].

Regional drivers that shape the national average

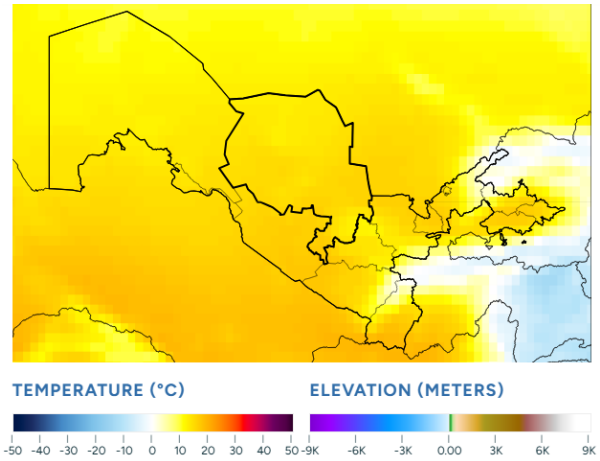

Figure 1.10 *Spatial distribution of mean air temperature over Uzbekistan* [21].

The national mean is a practical modeling input, but it must be physically interpreted as the result of three dominant controls: (i) latitude (north–south gradient), (ii) elevation (cooling with altitude), and (iii) surface aridity/vegetation (stronger surface heating and larger diurnal swing in deserts). WorldClim's high-resolution surfaces support this interpretation by showing how warm lowlands and cooler elevated/valley zones coexist within the same national boundary, producing a national mean that is meaningful for annual fleet-level BEV assessment [19].

Working-hour bias: why daytime exposure must be separated from daily averages

A crucial national observation is that working-hour temperatures are consistently higher than 24-hour means, because the 09:00–17:00 window excludes nocturnal cooling and covers the peak solar-heating period. In the Uzbekistan composite, the annual difference is about +1.6 °C, with the largest differences in summer. This is directly relevant to BEVs: HVAC cooling demand is correlated with daytime heat, and battery thermal exposure during driving is better represented by working-hour temperature than by a 24-hour mean [17], [18].

Implications for BEV annual performance and why these vectors are "model-critical"

For BEV modeling, temperature influences (i) battery internal resistance and usable energy at low temperatures, (ii) auxiliary energy demand (heating/cooling), and (iii) thermal constraints affecting charging/regen behavior. Because real driving happens mostly during daytime, the working-hour vector is the primary input for on-road energy consumption, while the 24-hour vector is a more appropriate descriptor for idle/overnight thermal boundary conditions (parking, home charging exposure). Using both vectors allows the annual model to separate "operating exposure" from "ambient baseline exposure," improving realism without adding unnecessary complexity[16].

***Table 1.1**. Uzbekistan national monthly temperature vectors for BEV simulation [17]*

Month	Working-hour mean (°C)	24 h daily mean (°C)	Typical regional span (North → South, °C)	Remarks
January	−1.8	−3.1	−10 … +5	Coldest in the north; milder south
February	1.9	0.4	−7 … +8	Gradual warming
March	8.6	7	2 … 15	Strong N–S gradient
April	16.3	14.7	10 … 22	Spring stabilization
May	23.2	21.7	17 … 28	Warm nationwide
June	29.3	27.6	25 … 35	Onset of hot season
July	31.8	30	27 … 40	Peak heat; max solar load
August	30.9	29.1	26 … 38	Persistent dry heat
September	25	23.3	20 … 30	Cooling trend
October	16.8	15.3	10 … 22	Comfortable days, cool nights
November	8.5	7	3 … 13	Rapid autumn drop
December	1.3	−0.1	−6 … +7	Early frosts
Annual mean	**17**	**15.4**	—	**Working-hours ≈ +1.6 °C warmer**

***Table 1.2.** Working-hour bias and BEV relevance (Uzbekistan national interpretation) [17], [18]*

Period	Typical WH–24h difference	Physical reason	Direct BEV consequence
Winter (Dec–Feb)	~+1 to +2 °C	Daytime solar heating vs cold nights	Heating demand persists; cold battery impacts
Spring/Autumn	~+1 to +2 °C	Rapid transitions; strong daytime warming	Efficient "shoulder seasons" with low HVAC load
Summer (Jun–Aug)	~+2 °C (often highest)	Peak insolation in 09:00–17:00	Higher A/C load → higher kWh/100 km, lower range
Annual	**~+1.6 °C**	Consistent exclusion of night cooling	Better annual BEV realism vs using only daily means

1.3. Temperature Effects and Battery Degradation Mechanisms

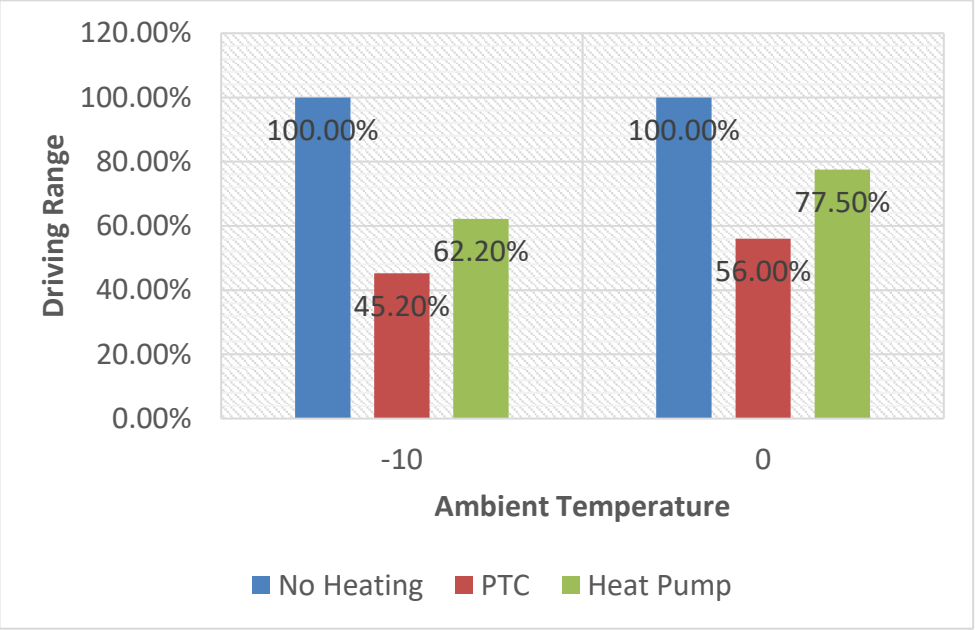

***Figure 1.11**. Effect of heating a BEV on driving range [22].*

Ambient temperature is a critical external parameter governing the real-world performance of battery electric vehicles (BEVs). Unlike internal combustion vehicles, BEVs rely entirely on electrochemical energy storage, making both propulsion efficiency and auxiliary energy demand strongly temperature-dependent. Numerous experimental and field studies confirm that deviations from the optimal thermal window led to significant reductions in driving range and energy efficiency, particularly under cold operating conditions [22], [23].

At the vehicle level, the impact of ambient temperature on BEV range can be interpreted through its influence on total energy consumption per unit distance. The driving range R can be expressed as:

$$R = \frac{E_{usable}(T)}{e_{trac} + e_{aux}(T)}$$

where $E_{\text{usable}}(T)$ is the temperature-dependent usable battery energy, $e_{\text{trac}}$is the traction energy per kilometer, and $e_{\text{aux}}(T)$represents auxiliary loads dominated by HVAC demand. Experimental results from cold-climate testing of production BEVs show that, as ambient temperature drops below 0 °C, HVAC power demand increases sharply, causing auxiliary loads to become a dominant contributor to total energy consumption [23].

$$R_{int}(T) = R_{ref} exp\left[\alpha\left(\frac{1}{T} - \frac{1}{T_{ref}}\right)\right]$$

where $R_{\text{int}}$is the internal resistance, $T$is absolute temperature, and $\alpha$is an empirically derived coefficient dependent on cell chemistry. As resistance increases, voltage losses under load rise, reducing effective battery capacity and limiting regenerative braking capability.

Battery thermal behavior and temperature distribution further influence BEV performance. NREL modeling studies demonstrate that non-uniform temperature fields within the battery pack can exacerbate localized aging and reduce overall efficiency, particularly during cold starts (NREL Battery Thermal Management System Design Modeling). Advanced thermal management strategies—such as heat pumps, waste-heat recovery, and thermal storage—have been shown to reduce HVAC energy consumption by up to 40–60 % at sub-zero temperatures, translating directly into measurable range extensions [22].

Beyond immediate performance effects, temperature also plays a decisive role in battery aging and degradation. Elevated temperatures accelerate calendar aging, while low-temperature operation increases mechanical and electrochemical stress during charge and discharge cycles. Long-term studies indicate that frequent operation outside the optimal temperature range of approximately 15–35 °C leads to accelerated capacity fade and reduced battery lifetime [24].

1.3.1. Effect of Ambient Temperature on BEV Energy Consumption and Driving Range

Ambient temperature has a direct and measurable influence on the energy consumption of battery electric vehicles (BEVs) by altering the balance between traction energy and auxiliary loads, most notably heating, ventilation, and air conditioning (HVAC). Experimental and field studies consistently show that temperature-dependent increases in energy consumption, rather than a simple reduction in nominal battery capacity, are the dominant cause of range degradation under non-optimal climatic conditions [23], [25].

At mild ambient temperatures, typically in the range of 15–25 °C, total BEV energy consumption is dominated by traction power. Under these conditions, HVAC systems operate intermittently and at relatively low power levels, resulting in a limited impact on total battery energy use. As ambient temperature decreases, however, the heating demand required to maintain cabin comfort increases rapidly, leading to a substantial rise in auxiliary energy consumption even when the driving profile remains unchanged [25].

The total electrical energy drawn from the battery during a driving cycle can be expressed as:

$$E_{tot}(T) = E_{trac} + E_{HVAC}(T) + E_{aux,other}$$

where $E_{\mathrm{HVAC}}(T)$is the dominant temperature-dependent term, while traction energy E_{trac}depends primarily on vehicle mass, aerodynamic drag, rolling resistance, and the selected drive cycle [23]. This formulation highlights that cold-weather range losses are primarily driven by auxiliary loads.

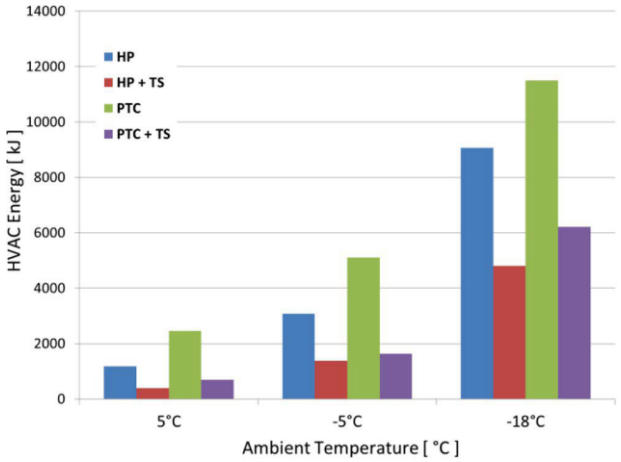

Figure 1.12 *Comparison of HVAC energy consumption for different thermal system configurations at various ambient temperatures[22].*

Figure 1.12 compares HVAC energy consumption for several thermal system configurations—including baseline PTC heating, heat-pump systems, and systems incorporating thermal storage—across ambient temperatures of 5 °C, −5 °C, and −18 °C. The figure clearly shows that HVAC energy consumption increases significantly as ambient temperature decreases for all system types. However, the magnitude of this increase strongly depends on the adopted heating architecture. Systems combining heat pumps with thermal storage exhibit substantially lower HVAC energy consumption than baseline PTC systems, particularly at moderate sub-zero temperatures [25].

At very low ambient temperatures (−18 °C), Figure 1.3.1-1 also indicates the onset of an HVAC saturation regime. In this regime, heating systems operate near their maximum capacity, and further reductions in ambient temperature do not produce proportional increases in HVAC energy consumption. This behavior has important implications for range modeling, as it explains why energy consumption—and consequently driving range—does not continue to degrade linearly at extreme cold conditions.

In addition to HVAC demand, ambient temperature affects BEV energy consumption through battery efficiency. As temperature decreases, increased internal resistance leads

to higher ohmic losses during discharge, reducing the fraction of electrical power converted into useful mechanical output. This effect can be represented as

$$\eta_{bat}(T) = 1 - \frac{I^2 R_{int}(T)}{P_{elec}}$$

where $R_{\text{int}}(T)$increases with decreasing temperature (Delos Reyes et al., 2016). Although secondary compared to HVAC loads, this mechanism contributes to cumulative energy losses during prolonged cold-weather operation.

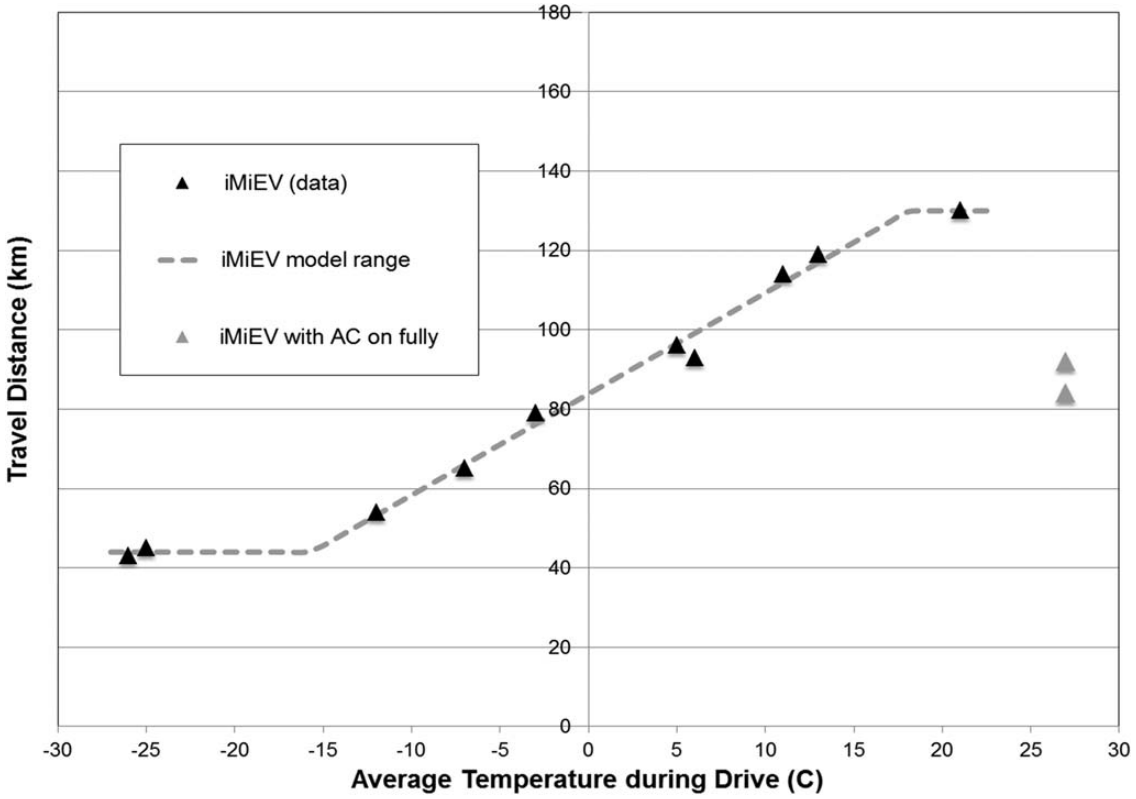

Figure 1.13. *Driving range as a function of ambient temperature with linear-segment interpretation [23].*

Figure 1.13 illustrates that, within the intermediate temperature range (approximately +20 °C to −15 °C), BEV driving range decreases almost linearly with decreasing ambient temperature. This behavior reflects the combined effects of increasing HVAC energy demand and declining battery efficiency. The temperature sensitivity of driving range in this region can be approximated as:

$$R(T) = R_0 - k(T_0 - T)$$

where the coefficient $k$typically lies between 2.5 and 3.0 km / °C, depending on vehicle design and HVAC configuration (Delos Reyes et al., 2016). This relationship is particularly useful for vehicle-level simulations and climate-specific range prediction models[23].

1.3.2. HVAC and Auxiliary Energy Consumption

Heating, Ventilation, and Air Conditioning (HVAC) systems represent one of the most significant auxiliary energy consumers in battery electric vehicles (BEVs), particularly under hot and cold ambient conditions. Unlike internal combustion engine vehicles, BEVs cannot rely on engine waste heat for cabin conditioning and must supply all thermal comfort and defrosting demands directly from the high-voltage battery. As a consequence, HVAC operation introduces a direct and temperature-dependent penalty on vehicle energy consumption and driving range.

At moderate ambient temperatures, HVAC systems operate intermittently and account for a relatively small fraction of total vehicle energy use. However, as ambient temperature deviates from the thermal comfort zone (approximately 20–25 °C), HVAC power demand increases rapidly. At low temperatures, electric heating becomes dominant, while at high temperatures cooling and dehumidification loads prevail. Vehicle-level studies show that under extreme ambient conditions HVAC energy consumption may exceed 30–50 % of total onboard energy usage, especially during urban driving with low traction power demand [4], [26].

The total electrical energy drawn from the traction battery can be expressed as:

$$E_{HV} = E_{trac} + E_{HVAC+}E_{aux}$$

where $E_{\text{trac}}$is the traction energy, $E_{\text{HVAC}}$is the energy consumed by cabin and battery thermal management, and E_{aux}represents other auxiliary loads such as lighting, infotainment, and control electronics. Among these terms, E_{HVAC}exhibits the strongest dependence on ambient temperature.

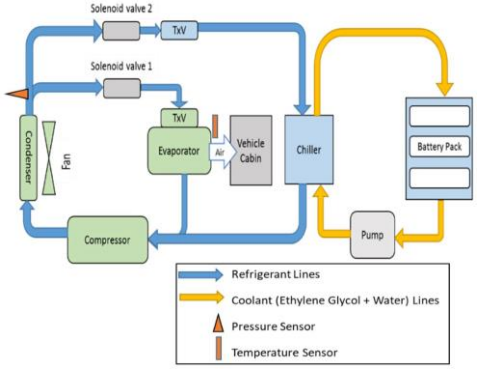

Figure 1.14. *Schematic architecture of the HVAC system for cabin and battery cooling in an*

electric vehicle[26].

Figure 1.14 illustrates a representative HVAC architecture used in modern BEVs, based on a vapor-compression refrigeration cycle with shared cooling capability for both the passenger cabin and the battery pack. The system employs an electrically driven compressor, a PTC heater for cabin heating, and solenoid-controlled refrigerant paths to balance thermal demands between cabin comfort and battery temperature regulation. This shared architecture highlights why HVAC operation directly affects not only passenger comfort but also battery operating conditions and efficiency.

From an energy-consumption perspective, heating efficiency is commonly characterized using the coefficient of performance (COP):

$$COP_{heat} = \frac{Q_{cabin}}{P_{HVAC}}$$

where $Q_{\text{cabin}}$is the thermal power delivered to the cabin and $P_{\text{HVAC}}$is the electrical power drawn from the battery. Resistance-based PTC heaters typically exhibit COP values close to unity, whereas heat-pump systems can achieve COP values between 2 and 3 at moderate ambient temperatures, substantially reducing energy consumption [22], [26].

Transient and steady-state HVAC energy demand

HVAC energy consumption is highly transient in nature. Immediately after vehicle start-up, the HVAC system operates at maximum capacity to bring the cabin temperature to the user-defined setpoint. During this phase, HVAC power demand can reach 4–6 kW in cold environments. Once thermal equilibrium is reached, power demand decreases to a steady-state level required to offset heat losses to the environment.

Table 1.3. Typical HVAC power demand in cold conditions[27]

Ambient temperature	Operating phase	HVAC power (kW)
−18 °C	Transient warm-up	4.5–6.0
−18 °C	Steady-state	3.0–4.0
−7 °C	Transient warm-up	3.0–4.0
−7 °C	Steady-state	2.0–3.0

These repeated transient heating phases are particularly detrimental during short urban trips, where the vehicle rarely reaches steady-state thermal conditions.

Contribution of HVAC to total vehicle energy consumption

Vehicle-level measurements indicate that the relative contribution of HVAC energy consumption depends strongly on the driving cycle. In low-speed urban driving, traction power demand is limited, causing HVAC energy to represent a larger fraction of total consumption. Conversely, during highway driving, higher traction power reduces the

relative impact of HVAC loads.

Table 1.4. HVAC share of total energy consumption[27]

Driving cycle	Ambient temperature	HVAC share (%)
Urban (UDDS)	−18 °C	45–60
Urban (UDDS)	35 °C	25–35
Highway (HWFET)	−18 °C	20–30
Highway (HWFET)	35 °C	10–15

HVAC and auxiliary energy consumption constitute a dominant temperature-dependent loss mechanism in BEVs. System architecture, control strategy, and ambient conditions jointly determine the magnitude of this effect. Accurate modeling of HVAC loads is therefore essential for reliable BEV energy-consumption and range prediction, especially for regions characterized by large seasonal temperature variations.

1.3.3. Charging/Discharging Behavior and Vehicle Efficiency

The charging and discharging behavior of lithium-ion batteries in battery electric vehicles (BEVs) is strongly influenced by temperature, current rate, and thermal boundary conditions. These factors jointly determine vehicle-level efficiency, available power, and long-term durability. Unlike steady laboratory cycling, real-world BEV operation involves highly transient current profiles, repeated partial charging, and temperature gradients within the battery pack, all of which affect electrical efficiency and degradation mechanisms.

During discharge, battery efficiency is primarily governed by internal resistance and electrochemical overpotentials. At low ambient temperatures, increased ionic resistance and reduced reaction kinetics lead to higher voltage losses under load, thereby reducing usable energy and traction efficiency. Vehicle-level measurements confirm that even when HVAC effects are excluded, cold-temperature operation results in measurable efficiency losses due to increased battery internal resistance and powertrain losses [3], [23].

At the cell level, the total heat generation during charge and discharge can be expressed as the sum of irreversible Joule heating and reversible entropic heat:

$$\dot{Q} = i^2 R_{int} + iT\frac{\partial V_{oc}}{\partial T}$$

where $i$is the current, $R_{\text{int}}$is the internal resistance, and $\partial V_{\text{oc}}/\partial T$represents the entropy coefficient of the electrochemical reaction (Jeon & Baek, 2011). This formulation highlights that both current magnitude and temperature-dependent electrochemical properties directly influence efficiency and thermal behavior.

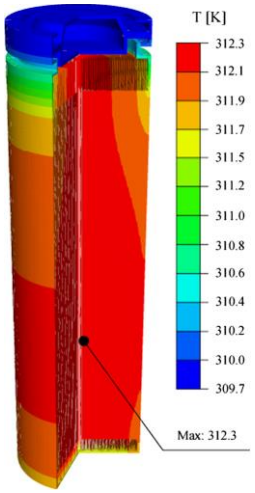

***Figure 1.15.** Non-uniform temperature distribution [28]*

Figure 1.15 illustrates the non-uniform temperature distribution that develops inside a cylindrical lithium-ion cell during discharge. The highest temperature is observed near the core of the cell, while the surface remains cooler due to convective heat transfer. Although the absolute temperature rise at moderate discharge rates may appear limited, even small internal gradients can accelerate aging mechanisms when repeated over thousands of cycles. This effect becomes more pronounced at higher C-rates, where Joule heating increases quadratically with current [28].

From a vehicle-efficiency perspective, elevated internal temperature during discharge has a dual effect. In moderate conditions, a slight temperature rise can temporarily reduce internal resistance and improve instantaneous efficiency. However, sustained high temperatures accelerate degradation processes, leading to long-term efficiency loss and reduced usable capacity. Conversely, operation at low temperatures results in lower instantaneous efficiency due to increased resistance and reduced power capability, particularly during high-load events such as acceleration or hill climbing [28].

Charging behavior and efficiency limitations

Charging efficiency is similarly temperature-dependent. At low temperatures, lithium-ion diffusion within the anode becomes sluggish, limiting charge acceptance and increasing the risk of lithium plating under high charging currents. To mitigate this risk, BEV battery management systems (BMS) often reduce allowable charging power in cold conditions, directly increasing charging time and reducing overall system efficiency. While this strategy preserves safety, it introduces operational inefficiencies that are especially relevant for fast-charging scenarios.

During high-temperature charging, increased side reactions and accelerated solid-electrolyte interphase (SEI) growth reduce coulombic efficiency. Over repeated cycles,

these losses accumulate and manifest as measurable capacity fade and increased internal resistance. Vehicle-level studies confirm that aggressive charging strategies at elevated temperatures significantly shorten battery lifetime, even when nominal efficiency during individual charging events appears high [23].

The round-trip energy efficiency of the battery during charge–discharge operation can be approximated as:

$$\eta_{rt} = \frac{E_{dis}}{E_{ch}} = 1 - \frac{E_{loss}}{E_{ch}},$$

where E_{loss}includes ohmic losses, polarization losses, and parasitic side reactions. Temperature influences all three terms, making thermal management an essential component of efficiency optimization

Long-term implications for efficiency and degradation

Repeated exposure to unfavorable charging and discharging conditions leads to cumulative degradation effects that ultimately reduce vehicle efficiency. Capacity loss reduces usable energy, while internal resistance growth increases losses during both charge and discharge. Although degradation is addressed in detail in subsequent sections, it is important to note that efficiency loss and degradation are tightly coupled phenomena.

Typical degradation tendencies for BEV lithium-ion batteries subjected to repeated charge–discharge cycles under controlled thermal conditions. These values represent order-of-magnitude trends, not exact predictions[28].

Table 1.5 Typical capacity degradation tendency of BEV lithium-ion batteries with cycling [23], [28]

Number of equivalent full cycles	Typical capacity fade (%)	Dominant contributing factors
1 000 cycles	5–8 %	SEI growth, mild resistance increase
2 000 cycles	10–15 %	Accelerated SEI thickening, lithium loss
3 000 cycles	18–25 %	Increased internal resistance, electrode aging
4 000+ cycles	>30 %	Structural degradation, reduced charge acceptance

1.4. Economic, Operational, and Policy Considerations

The transition to battery electric vehicles (BEVs) introduces a tightly coupled set of economic, operational, and policy challenges that extend beyond vehicle-level performance and directly influence national energy systems and consumer decision-making. In emerging economies such as Uzbekistan, where road transport remains

dominated by fossil fuels, electrification pathways are shaped by fuel price structures, infrastructure readiness, and long-term policy coordination. Agent-based modelling of Uzbekistan's transport sector demonstrates that, in the absence of sustained policy intervention, fossil fuel dominance persists despite technological progress, leading to transport emissions exceeding 41 $MtCO_2$ annually by mid-century. These findings highlight that market forces alone are insufficient to drive large-scale electrification without coordinated regulatory and fiscal measures [29].

From an operational perspective, charging behavior and infrastructure deployment strongly affect system-level costs and grid interaction. Studies on charging optimization for electric vehicle fleets show that unmanaged charging can significantly increase operational expenditure, whereas coordinated overnight or off-peak charging strategies reduce electricity costs and peak load stress. In particular, scheduling-based charging optimization demonstrates measurable reductions in energy-related operating costs when charging is aligned with low-tariff periods, emphasizing the importance of pricing mechanisms and infrastructure planning in large-scale electrification scenarios. These operational insights are directly transferable to passenger BEV adoption, where similar cost-saving mechanisms can be leveraged through smart charging policies [30].

Infrastructure planning represents a critical policy lever influencing both operational efficiency and user confidence. Urban charging studies reveal that an imbalanced distribution between residential and commercial charging stations can lead to underutilization and increased system costs. A mixed charging ecosystem—combining home charging, workplace charging, and public fast chargers—is shown to minimize infrastructure redundancy while improving accessibility. For cities in Uzbekistan, where multi-family housing and limited private parking are common, such planning principles are essential to avoid reinforcing range anxiety and slowing market uptake [31].

At the policy and market level, evidence from Central Asia indicates that fiscal incentives, import tax exemptions, and clear national electrification targets significantly improve BEV competitiveness. A Total Cost of Ownership (TCO) assessment for Kyrgyzstan—an economically and climatically comparable country—shows that BEVs can already achieve lower lifetime costs than internal combustion vehicles under favorable electricity pricing and tax exemptions. Importantly, the study emphasizes that consumer adoption is highly sensitive to upfront cost signals and charging availability, reinforcing the need for integrated policy frameworks rather than isolated incentives. These insights are directly applicable to Uzbekistan's ongoing transport decarbonization strategy [30].

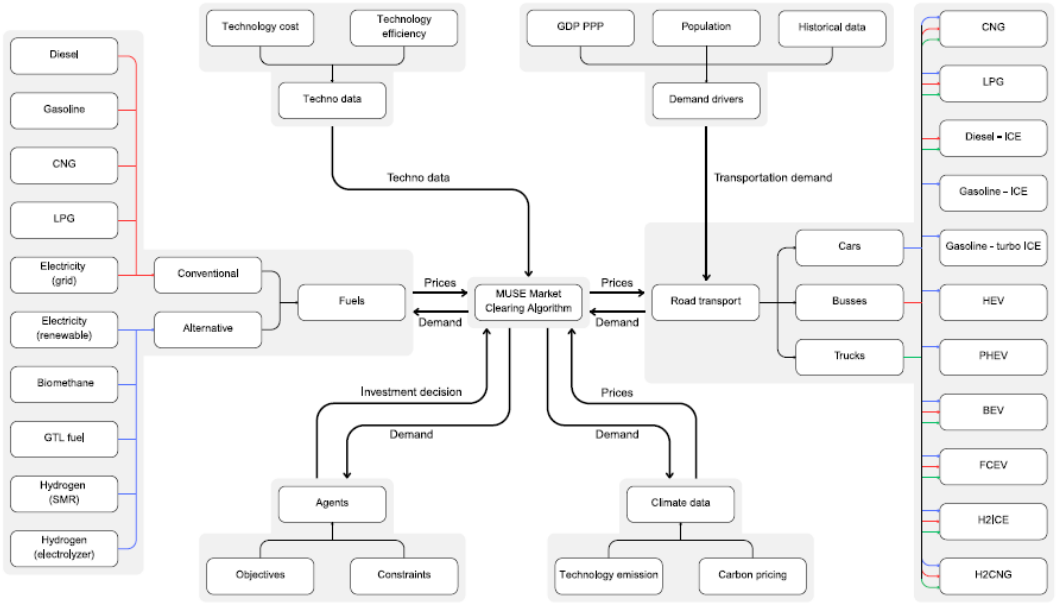

Figure 1.16. *Agent-based modelling structure and energy–emissions pathways for Uzbekistan's road transport sector [29]*

1.4.1. Calendar and Cycle Ageing, SEI Growth, and Lithium Plating

Battery degradation in lithium-ion batteries used in battery electric vehicles (BEVs) originates from a combination of time-dependent and usage-dependent mechanisms, commonly referred to as calendar ageing and cycle ageing, respectively. Both processes are strongly influenced by temperature, state of charge (SOC), and current rates, but their relative importance differs significantly under real-world vehicle operating conditions.

Calendar ageing describes degradation occurring during storage or idle periods, even in the absence of cycling. It is primarily associated with continuous side reactions at the electrode–electrolyte interface, most notably the growth and transformation of the solid electrolyte interphase (SEI) layer on the graphite anode. Experimental studies show that elevated temperature and high SOC accelerate calendar ageing by enhancing electrolyte decomposition kinetics and lithium consumption [25], [32].

As the SEI thickens over time, lithium inventory is irreversibly reduced, leading to capacity fade and increased internal resistance.

The rate of calendar ageing can be approximated by an Arrhenius-type relationship:

$$k_{cal} = k_0 exp\left(-\frac{E_\alpha}{RT}\right)$$

where $k_{\text{cal}}$is the degradation rate constant, $E_a$is the activation energy of side reactions,

*R*is the universal gas constant, and *T*is the absolute temperature (Elsevier, 2019). This relationship explains why prolonged exposure to high ambient temperatures significantly accelerates capacity loss during storage.

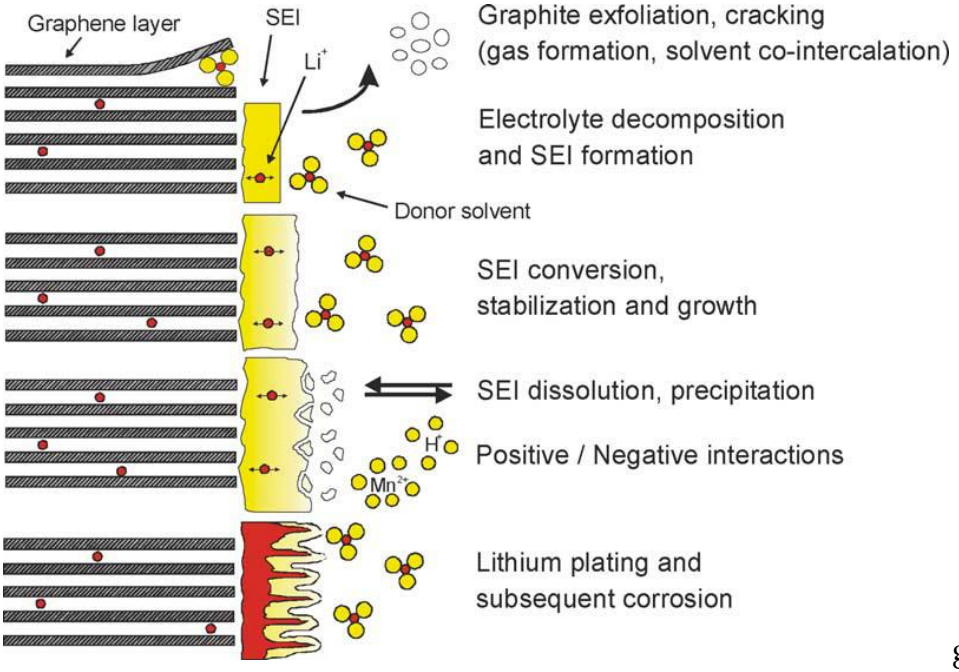

growth.

Figure 1.17. *Changes at the anode–electrolyte interface illustrating SEI formation and growth [32].*

Figure 1.17 illustrates how continuous electrolyte decomposition leads to progressive SEI growth on the graphite anode. While an initial SEI layer is essential for battery stability, ongoing SEI thickening increases ionic transport resistance and contributes to power fade over long-term operation.

Cycle ageing, in contrast, results from repeated charge–discharge cycling and is the dominant degradation mechanism under typical BEV usage. It is driven by lithium inventory loss, mechanical stress in active materials, and irreversible side reactions that intensify with increasing depth of discharge (DOD), current rate, and temperature [3], [24].

Repeated cycling causes structural changes in electrodes and accelerates SEI growth beyond that observed during storage alone.

The total capacity loss can be expressed as the combined contribution of calendar and cycle ageing:

$$\Delta Q = \Delta Q_{\text{cal}} + \Delta Q_{\text{cyc}},$$

where ΔQ_{cyc}generally dominates for vehicles subjected to frequent driving and charging events (SAE 2020-01-1188).

A particularly critical cycle-induced degradation mechanism is lithium plating, which occurs primarily during charging at low temperatures or high current rates. Under these conditions, lithium ions cannot intercalate into the graphite anode fast enough and instead deposit as metallic lithium on the anode surface. This process not only reduces the amount of cyclable lithium but also poses safety risks due to dendrite formation [3], [32].

Subsequent reactions between plated lithium and electrolyte further accelerate SEI growth and capacity loss.

Table 1.6. Comparison of calendar and cycle ageing mechanisms in BEV lithium-ion batteries[25], [32]

Ageing type	Dominant conditions	Main mechanisms	Relative importance in BEVs
Calendar ageing	High SOC, high temperature, long storage	SEI growth, electrolyte decomposition	Secondary
Cycle ageing	Repeated cycling, high DOD, high C-rate	SEI thickening, lithium loss, mechanical stress	Dominant
Lithium plating	Low temperature, fast charging	Metallic lithium deposition, SEI reformation	Critical risk factor

Thesis statement

Based on the reviewed literature, calendar ageing is not the dominant degradation mechanism during everyday BEV operation, as vehicles typically experience frequent cycling rather than prolonged storage at high SOC. Cycle ageing is the primary contributor to battery degradation in BEVs, driven by repeated charge–discharge events, temperature-dependent SEI growth, and lithium plating under unfavorable charging conditions. Calendar ageing becomes significant mainly during extended idle periods or sustained high-SOC storage, whereas real-world vehicle usage is governed predominantly by cycle-induced degradation processes.

1.4.2. Temperature-Driven Energy Cost Variations and Charging Frequency

Temperature variations affect the economic performance of battery electric vehicles (BEVs) primarily through changes in auxiliary energy demand rather than through propulsion efficiency alone. Under cold and hot ambient conditions, additional electrical energy is required to maintain acceptable cabin comfort, leading to higher total energy consumption per trip. This increase directly raises operating costs and accelerates the frequency of battery recharging, particularly in urban and short-trip driving where auxiliary loads represent a larger share of total energy use. Field studies conducted under real driving conditions confirm that temperature-dependent auxiliary loads constitute a

major contributor to seasonal energy penalties in BEV operation [23].

The heating, ventilation, and air-conditioning (HVAC) system is the dominant temperature-sensitive subsystem influencing BEV energy consumption. Experimental measurements reported in SAE literature show that cabin heating demand in winter conditions can exceed 4–5 kW during cold start and remain significant throughout the trip, substantially increasing total electrical energy use. Similarly, cooling loads under high ambient temperatures impose a measurable energy penalty, although typically lower than heating demand. The auxiliary energy consumption associated with thermal comfort can be expressed as:

$$E_{HVAC} = \int_0^t P_{HVAC}(T_a)dt$$

where P_{HVAC} increases as a function of ambient temperature deviation from the comfort setpoint. As a result, lower ambient temperatures lead to higher energy consumption per kilometer and increased charging frequency [33].

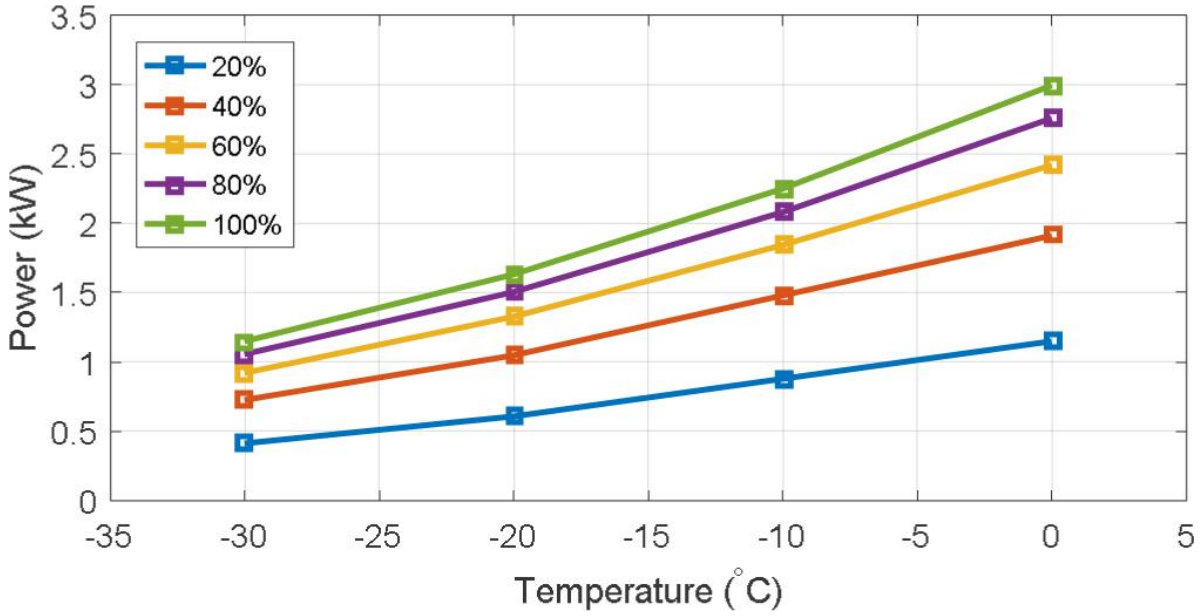

Figure 1.18. *Contribution of HVAC systems to total BEV energy consumption under heating and cooling operation, illustrating the strong dependency of auxiliary loads on ambient temperature [33]*

Advanced HVAC technologies, particularly heat-pump-based systems, have been introduced to mitigate temperature-driven energy penalties. Control-oriented studies demonstrate that optimized heat-pump operation can reduce HVAC energy consumption by exploiting cabin thermal inertia and staged heating strategies during vehicle warm-up. However, even with optimized control trajectories, HVAC systems remain a substantial energy consumer under extreme ambient conditions. This indicates

that while technological improvements can reduce operating cost sensitivity to temperature, they cannot eliminate seasonal variations in energy demand [34].

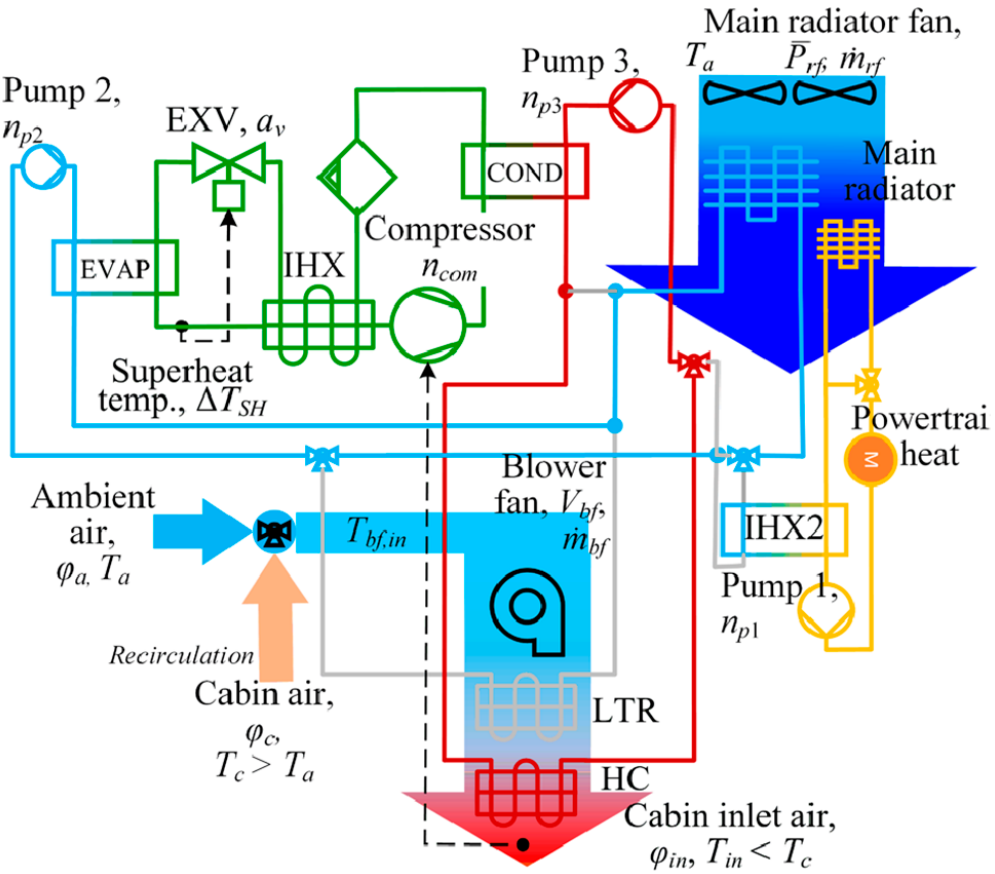

Figure 1.19. *Schematic representation of a heat-pump-based HVAC system for BEVs, illustrating refrigerant and coolant loops influencing cabin heating efficiency and energy consumption[34].*

From an economic standpoint, increased energy consumption per trip directly affects charging behavior. As temperature-driven auxiliary loads increase the required charging energy, users are exposed more frequently to electricity tariffs, particularly under time-dependent pricing schemes. The cumulative charging cost over a given period can be expressed as:

$$C_{charge} = \sum_{i=1}^{N} E_i * \lambda(t_i)$$

where $E_i$represents the energy of each charging event and $\lambda(t_i)$the electricity price at the charging time. Under extreme temperature conditions, both $E_i$and the number of charging events Nincrease, reinforcing the importance of efficient HVAC design and cost-aware charging strategies for minimizing operational expenses [35].

1.4.3. Range Anxiety, Infrastructure, and Market Adaptation in Uzbekistan

Range anxiety refers to the concern that a battery electric vehicle (BEV) may not have sufficient energy to complete a planned trip, and it remains a dominant barrier to adoption in regions with sparse charging infrastructure and high climatic variability. In continental climates such as Uzbekistan's, this concern is amplified by seasonal temperature effects that reduce effective driving range and increase uncertainty in energy availability. Even when nominal vehicle range is adequate, users tend to base their perception on worst-case scenarios, particularly winter operation and long-distance intercity travel. Empirical studies confirm that such perception-based barriers persist independently of actual vehicle capability and must therefore be addressed through infrastructure visibility and policy support rather than vehicle technology alone [23].

From a user-centric perspective, perceived range adequacy depends on the balance between usable battery energy and expected energy demand under real-world conditions. This relationship can be expressed as:

$$R_{eff} = \frac{E_{usable}}{e_{drive} + e_{aux}}$$

where $E_{\text{usable}}$is the usable battery energy, $e_{\text{drive}}$is traction energy per kilometer, and e_{aux}represents auxiliary loads such as heating and cooling. In cold or hot conditions, e_{aux}increases significantly, reducing effective range and reinforcing user anxiety. In the absence of frequent and reliable charging options, this perceived reduction directly influences purchase decisions and daily usage patterns [23].

Charging infrastructure deployment plays a decisive role in mitigating range anxiety and enabling market adaptation. Urban infrastructure planning studies show that an unbalanced concentration of charging stations—either predominantly residential or commercial—fails to meet diverse user needs and limits utilization efficiency. A mixed infrastructure strategy that integrates residential charging with workplace and public fast-charging facilities significantly improves both actual accessibility and perceived reliability. For Uzbekistan, where a large share of the urban population resides in multi-apartment buildings with limited private parking, public and semi-public charging infrastructure is essential to support early-stage BEV adoption [36].

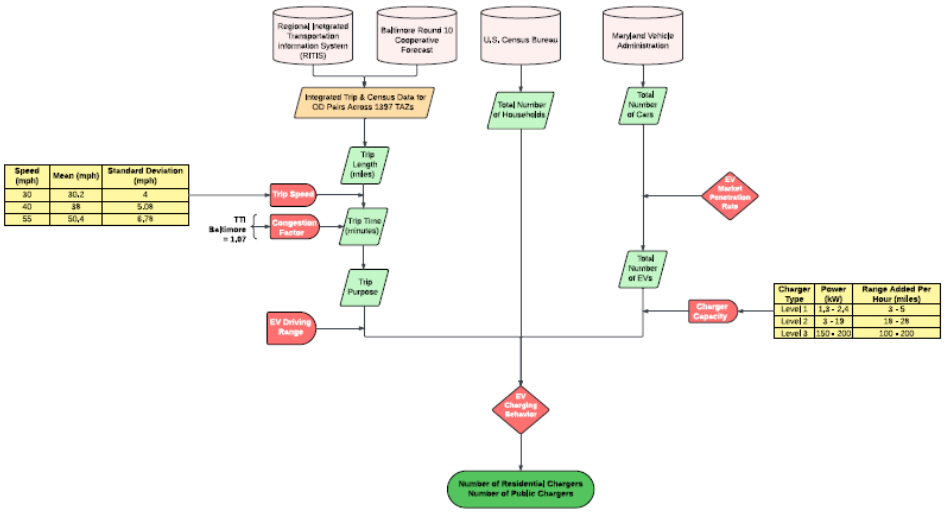

Figure 1.20. *Conceptual illustration of balanced residential and commercial EV charging infrastructure deployment, highlighting its role in improving accessibility and reducing range anxiety [36].*

Market adaptation to BEVs in Central Asia is strongly influenced by policy incentives and infrastructure rollout timing. Evidence from Kyrgyzstan—a geographically, economically, and climatically comparable country—demonstrates that EV adoption accelerates when fiscal incentives coincide with visible infrastructure expansion. Import duty exemptions, reduced registration taxes, and free or subsidized public charging have been shown to lower entry barriers and improve consumer confidence. Importantly, the study highlights that infrastructure availability functions as a confidence signal, reducing perceived risk even before high utilization levels are reached. These findings are directly transferable to Uzbekistan's emerging BEV market [30].

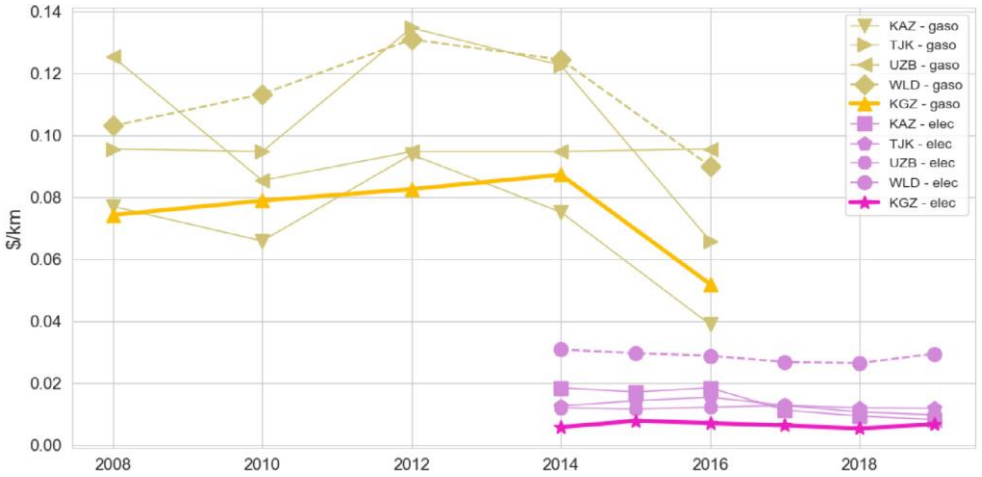

Figure 1.21. *Comparison of energy cost per kilometer for electric and gasoline vehicles in Central Asian countries, illustrating the economic conditions supporting BEV adoption and reduced range anxiety [30].*

At the system level, infrastructure sufficiency can be evaluated using a charger-to-vehicle ratio, defined as:

$$I_c = \frac{N_{charges}}{N_{EV}}$$

where $N_{\text{chargers}}$is the number of publicly accessible charging points and $N_{\text{EV}}$is the number of registered electric vehicles. Low values of $I_c$are associated with increased range anxiety and slower market uptake. For Uzbekistan, proactive infrastructure deployment aligned with projected BEV growth is therefore critical to avoid reinforcing negative perceptions and to ensure a smooth transition toward electrified mobility *[30]*.

1.4.4. Economic Implications for Consumers and National Energy Strategy

The adoption of battery electric vehicles (BEVs) has direct economic implications for consumers through changes in fuel expenditure, maintenance costs, and exposure to long-term energy price volatility. In Uzbekistan, where road transport is currently dominated by fossil fuels, the transition to electricity-based mobility represents a structural shift in household transport economics. Long-term transport energy modeling indicates that, without targeted policy intervention, BEV adoption remains constrained by higher upfront costs despite lower operating expenses. These findings highlight the need for coordinated fiscal policies to make lifecycle cost advantages visible to consumers[29].

From a consumer perspective, the economic attractiveness of BEVs can be assessed using a levelized cost of driving framework that accounts for capital investment and operational expenses over the vehicle lifetime. This can be expressed as:

$$LCOD = \frac{CAPEX + \sum_{t=1}^{n} \frac{OPEX_t}{(1+r)^t}}{\sum_{t=1}^{n} \frac{D_t}{(1+r)^t}}$$

where $CAPEX$denotes vehicle purchase cost, $OPEX_t$includes energy and maintenance costs, $D_t$is the annual driving distance, and $r$is the discount rate. Scenario-based modeling for Uzbekistan shows that BEVs reach cost parity with internal combustion vehicles only under stable electricity prices and supportive fiscal policies, reinforcing the strategic importance of national pricing frameworks[29].

At the national level, large-scale BEV deployment significantly affects electricity demand growth and infrastructure investment requirements. Transport electrification scenarios indicate that electricity demand from road transport could reach several tens of petajoules per year by mid-century, requiring coordinated expansion of generation capacity and

grid infrastructure. Integrating transport electrification into national energy planning is therefore essential to avoid cost escalation and ensure system reliability, particularly under rapid adoption trajectories [29].

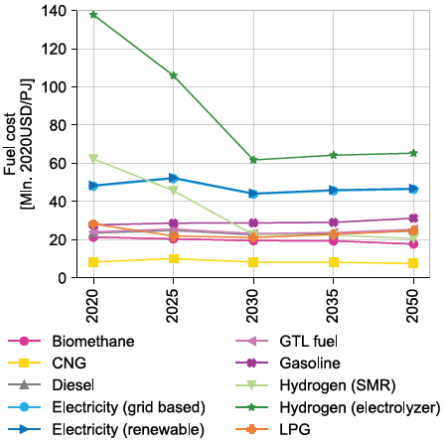

Figure 1.22. *Projected evolution of transport energy demand and fuel mix in Uzbekistan under electrification scenarios[29].*

In addition to energy demand growth, charging cost structures play a crucial role in shaping both consumer behavior and national energy efficiency. Pricing-based charging strategies encourage off-peak electricity use, reducing household charging costs while supporting grid stability. The cumulative charging cost can be expressed as:

$$C_{charge} = \sum_{i=1}^{N} E_i * \lambda(t_i)$$

where $E_i$is the charged energy and $\lambda(t_i)$is the time-dependent electricity price. Studies on charging price optimization show that such mechanisms reduce system-level peak loads and enhance the economic sustainability of BEV adoption, aligning consumer benefits with national energy strategy objectives[35].

2. Mathematical Modelling and Experimental Methodology

2.1. Mathematical Modelling Framework and System Architecture

2.1.1. Overall, BEV Modelling Architecture and Simulation Scope

The Battery Electric Vehicle (BEV) simulation model developed in this study is implemented in MATLAB/Simulink using Powertrain Blockset and Simscape, following a modular, physics-based modeling philosophy. The model architecture adopts a backward-facing longitudinal approach, where the vehicle motion prescribed by the driving cycle defines the propulsion demand, while electrical energy is supplied by the battery and converted into mechanical motion at the wheels. This approach ensures numerical robustness, transparency of energy flows, and realistic interaction between subsystems under transient driving conditions [37].

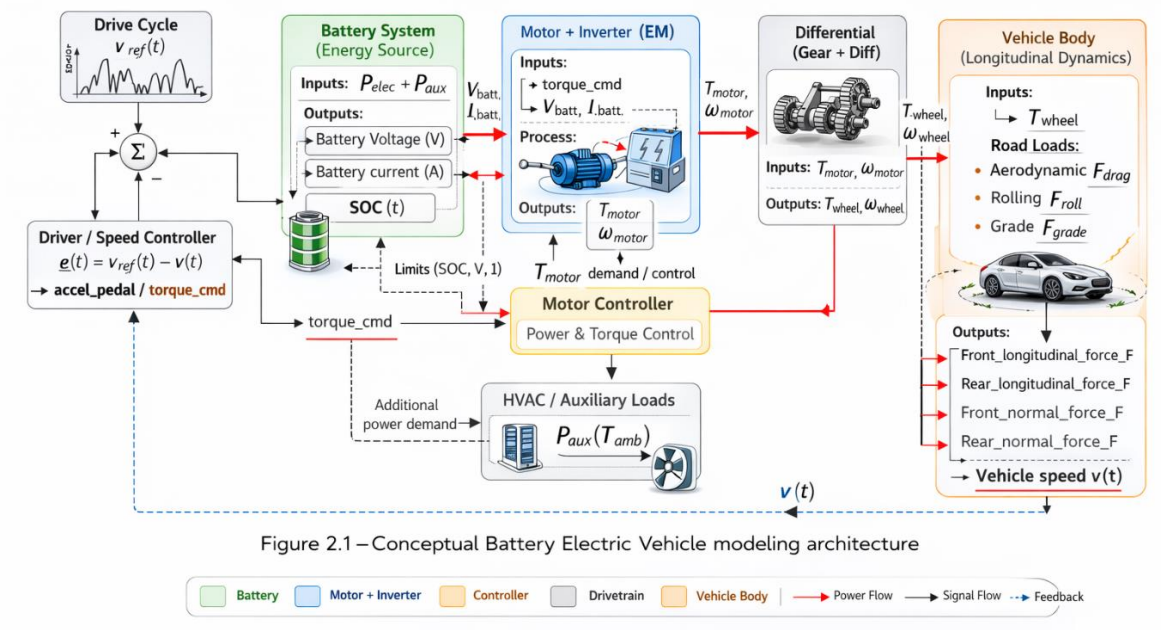

Figure 2.1 – Conceptual Battery Electric Vehicle modeling architecture

Figure 2.1 *– Conceptual Battery Electric Vehicle modeling architecture adopted in this study.*

Figure 2.1 illustrates the high-level conceptual architecture of the BEV model adopted in this work. The system is composed of five main subsystems: Driving Cycle and Driver, Battery and Electrical Energy Source, Electric Motor and Power Electronics, Drivetrain and Differential, and Vehicle Body. Each subsystem represents a physical domain and exchanges information through clearly defined signals, such as speed, torque, current, and voltage. The figure is intended to explain system logic and causality, while avoiding implementation-level details that are addressed in subsequent sections[37], [38].

Driving Cycle, Driver, and Vehicle Demand Flow

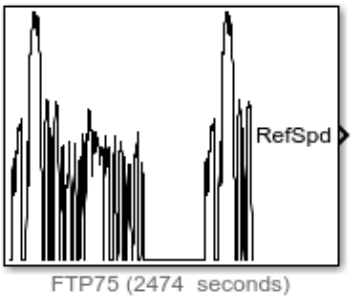

Figure 2.2. *The Drive Cycle Source block [37].*

The simulation is initiated by a Driving Cycle block, which provides a reference vehicle speed profile as a function of time. This reference does not directly impose vehicle motion; instead, it is processed by a Longitudinal Driver subsystem that compares the reference speed with the actual vehicle speed and generates accelerator and braking commands. These commands represent driver intent rather than physical forces, allowing the feasibility of the request to be enforced by the propulsion and energy subsystems. This structure enables realistic reproduction of transient behavior, including acceleration, cruising, and deceleration phases[37].

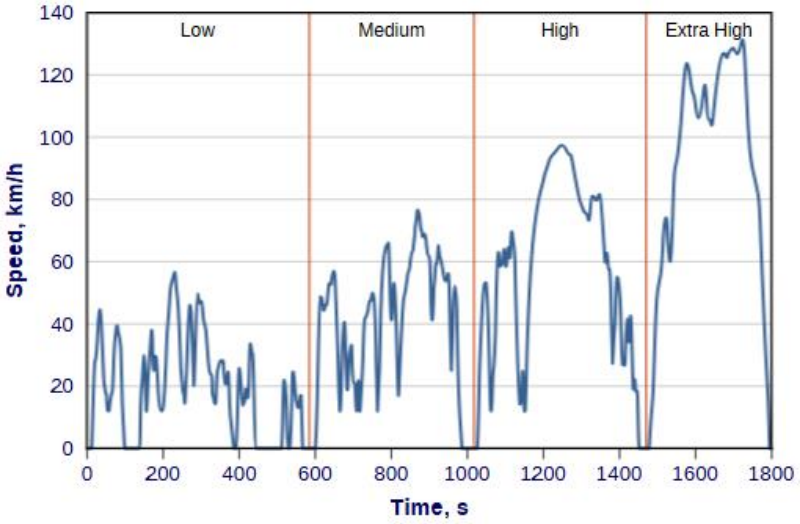

Figure 2.3. *WLTP cycle for Class 3b vehicles [39].*

The Worldwide Harmonized Light Vehicles Test Procedure (WLTP) was selected as the reference regulatory framework for defining vehicle operating conditions, with specific adoption of the WLTP Class 3 driving cycle. WLTP Class 3 is intended for passenger vehicles with relatively high power-to-mass ratios and is therefore well aligned with the performance envelopes of modern battery-electric vehicles, particularly the Chevrolet Bolt EV and Volkswagen e-Golf 2017. Compared with earlier regulatory cycles, WLTP incorporates higher average speeds, stronger transient accelerations, and a broader distribution of operating points, resulting in more realistic traction power demand and electrical loading. For the Nissan Leaf, representing an earlier generation BEV, the WLTP Class 3 cycle still provides a standardized benchmark suitable for comparative analysis [40].

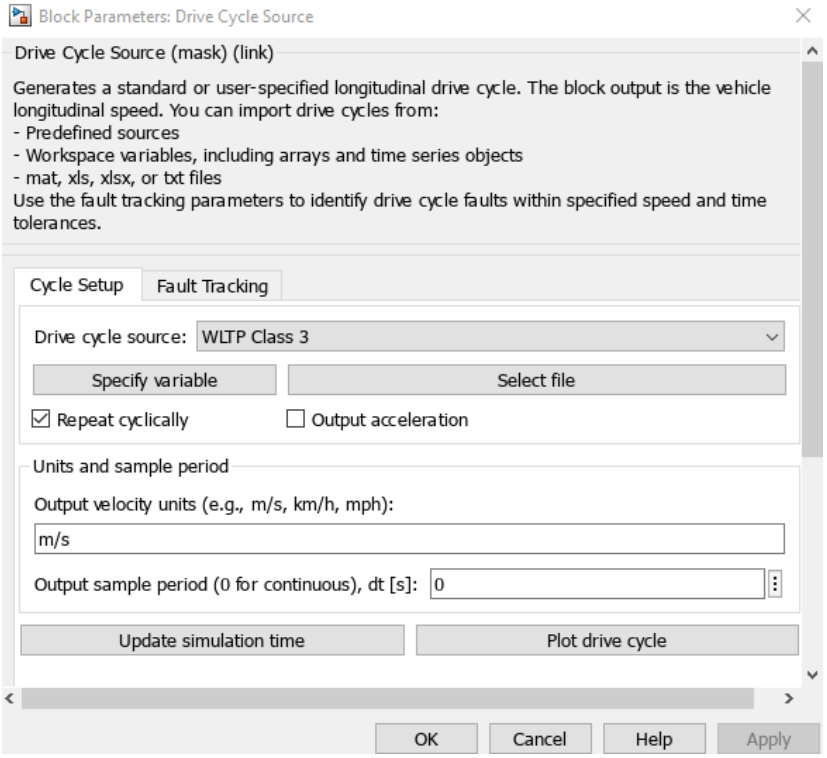

Figure B: *Block parameter window showing selection of WLTP Class 3[37], [41]*

Global Vehicle Dynamics Representation

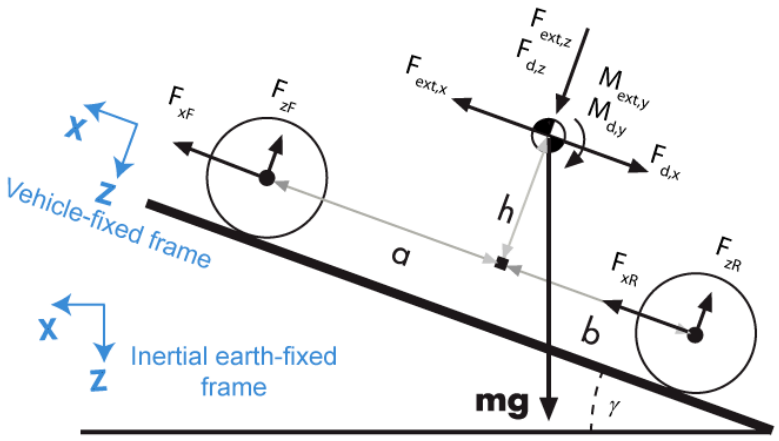

Figure 2.4. *Longitudinal force components acting on a vehicle on an inclined road [37]*

The Vehicle Body 1DOF Longitudinal block in MathWorks Simulink represents the vehicle as a rigid body constrained to one-dimensional longitudinal motion along the road. The positive direction corresponds to forward vehicle travel, while reverse motion is represented by negative velocity. Vertical, lateral, and pitch dynamics are neglected, allowing the model to focus on longitudinal behavior only.

The vehicle dynamics are governed by Newton's second law, where the net longitudinal force determines acceleration. The force balance acting on the vehicle body is expressed as

$$F_b = F_{xF} + F_{xR} - F_{d,x} + F_{\text{ext},x} - mg\sin(\gamma),$$

with $F_b = ma$. Here, $F_{xF}$and F_{xR}denote the longitudinal tire forces at the front and rear axles, $F_{d,x}$represents aerodynamic drag, $F_{\text{ext},x}$includes external longitudinal disturbances, and $mg\sin(\gamma)$accounts for the gravitational component due to road grade γ. By integrating acceleration over time, the block computes vehicle velocity and position, making it suitable for drive-cycle tracking and energy-consumption analysis [37].

Energy Conversion Chain: Battery to Wheels

The propulsion energy path in the BEV model follows a clear and physically consistent sequence: battery → power electronics → electric motor → drivetrain → wheels. Electrical energy stored in the battery is converted into mechanical torque by the electric motor and transmitted to the wheels through a fixed-ratio drivetrain. The overall power flow can be summarized at a system level by:

$$P_{battery} = \frac{P_{wheel}}{\eta_{drivetrain}}$$

where $\boldsymbol{P}_{\text{wheel}}$is the mechanical power required at the wheels and $\boldsymbol{\eta}_{\text{drivetrain}}$represents the

combined efficiency of the electric motor, inverter, and drivetrain. Detailed component-level modeling of this energy conversion chain is addressed in the following subsections [37], [38].

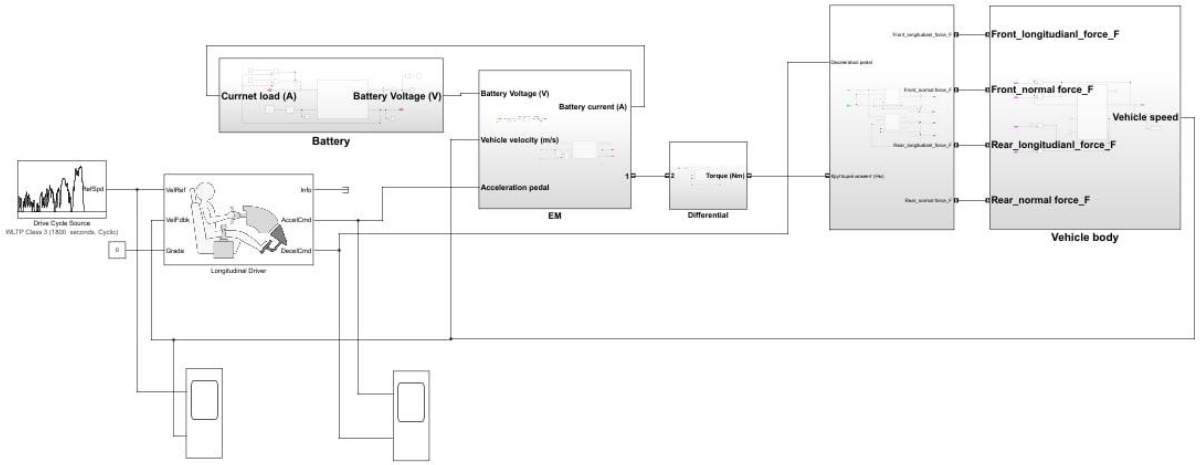

Figure 2.5 *– Detailed MATLAB/Simulink implementation of the Battery Electric Vehicle model.*

Figure 2.5 shows the detailed Simulink realization of the conceptual architecture presented in Figure 2.1. Each conceptual subsystem is implemented using standard library blocks and explicitly parameterized by the author. Signal routing and feedback paths connect the vehicle dynamics, driver, electric drivetrain, and battery subsystems, forming a closed-loop system. This figure demonstrates the practical realization of the modeling framework rather than introducing new conceptual information[37].

Regenerative Braking and Energy Recovery

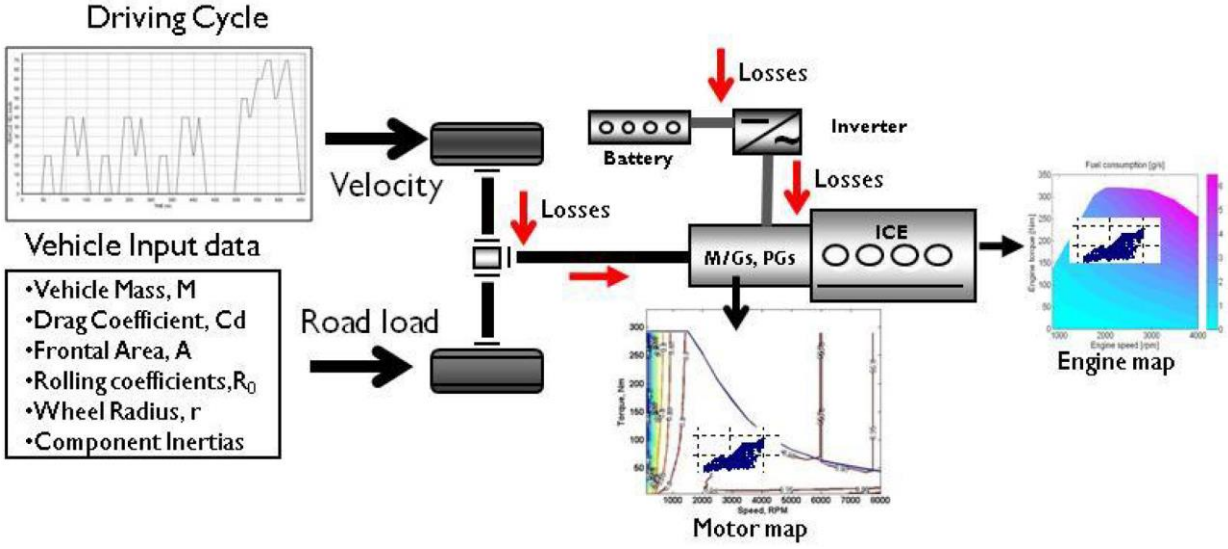

Figure 2.6 *– Energy flow and regenerative braking operation in a Battery Electric Vehicle [9].*

During deceleration, the BEV model prioritizes regenerative braking, allowing the electric motor to operate as a generator and convert kinetic energy back into electrical energy stored in the battery. Mechanical braking is applied only when regenerative capability is insufficient. This energy recovery mechanism is particularly important for urban driving conditions and significantly influences overall vehicle efficiency[9], [37].

2.1.2. Longitudinal Driver PI Speed-Tracking Controller

The Longitudinal Driver subsystem represents the virtual driver responsible for tracking a prescribed drive cycle by regulating vehicle speed through accelerator and brake commands. In this thesis, the driver is implemented using a Proportional–Integral (PI) controller, following the structure described in the MathWorks Longitudinal Driver block (Vehicle Dynamics Blockset) documentation. The objective of the controller is to minimize the speed tracking error between the reference velocity $v_{ref}(t)$and the measured vehicle velocity $v(t)$ [37].

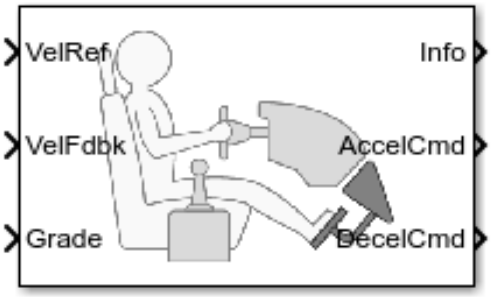

Figure 2.7 *– Longitudinal Driver PI control structure used for speed tracking in the BEV model*[37]

The control error is defined as:

$$e(t) = v_{ref}(t) - v(t)$$

The PI controller computes the control action:

$$u(t) = K_p e(t) + K_i \int_0^t e(\tau)\, d\tau$$

where $K_p$is the proportional gain and $K_i$is the integral gain. The proportional term ensures fast response to transient speed deviations, while the integral term eliminates steady-state tracking error caused by disturbances such as aerodynamic drag or road grade.

The controller output $u(t)$is mapped into accelerator and brake commands through saturation and logic separation. When $u(t) > 0$, the signal generates a throttle request for the electric powertrain; when $u(t) < 0$, it produces a brake command. This ensures that traction and braking forces are not simultaneously applied under normal operating conditions. Such signal conditioning is consistent with the block-level implementation

described in the MathWorks documentation [37].
The longitudinal driver interacts directly with the global vehicle dynamics equation:

$$m\frac{dv}{dt} = F_{drive} - F_{brake} - F_{resist}$$

where F_{drive} is generated by the electric motor in response to throttle input, F_{brake} corresponds to the commanded braking torque, and F_{resist} includes aerodynamic drag, rolling resistance, and road grade forces. Through this closed-loop interaction, the driver block provides dynamic coupling between the drive cycle input and the propulsion system response.
To ensure stable and realistic speed tracking, controller gains $K_p$and $K_i$are tuned to balance responsiveness and smoothness. Excessive proportional gain may introduce oscillations, while high integral gain can cause wind-up effects. Therefore, anti-windup protection and actuator saturation limits are implemented, as recommended in the MathWorks reference model guidelines [37].

2.1.3. Battery System and Electrical Energy Source Model

The battery system represents the primary energy source of the Battery Electric Vehicle (BEV) and plays a central role in determining vehicle range, performance, and operational constraints. In this work, the battery subsystem is implemented in MATLAB/Simulink using Powertrain Blockset, adopting a datasheet-based lithium-ion battery model. The model captures the interaction between electrical load, terminal voltage, temperature, and State of Charge (SOC), enabling realistic simulation of battery behavior under dynamic driving conditions. The selected modeling approach balances physical fidelity and computational efficiency, making it suitable for system-level BEV studies [37], [42].

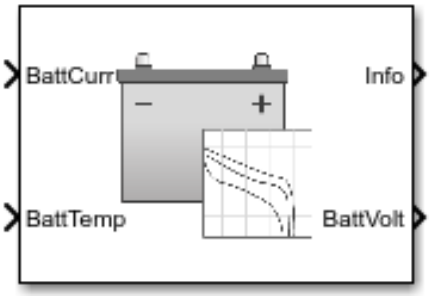

***Figure 2.8** – Datasheet-based lithium-ion battery model used in the BEV simulation framework [37].*

The battery subsystem is implemented using a datasheet battery block, which relies on manufacturer-provided characteristics such as open-circuit voltage curves, internal resistance, nominal capacity, and temperature dependency. Unlike purely equivalent-

circuit models, this formulation directly links electrical behavior to SOC and temperature through lookup tables. This allows the model to reproduce realistic voltage sag during high current demand and voltage recovery during low-load or regenerative operation, which are essential features for accurate BEV simulation [37], [42].

Integration with the BEV Energy Flow

In the overall BEV architecture, the battery block receives battery current demand from the electric motor and inverter subsystem and outputs the corresponding terminal voltage and SOC information. The electrical coupling ensures that the motor torque capability is implicitly limited by battery voltage and current constraints. This closed-loop interaction reflects real vehicle behavior, where propulsion performance is directly influenced by battery operating conditions. The battery model therefore acts not only as an energy source but also as a system-level constraint on vehicle dynamics[9], [37].

Electrical Behavior and Terminal Voltage Calculation

At each simulation step, battery terminal voltage is computed as the difference between open-circuit voltage and internal losses. In simplified form, the relationship can be expressed as:

$$V_{bat} = V_{OC}(SOC, T) - I_{bat} * R_{int}(SOC, T)$$

where $V_{OC}$is the SOC- and temperature-dependent open-circuit voltage, $I_{bat}$is the battery current, and R_{int}represents internal resistance. This formulation, embedded internally within the MathWorks battery block, enables accurate prediction of voltage drop under high load and voltage rise during regenerative charging[37], [42].

State of Charge Computation and Energy Tracking

The battery SOC is computed using Coulomb counting, which integrates the battery current over time relative to nominal capacity. In discrete form, SOC evolution can be expressed as:

$$SOC(k) = SOC(k-1) - \frac{I_{bat}(k)\Delta t}{Q_{nom}}$$

where $Q_{nom}$is the nominal battery capacity. Although this method is sensitive to current measurement accuracy, it remains the standard approach in simulation environments. The model provides SOC as an output signal, which is used by higher-level control logic and safety limits in the BEV system [37].

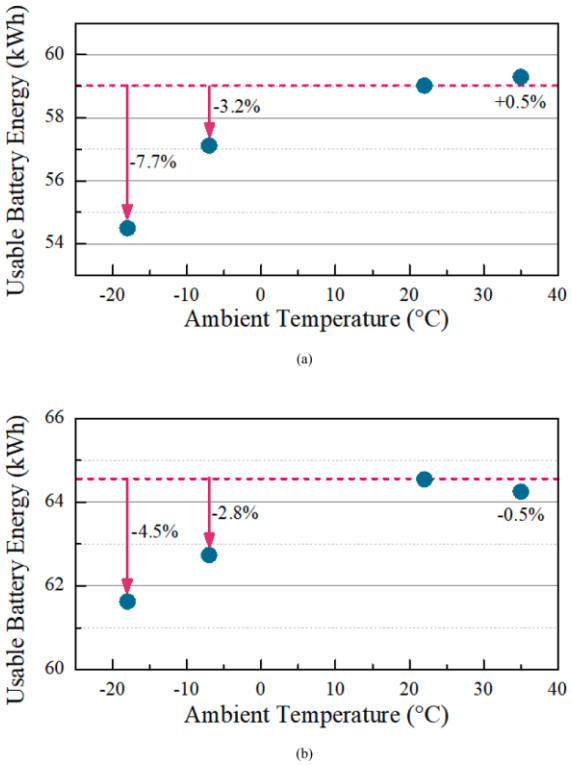

Figure 2.9 *– Usable battery energy of electric vehicles depending on ambient temperature [4].*

The battery model incorporates temperature as an explicit input, allowing internal resistance and voltage behavior to vary with thermal conditions. This feature is critical for BEV studies involving climatic effects, as low temperatures increase internal resistance and reduce available power, while high temperatures may accelerate degradation. In the present model, battery temperature is supplied as an external signal, enabling future extension toward coupled electro-thermal simulations[4], [37], [42].

In addition to its direct influence on electrochemical behavior, ambient temperature significantly affects auxiliary electrical loads, particularly the Heating, Ventilation, and Air Conditioning (HVAC) system, which represents a major non-traction energy consumer in Battery Electric Vehicles. To account for this effect at system level, an additional constant electrical load is introduced in the battery subsystem as a function of ambient temperature. This auxiliary load is superimposed on the traction power demand and directly increases battery current draw, thereby influencing State of Charge evolution and vehicle range.

The magnitude of the HVAC load is defined based on experimentally measured real-world data reported in large-scale studies, including the NREL EV Climate Loads Report (2018), the AAA EV Cold-Weather Study (2019), and INL AVTA mixed-route datasets. Different temperature bands are associated with representative low, mild, and high auxiliary load levels. The numerical values corresponding to these operating conditions

will be provided and discussed in detail in a dedicated subsection later in this work[43], [44], [45].

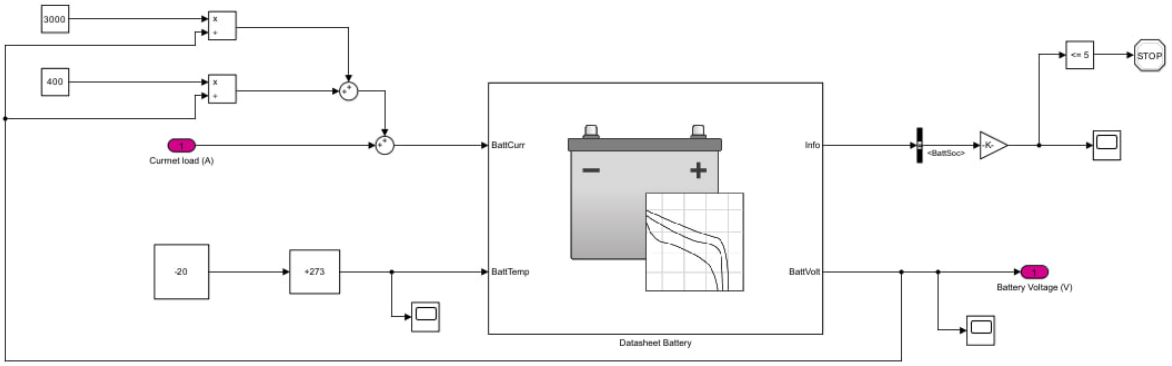

***Figure 2.10** – Battery subsystem implementation in MATLAB/Simulink with SOC and voltage monitoring.*

As shown in Figure 2.6, the battery subsystem includes monitoring logic for SOC and terminal voltage. Threshold blocks are used to detect low SOC or voltage conditions, which can be linked to simulation stop criteria or power limitation logic. This structure mirrors real battery management system (BMS) functions at a simplified level and ensures that the BEV model operates within physically realistic limits [37], [46].

Role of the Battery Model in BEV Performance Analysis

The implemented battery system provides the foundation for evaluating BEV range, energy consumption, and power availability under different driving cycles. Because voltage and SOC dynamically respond to current demand, the model naturally captures the coupling between vehicle dynamics and energy usage. This makes the battery subsystem suitable for further studies on range uncertainty, efficiency variation, and climate-dependent performance.

2.1.4. Electric Motor, Power Electronics, and Torque Generation Model

The electric motor and power electronics subsystem implemented in this study represents the traction unit responsible for converting electrical energy from the battery into mechanical torque at the wheels. The model is developed using a backward-facing, map-based approach, where driver demand and vehicle operating conditions determine motor torque and electrical power requirements. This modeling philosophy is widely adopted in propulsion system assessment studies, as it enables efficient evaluation of energy consumption and component loading over standardized driving cycles [9].

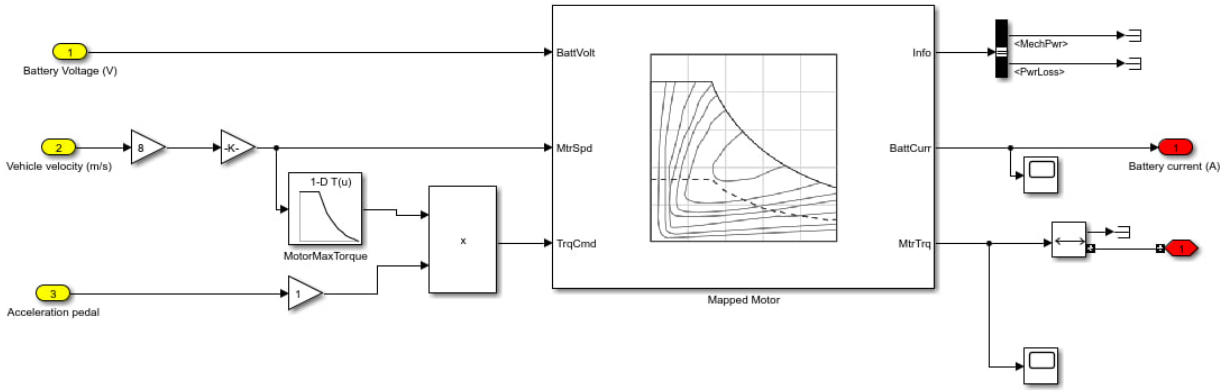

Figure 2.11.– *Electric motor and power electronics subsystem implemented in MATLAB/Simulink.*

As shown in Figure 2.X, the motor subsystem receives battery voltage, vehicle speed, and accelerator pedal position as its primary inputs. Vehicle speed is converted internally into motor angular speed through the drivetrain and wheel radius, while battery voltage defines the instantaneous electrical boundary conditions imposed by the energy storage system. The accelerator pedal position represents the driver's torque request and is normalized to provide a scalable command signal. This signal structure reflects the backward propagation of power demand from the wheels to the energy source, which is a standard approach in SAE-based propulsion modeling [9], [37]. Torque generation within the model is governed by a speed-dependent maximum torque map, which defines the physical capability of the electric motor at each operating speed. The driver-requested torque is obtained by scaling the maximum available torque with the accelerator pedal position, ensuring that the commanded torque remains within motor and inverter limits. This implementation allows the model to naturally capture torque saturation at high speeds due to voltage and power constraints, which is essential for realistic propulsion behavior. The torque command is expressed as:

$$T_{cmd} = \alpha T_{max}(\omega_m)$$

where α is the normalized pedal input and $T_{max}(\omega_m)$is the maximum motor torque as a function of motor angular speed ω_m[9], [37].

After torque determination, the motor block evaluates the mechanical output power and converts it into electrical power demand using a two-dimensional efficiency map representing combined motor and inverter losses. Mechanical power is computed as:

$$P_{mech} = T_m * \omega_m ana$$

and the required electrical input power is obtained from:

$$P_{elec} = \frac{P_{mech}}{\eta(\omega_m, T_m)}$$

where $\eta(\omega_m, T_m)$is the efficiency value interpolated from the map. This efficiency-based formulation enables accurate representation of power losses without explicitly modeling inverter switching dynamics, which is consistent with SAE-recommended system-level simulation practices [9], [47].

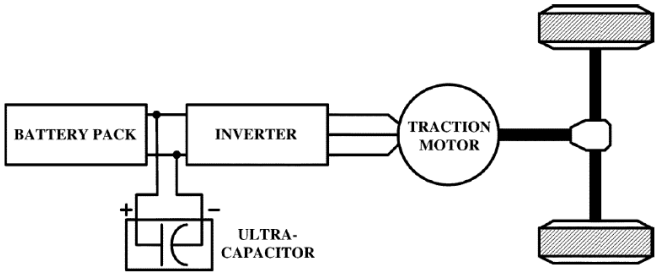

Figure 2.12 *– Typical electric vehicle drivetrain topology (battery–inverter–traction motor–wheels) [47].*

The electrical power demand calculated by the motor block is converted into battery current using the instantaneous battery voltage. This current output directly interfaces with the battery subsystem, ensuring consistent energy flow between the traction system and the energy source. This coupling is critical for evaluating battery loading, voltage drop, and overall energy consumption during dynamic driving conditions, as emphasized in SAE propulsion architecture comparisons[9], [37].

Table 2.1. – Functional Description of the Electric Motor and Power Electronics Model[37]

Model Function	Inputs	Outputs	Description
Driver Demand Processing	Pedal position	Torque request	Converts driver input into torque command
Torque Limitation	Motor speed	Max torque	Enforces motor capability limits
Efficiency Mapping	Torque, speed	Power losses	Models motor–inverter efficiency
Power Conversion	Battery voltage	Battery current	Couples traction demand to battery

2.1.5. Gearbox modeled as a single stage reducer with differential

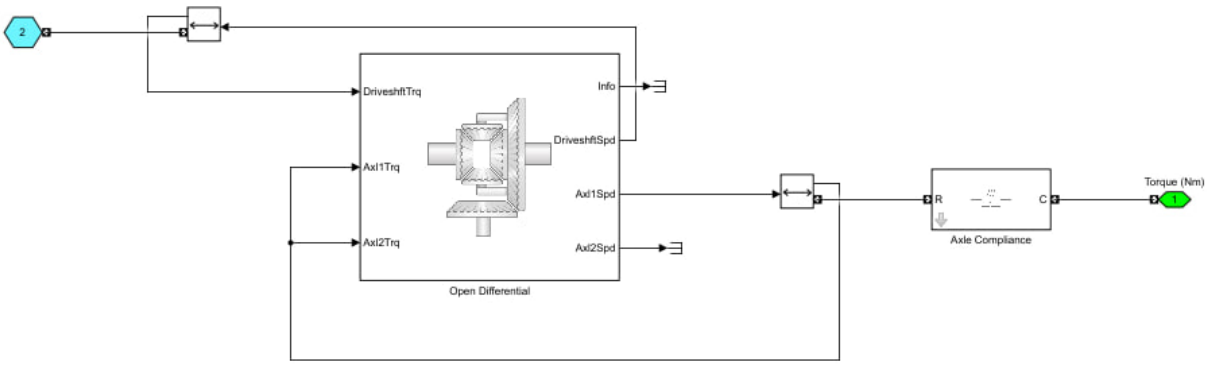

Figure 2.13 *– Simulink implementation of the drivetrain and open differential transmission subsystem, including axle compliance, used in the BEV model.*

The drivetrain and differential transmission subsystem represent the mechanical link between the electric traction motor and the driven wheels, converting motor torque into wheel torque while allowing speed differentiation between left and right wheels during cornering. In the present BEV model, this subsystem is implemented using an open differential architecture combined with axle compliance, following the modeling philosophy recommended in the MathWorks Driveline and Simscape Multibody libraries. This approach enables accurate representation of torque distribution, rotational inertia effects, and driveline flexibility under transient operating conditions[37]. As shown in Figure 2.13, the open differential block receives the input driveshaft torque from the upstream electric motor and splits it between the two output axle shafts. The differential enforces equal torque delivery to both wheels while allowing different rotational speeds, which is essential during vehicle cornering. In accordance with MathWorks' implementation, the differential is modeled using a torque-balance formulation rather than rigid kinematic constraints, allowing seamless integration with compliant drivetrain elements and numerical stability in dynamic simulations [37].

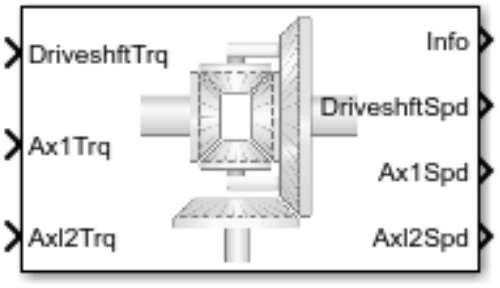

Figure 2.14 – Conceptual representation of open differential torque and speed distribution with compliant axle shafts [37]**.**

The governing torque relationship for an ideal open differential can be expressed as

$$T_L = T_R = \frac{T_{in}}{2}$$

where $T_{in}$is the input torque from the driveshaft, and T_L, $T_R$are the torques transmitted to the left and right axles, respectively. Simultaneously, the kinematic constraint on angular velocities is defined as

$$\omega_{in} = \frac{\omega_L + \omega_R}{2}$$

ensuring conservation of power while allowing wheel speed differentiation. These equations are internally handled by the Simulink differential block and form the basis for power-split behavior under all driving conditions [37].

To capture real drivetrain behavior beyond ideal rigid transmission, an axle compliance block is introduced downstream of the differential. This element models the torsional elasticity and damping of the axle shafts, which are known to significantly influence driveline oscillations, torque ripple transmission, and NVH behavior. The compliant axle is represented using a linear torsional spring-damper formulation, where the transmitted torque is given by

$$T_{axle} = k_\theta(\theta_{in} - \theta_{out}) + c_\theta\left(\dot{\theta}_{in} - \dot{\theta}_{out}\right)$$

with $k_\theta$denoting torsional stiffness and $c_\theta$the damping coefficient. Such representation follows standard drivetrain modeling practice in both MathWorks documentation and automotive literature [37], [48].

Including axle compliance is particularly important for BEV applications, as electric motors can generate high torque gradients during rapid acceleration and regenerative braking. Without compliance, these transients would unrealistically propagate instantaneously to the wheels. The adopted compliant model allows torque oscillations and phase delays to emerge naturally, improving fidelity in traction, ride comfort, and durability analyses [9].

Furthermore, the selected open differential configuration reflects a common and robust solution for single-motor BEVs targeting efficiency and simplicity. While torque-vectoring differentials can enhance handling, the open differential remains suitable for range and energy-focused studies, particularly when combined with accurate tire and vehicle dynamics models. This modeling choice aligns with the scope of the present work, which prioritizes energy consumption, thermal effects, and climate-dependent range assessment rather than advanced handling control [9], [37].

The electric motor and power electronics subsystem implemented in this study represents

the traction unit responsible for converting electrical energy from the battery into mechanical torque at the wheels. The model is developed using a backward-facing, map-based approach, where driver demand and vehicle operating conditions determine motor torque and electrical power requirements. This modeling philosophy is widely adopted in propulsion system assessment studies, as it enables efficient evaluation of energy consumption and component loading over standardized driving cycles [46].

2.1.6. Vehicle Body, Longitudinal Wheel, and Brake Dynamics

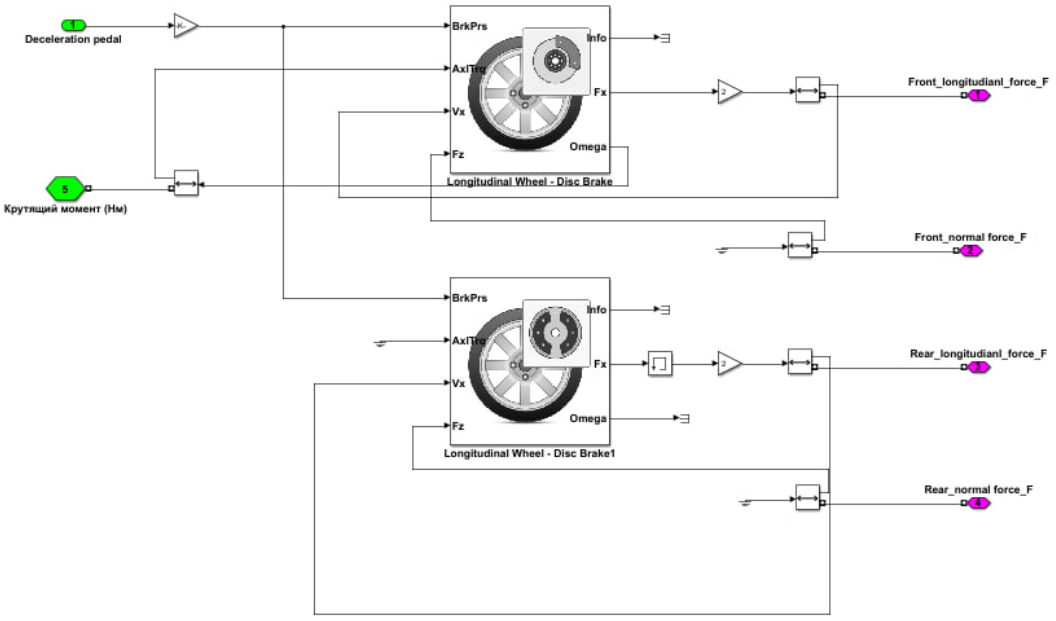

Figure 2.15 *– Simulink implementation of the Vehicle Body, Longitudinal Wheel, and Disc Brake subsystems used in this study.*

The longitudinal dynamics of the vehicle are modeled using a modular structure based on Simscape Driveline, integrating the Vehicle Body, Longitudinal Wheel, and Disc Brake subsystems. This structure follows the modeling philosophy recommended by MathWorks, where each physical component is represented by a dedicated block with clearly defined mechanical interfaces. Such an approach enables transparent force transmission from braking actuation to vehicle deceleration and ensures numerical robustness under transient and low-speed conditions [37].

The Vehicle Body block represents the lumped longitudinal motion of the vehicle mass and forms the inertial core of the model. It accounts for vehicle mass, road grade, aerodynamic drag, and externally applied longitudinal forces. The block receives the summed longitudinal tire forces generated at the wheels and computes the resulting vehicle acceleration and velocity. The governing longitudinal equation implemented

internally by the block can be expressed as:

$$m\dot{v}_x = \sum F_x - F_{drag} - mgsin(\alpha)$$

where $m$is vehicle mass, $F_x$represents the tire longitudinal forces, and $\alpha$is the road grade angle [37]. [37]

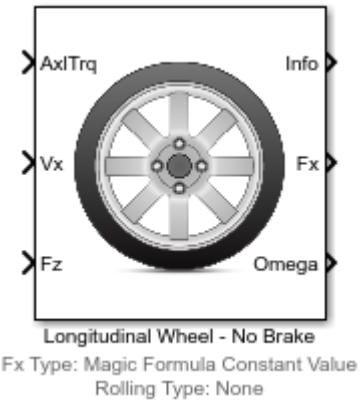

Figure 2.16 – Longitudinal Wheel and Disc Brake blocks showing slip-based force generation and braking torque application [37].

The Longitudinal Wheel block models the rotational dynamics of each wheel and the interaction between the tire and the road surface. It computes longitudinal tire force based on wheel angular speed, vehicle velocity, normal load, and slip ratio. During braking, slip is defined in a numerically stable form as:

$$s = \frac{\omega R - v_x}{|v_x|}$$

where ω is wheel angular speed, $R$is the effective rolling radius, and $v_x$is vehicle longitudinal velocity. This formulation avoids singularities as wheel speed approaches zero and is particularly suitable for low-speed braking simulations [37], [49].

The Disc Brake subsystem converts the brake pedal input into a mechanical braking torque applied to the wheel. In the implemented model, brake pressure is mapped to a normal clamping force acting on the brake pads, generating a friction torque opposing wheel rotation. The braking torque can be expressed as:

$$T_b = \mu_b F_n R_m$$

where μ_b is the brake friction coefficient, F_n is the pad normal force, and R_m is the mean effective brake radius. This formulation is consistent with both Simscape brake blocks and standard disc brake theory.

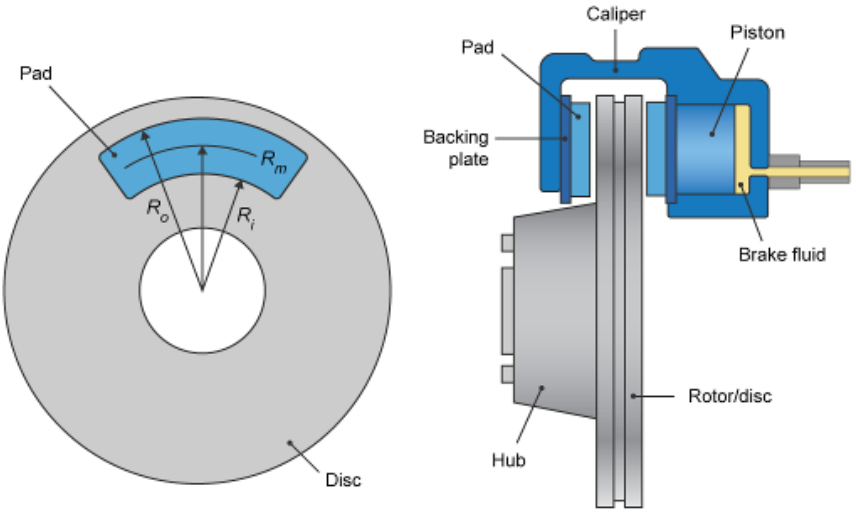

Figure 2.17 *– Schematic representation of disc brake force and torque generation[37].*

A key advantage of the adopted modeling approach is the continuous coupling between brake torque, wheel dynamics, and tire force generation. As braking torque increases, wheel angular speed decreases, leading to higher slip ratios and increased longitudinal tire forces until friction saturation is reached. This interaction naturally reproduces realistic braking behavior without relying on discontinuous friction switching, which is known to cause numerical oscillations near zero speed [37], [49].

At very low speeds, the interaction between disc brake friction and tire–road friction becomes critical for accurately capturing deceleration smoothness and potential jerk phenomena. The Simscape-based formulation ensures that braking forces remain physically consistent even when wheel speed approaches zero, enabling reliable analysis of comfort-related metrics and control strategies. This capability is essential for BEV studies, where regenerative and friction braking interactions are strongly speed dependent [37], [49].

2.1.7. Model Coupling, Signal Interfaces, and Output Consistency

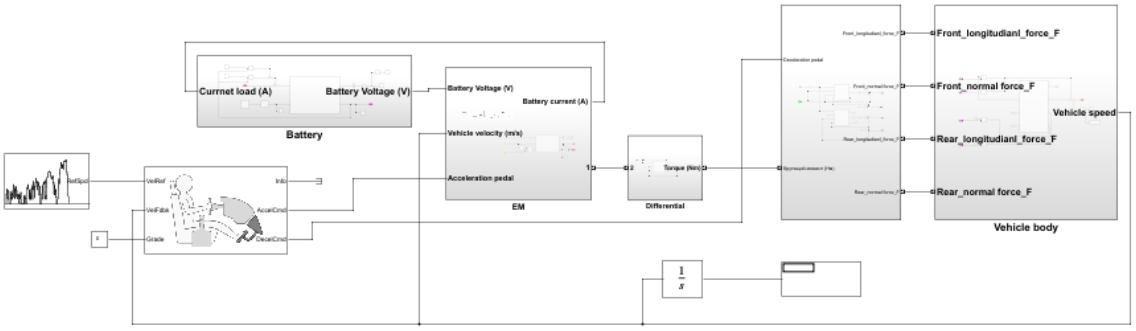

Figure 2.18 *– Overall, MATLAB/Simulink BEV model architecture and signal coupling*

.

The Battery Electric Vehicle (BEV) model is implemented in MATLAB/Simulink using a modular subsystem structure consistent with the component-based description introduced in Sections 2.1.1–2.1.5. Each main element of the propulsion system—Driving Cycle, Longitudinal Driver, Battery System (Electrical Energy Source), Electric Machine (EM) with Inverter, Drivetrain and Differential, and Vehicle Body—is modeled as an independent block with clearly defined input and output signals. This architecture enables clear separation of physical domains while maintaining a coherent system-level representation of BEV longitudinal behavior[37].

Model coupling follows a closed-loop longitudinal control structure. The Driving Cycle block provides a reference vehicle speed, which is compared with the actual vehicle speed in the Longitudinal Driver model. Based on this error, the driver generates accelerator and brake commands that are converted into a traction torque request for the Electric Machine. The produced electromagnetic torque is transmitted through the Drivetrain and Differential to the Vehicle Body, while the resulting vehicle speed is fed back to the driver. This feedback mechanism ensures consistency between demanded and achieved vehicle motion under transient driving conditions[37].

The Battery System supplies electrical power to the inverter–electric machine assembly through current and voltage signals. Battery state evolution is calculated internally using the Coulomb counting approach, commonly adopted in BEV system studies:

$$SOC(t) = SOC(0) - \frac{1}{C_n}\int_0^t I(\tau)\,d\tau$$

where $C_n$is the nominal battery capacity and $I(t)$is the battery current. The battery terminal voltage is evaluated using an equivalent circuit formulation, ensuring consistency with the battery modeling approach introduced earlier in Section 2.1.2 [37], [42].

The Electric Machine converts electrical input power into mechanical torque according to the power balance relationship:

$$T_{EM} = \eta_{EM} \frac{P_c}{\omega_{EM}}$$

where $P_e$is the electrical power supplied by the Battery System, $\omega_{EM}$is the machine rotational speed, and η_{EM}represents the combined efficiency of the inverter and motor. This formulation ensures direct consistency between electrical energy consumption and mechanical traction generation[37].

Output consistency across the full BEV model is ensured by synchronized solver settings, unit coherence, and continuous feedback between subsystems. Battery power demand, electric machine torque, drivetrain transmission, and vehicle longitudinal dynamics remain mutually consistent throughout the simulation, avoiding artificial energy losses and numerical imbalance. This modeling approach follows MathWorks best practices for multi-domain physical system simulation and supports reliable BEV performance analysis[37].

2.1.8. Regenerative Braking Modeling

Regenerative braking is a fundamental energy recovery mechanism in battery electric vehicles (BEVs), enabling the conversion of vehicle kinetic energy into electrical energy during deceleration. In contrast to conventional friction braking systems—where kinetic energy is dissipated as heat—regenerative braking allows the traction motor to operate in generator mode, thereby improving overall vehicle efficiency and extending driving range.

In the MATLAB/Simulink environment, regenerative braking is implemented within the Electric Vehicle Reference Application of the Powertrain Blockset. During deceleration, the supervisory control system issues a negative torque request to the traction motor. When the commanded torque satisfies

$$T_{cmd} < 0,$$

the electric machine transitions from motoring to generating mode, enabling kinetic energy recovery and controlled energy flow from the drivetrain to the battery [37].

In this operating condition, the mechanical power at the motor shaft is expressed as:

$$P_{mech} = T_m \cdot \omega_m$$

where $T_m$is the motor torque and $\omega_m$is the motor angular velocity. For regenerative

operation ($T_m < 0$, $\omega_m > 0$), the mechanical power becomes negative, indicating energy flow from the wheels to the motor. The generated electrical power is then:

$$P_{elec} = \eta_m \, T_m \omega_m$$

and the power transferred to the battery is:

$$P_{battery} = \eta_{inv} \eta_m T_m \omega_m$$

where $\eta_m$and η_{inv}represent motor and inverter efficiencies, respectively .

Within the MATLAB reference architecture, regenerative braking torque is limited by both motor capability and battery charging constraints. The maximum regenerative torque is computed as:

$$T_{regen,max} = \min \left(T_{motor,limit}, \frac{V_{OCV} - V_{min}}{R_{int}} \cdot \frac{1}{\omega_m} \right)$$

where $V_{OCV}$is the open-circuit voltage and $R_{int}$is the battery internal resistance. This formulation ensures that the charging current does not exceed safe operational limits, particularly at high state-of-charge (SOC) or low battery temperature [9].

At low vehicle speeds, regenerative braking effectiveness decreases because the induced back electromotive force (EMF),

$$E = k_e \omega_m,$$

is proportional to motor speed. As $\omega_m \to 0$, the generated voltage and recoverable power diminish. Therefore, a brake blending strategy is implemented in the reference model, whereby friction brakes supplement regenerative torque to maintain the required deceleration while maximizing energy recovery[5].

The MATLAB laboratory framework thus provides a physics-based and control-oriented representation of regenerative braking, incorporating electromechanical energy conversion, inverter dynamics, and battery charge limitations. This modeling approach ensures accurate simulation of energy recovery behavior under varying speed, temperature, and SOC conditions, which is essential for range prediction and thermal analysis[11].

2.2. Vehicle Modeling Framework and Input Parameters

2.2.1. Reference Vehicle Selection and Specifications

The vehicles selected for this research represent three distinct technological generations in electric-vehicle (EV) development and are chosen to serve complementary analytical roles. The selection criteria include: (i) the availability of validated experimental data covering a wide ambient temperature range, (ii) relevance to Uzbekistan's market characteristics and continental climate, and (iii) sufficient diversity in battery capacity, thermal-management architecture, and overall drivetrain efficiency. Accordingly, the Nissan Leaf 24 kWh, Chevrolet Bolt EV 60 kWh, and Volkswagen e-Golf 2017, 35.8 kWh together form a comprehensive comparative basis for evaluating temperature-dependent performance and energy consumption behavior [44], [45].

Nissan Leaf (24 kWh)
The first-generation Nissan Leaf, produced between 2011 and 2013, represents early-stage EV technology employing a lithium-manganese-oxide (LMO) battery without active liquid cooling. Its battery pack consists of 48 modules (192 cells), rated at 360 V and 66 Ah nominal capacity. The vehicle's mass of 1 520 kg and 80 kW permanent-magnet synchronous motor yield an efficiency of approximately 6.2 km / kWh under moderate temperatures. Due to the absence of thermal regulation, its performance strongly depends on ambient temperature, with up to 30 % range loss observed below –10 °C and 10 % loss above 35 °C. This makes it a suitable reference for assessing the direct climatic impact on non-cooled battery systems [43].

Chevrolet Bolt EV (60 kWh)
The Chevrolet Bolt, launched in 2017, embodies the second generation of high-efficiency EVs with active liquid thermal management. It utilizes a 60-kWh lithium-ion pack (288 cells in 96 modules, 350 V nominal voltage) with a 150-kW drive motor and total vehicle mass of 1 625 kg. According to NREL AVTA Report DOE/AVTA-2019-T-02, the Bolt maintains > 90 % of its rated range at 0 °C and > 80 % at –10 °C, confirming the effectiveness of its closed-loop coolant circuit. Its combined WLTP energy consumption of 16.9 kWh / 100 km under mild conditions provides an intermediate benchmark between conventional and premium architectures, making it ideal for evaluating temperature-compensated range stability in Uzbekistan's mid-continental climate [44].

Volkswagen e-Golf 2017, DC Fast-Charging Version (35.8 kWh)

The 2017 Volkswagen e-Golf represents a mature European compact BEV platform developed on the conventional Golf architecture and equipped with active battery temperature management. The updated 2017 model features a 35.8 kWh nominal lithium-ion battery pack, with approximately 32–33 kWh usable energy, and a nominal system voltage of approximately 323 V.

The vehicle is driven by a 100 kW front-mounted electric motor and has a curb weight of approximately 1 567 kg. Compared with the first-generation Leaf, the e-Golf integrates an actively controlled thermal system that improves stability during both cold starts and high-temperature operation. Regulatory and independent benchmarking data indicate moderate seasonal variation in range, smaller than that observed in passively cooled systems but still noticeable under extreme temperatures [44].

Together, these three vehicles establish a representative cross-section of EV technologies—from passively cooled early designs to actively managed modern systems—allowing systematic evaluation of temperature influence on range, battery degradation, and operating cost under the climatic spectrum characteristic of Uzbekistan

Comparative Framework

Collectively, the selected vehicles cover a structured battery capacity spectrum:

- 24 kWh class (Leaf) – passive thermal management
- 35.8 kWh class (e-Golf) – active thermal management, compact platform
- 60 kWh class (Bolt EV) – high-capacity liquid-cooled architecture

This distribution enables systematic assessment of how battery size, usable energy fraction, and thermal-management design influence temperature-dependent driving range, degradation behavior, and operating cost under climatic conditions characteristic of Uzbekistan. By integrating OEM specifications with independently validated testing data, the vehicle selection ensures methodological robustness and reproducibility for subsequent modeling and simulation stages [43], [44].

2.2.2. Battery, Motor, and Drivetrain Parameters

The battery, electric motor, and drivetrain subsystems were parameterized using a two-level data strategy, combining certified vehicle-level testing data with component-level benchmarking and simulation-oriented sources. This approach ensures both physical consistency and traceability while addressing the limited availability of detailed component data in OEM technical brochures. Vehicle-level parameters such as mass, certified energy consumption, and range were obtained from standardized certification and testing programs and are primarily used for model validation, whereas component-level parameters required by the simulation

blocks were populated using benchmarking reports and simulation documentation specifically developed for powertrain modeling [50].

Battery subsystem parameterization

The battery model is implemented using the Datasheet Battery block, which represents lithium-ion battery behavior through lookup tables describing open-circuit voltage and internal resistance as functions of state of charge and temperature. This structure is consistent with system-level BEV modeling practice, where the objective is not cell-level electrochemical identification but the accurate reproduction of pack-level voltage response, power limitations, and thermal sensitivity. Rated battery capacity at nominal temperature, initial capacity, and the number of cells in series and parallel define the equivalent pack architecture, while OCV–SOC and resistance–SOC–temperature maps reproduce the observed voltage sag and efficiency degradation under cold and high-load conditions. Since such maps are not publicly released by OEMs, equivalent electrical representations are adopted, following recommended modeling practices in MATLAB/Simulink-based BEV simulations [37].

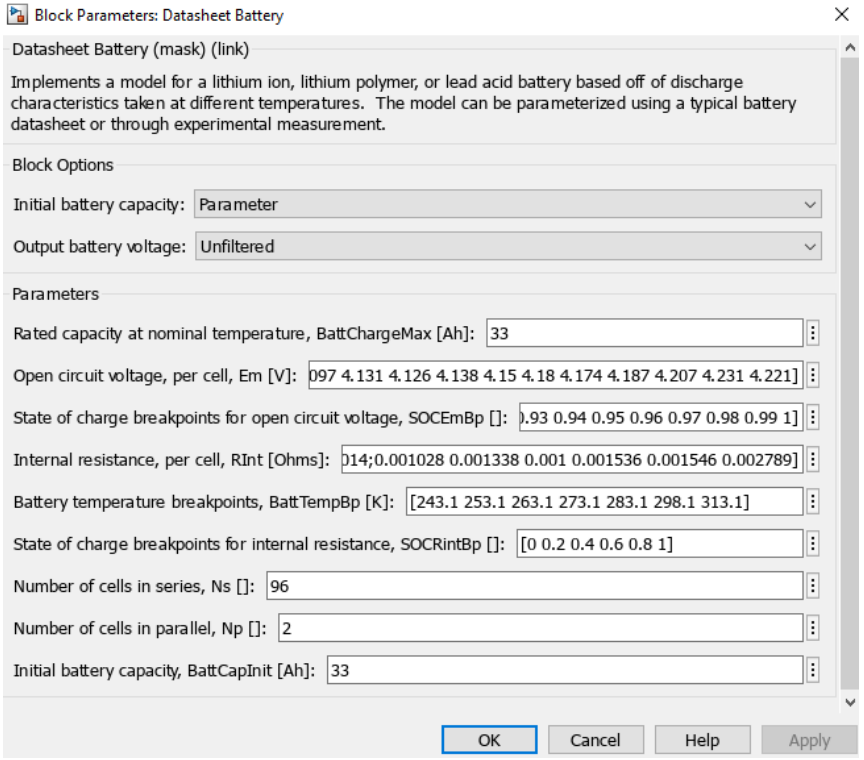

Figure 2.19 *– Battery block parameterization showing OCV–SOC and internal resistance lookup tables [37].*

Electric motor and inverter modeling

The traction system is modeled using a Mapped Motor representation, defined by a torque–speed envelope and a torque control time constant. This formulation

preserves the correct traction limits and power capability while maintaining low computational complexity, making it suitable for range and energy consumption studies. Maximum torque values are defined over a set of speed breakpoints, capturing the constant-torque and constant-power regions of the electric drive. A fixed response time constant is introduced to represent inverter and control dynamics at system level. Where detailed efficiency maps are unavailable, the motor efficiency and loss representation is calibrated to ensure agreement with certified energy consumption during drive-cycle simulations [37].

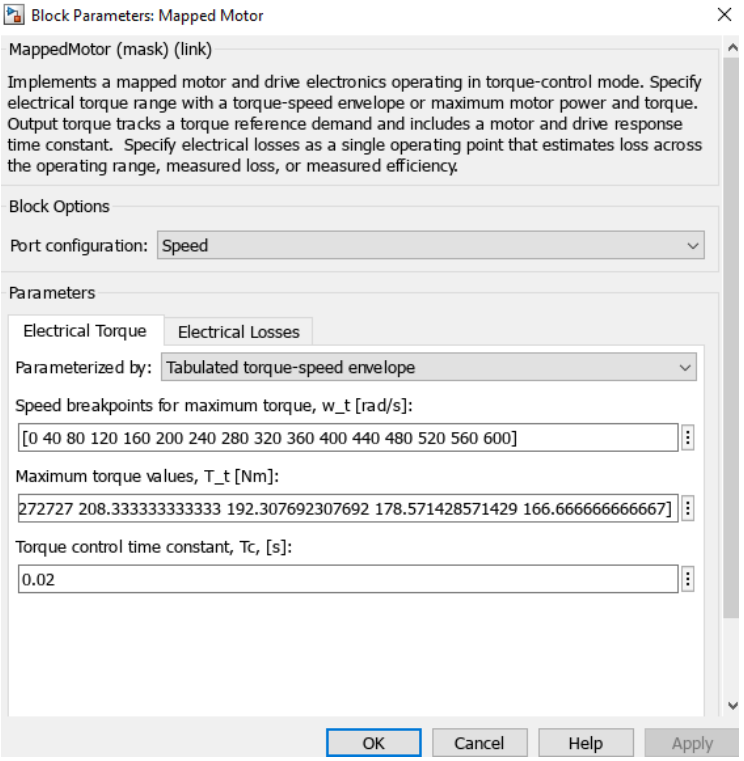

Figure 2.20 *– Electric motor torque–speed envelope and control parameters in the Mapped Motor block [37].*

Drivetrain and differential representation

The mechanical power transfer between the electric motor and the driven wheels is represented using an Open Differential block. The final drive ratio is defined as a vehicle-specific parameter when available from benchmarking sources, while carrier inertia, axle inertias, and viscous damping coefficients are introduced to capture driveline dynamics and ensure numerical stability. As these parameters are rarely disclosed in open literature, they are treated as calibration parameters, adjusted within physically realistic ranges to avoid non-physical oscillations and to reproduce smooth torque transmission during transient operation. This approach is consistent with established vehicle system modeling methodologies [51].

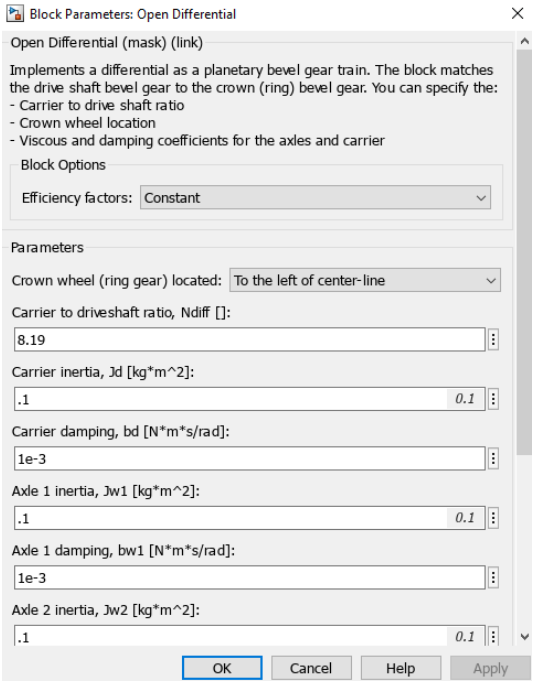

Figure 2.21 *– Differential and driveline parameterization including final drive ratio and inertial elements* ***[37].***

Table 2.2 – Summary of Battery, Motor, and Drivetrain Parameters Used in the Simulation [50], [51]

Parameter	Simulink name	Nissan Leaf 24 kWh	Chevrolet Bolt EV 60 kWh	Volkswagen e-Golf 2017
Battery capacity [Ah]	**BattChargeMax**	**66.2 Ah**	**174.4 Ah**	**110.2 Ah**
Cells in series	**Ns**	**96**	**96**	**88**
Cells in parallel	**Np**	**2**	**1**	**1**
Max motor torque [Nm]	**T_t,max**	**280**	**360**	**290**
Torque time constant [s]	**Tc**	**0.02**	**0.02–0.03**	**0.02–0.03**
Final drive ratio [-]	**Ndiff**	**8.19**	**7.05**	**9.747**
Driveline inertias	**Jd, Jw**	**Jd=0.015, Jw=0.040**	**Jd=0.015, Jw=0.040**	**Jd=0.010, Jw=0.020**
Driveline damping	**bd, bw**	**bd=1.5e-3, bw=2.0e-3**	**bd=1.5e-3, bw=2.0e-3**	**bd=1.0e-3, bw=1.5e-3**

Model validation linkage

To ensure consistency between component-level parameterization and vehicle-level behavior, the complete model is validated against certified energy consumption and range data from standardized testing programs. Parameters obtained from certification datasets define acceptance targets, while equivalent electrical and mechanical parameters are tuned only when deviations exceed reasonable uncertainty margins. This guarantees that calibration does not compensate for modeling errors but instead reflects unavoidable data unavailability in public sources [51].

2.2.3. Vehicle Mass, Aerodynamics, and Road Load Data

Vehicle mass, aerodynamic characteristics, and road load parameters play a dominant role in determining the longitudinal energy demand of battery electric vehicles and therefore directly affect predicted range and efficiency. In this study, these parameters were selected using standardized certification and testing datasets to ensure traceability and reproducibility, while their implementation in the simulation model follows established longitudinal vehicle dynamics formulations. The objective is to reproduce realistic traction force requirements over standard drive cycles and under varying environmental conditions, rather than to identify proprietary OEM design details [50].

Vehicle mass and geometric distribution

Vehicle mass is introduced as a fixed parameter in the longitudinal vehicle body model and represents the curb mass under standard test conditions. This value directly influences inertial forces during acceleration and deceleration, as well as rolling resistance and grade effects. The longitudinal position of the center of gravity relative to the front and rear axles is defined through geometric distances a and b, while the center-of-gravity height determines load transfer during traction and braking. These geometric parameters are required to correctly distribute normal forces between axles, which in turn affects tire longitudinal force generation and brake force allocation. When detailed OEM geometry data are unavailable, representative values consistent with vehicle class and layout are adopted and maintained constant across simulations to isolate the influence of climatic and operational variables [37].

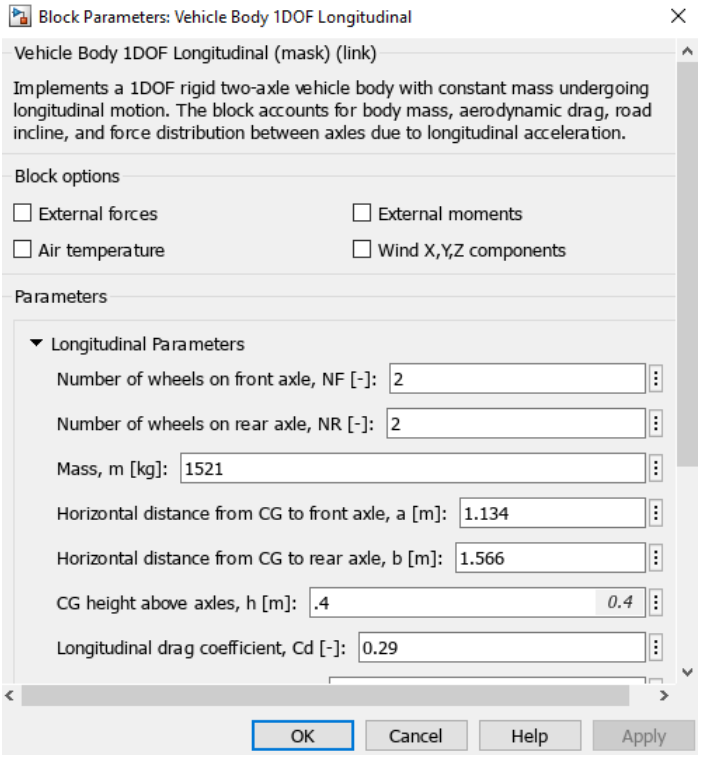

Figure 2.22 *– Vehicle body longitudinal parameterization including mass and center-of-gravity geometry [37].*

Aerodynamic characteristics

Aerodynamic drag is modeled using the conventional quadratic formulation, where the drag force is proportional to the air density, frontal area, drag coefficient, and the square of vehicle speed. In the present model, the drag coefficient (Cd) is introduced as an effective parameter that captures the combined influence of body shape, underbody flow, and auxiliary aerodynamic features. While frontal area values are not explicitly required by the selected vehicle body block, the adopted drag coefficient is consistent with certified aerodynamic performance reported in open datasets. Aerodynamic drag becomes the dominant resistance component at medium-to-high speeds and therefore has a strong influence on highway energy consumption and long-range capability, which is particularly relevant for the Volkswagen e-Golf 2017 configuration [50].

Road load and resistance modeling

The total longitudinal resistance acting on the vehicle is represented through rolling resistance, aerodynamic drag, and inertial forces. Rolling resistance effects are implicitly included through effective resistance terms and validated against

standardized coast down-derived road load data. Certified road load coefficients obtained from regulatory testing programs represent the combined effect of rolling resistance, drivetrain drag, and residual aerodynamic losses. In the simulation framework, these coefficients are not directly imposed but are instead used as validation references, ensuring that the modeled vehicle reproduces realistic traction force demand over standardized cycles. This methodology avoids overfitting while preserving physical interpretability of individual resistance components [51].

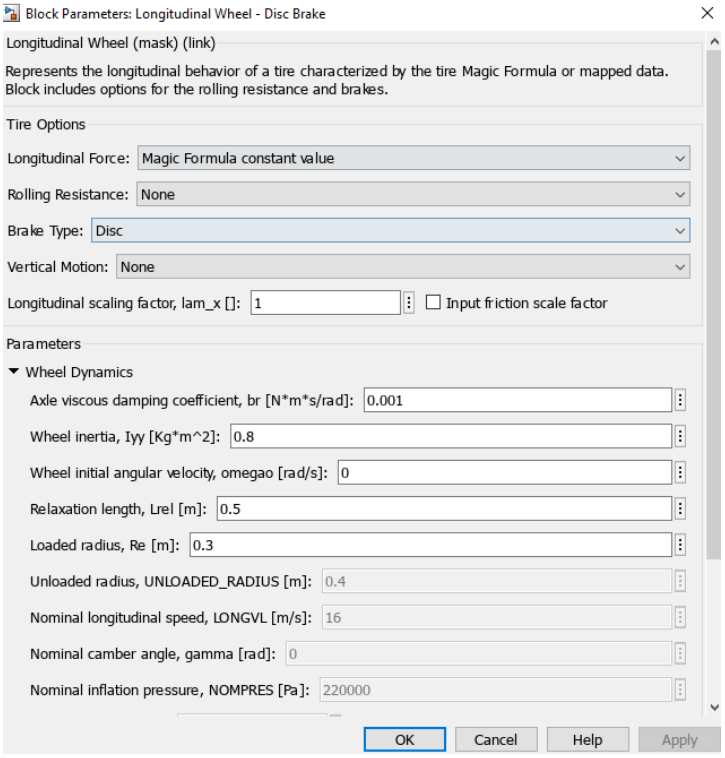

Figure 2.23 *– Longitudinal resistance and road load implementation within the vehicle dynamics subsystem [37].*

Implementation consistency across vehicles

For all three reference vehicles—the Nissan Leaf 24 kWh, Chevrolet Bolt EV 60 kWh, and Volkswagen e-Golf 2017—the same modeling structure is retained to ensure comparability. Differences in simulated energy consumption therefore arise solely from variations in vehicle mass, aerodynamic drag, and drivetrain efficiency, rather than from changes in model structure. This consistent formulation is essential for isolating the influence of climatic conditions and auxiliary loads in later sections of the study.

Table 2.3 – Summary of Vehicle Mass, Aerodynamics, and Road Load Data Parameters Used in the Simulation [50], [51]

Parameter	Simulink name	Nissan Leaf 24 kWh	Chevrolet Bolt EV 60 kWh	Volkswagen e-Golf 2017	Source	Notes
Vehicle mass [kg]	m	1521	1616	1567	EPA	Certified curb mass
Front wheels	NF	2	2	2	Model definition	Fixed
Rear wheels	NR	2	2	2	Model definition	Fixed
CG to front axle [m]	a	1.14	1.17	1.05	Representative	Geometry assumption
CG to rear axle [m]	b	1.54	1.43	1.58	Representative	Geometry assumption
CG height [m]	h	0.55	0.53	0.52	Representative	Load transfer
Drag coefficient [-]	Cd	0.28	0.308	0.27	EPA / benchmarks	Effective value
Frontal area [m²]	Af	2.27	2.39	2.27	Not explicit	Included in Cd
Air density [kg/m³]	rho	1.225	1.225	1.225	Standard	Sea-level reference

2.2.4. Data Sources, Assumptions, and Uncertainty

The modeling framework developed in this study relies exclusively on publicly accessible and independently verifiable data sources, combined with clearly stated assumptions, to ensure transparency and reproducibility. Vehicle-level inputs such as mass, certified energy consumption, and driving range are obtained from standardized certification and testing programs, which provide harmonized reference values across different manufacturers and vehicle classes. These data are

used primarily as validation targets, ensuring that the simulation outputs reproduce realistic vehicle behavior under regulated driving conditions rather than reflecting idealized or proprietary specifications[50].

Component-level parameters required by the battery, motor, and drivetrain subsystems—such as battery electrical maps, motor torque–speed envelopes, and drivetrain ratios—are derived from benchmarking-oriented datasets and simulation documentation specifically developed for powertrain analysis. Such sources provide internally consistent parameter sets suitable for system-level modeling, even when detailed OEM component data are not publicly disclosed. This approach is widely adopted in academic BEV studies and ensures that the model structure remains physically meaningful while avoiding unsupported assumptions regarding internal design details [37].

Several parameters relevant to longitudinal vehicle dynamics are not available in open-source documentation, including driveline inertias, damping coefficients, brake friction characteristics, and tire longitudinal coefficients. These quantities are therefore treated as assumed or calibrated parameters, selected within physically reasonable ranges reported in the literature. Calibration is applied conservatively and is limited to ensuring numerical stability and realistic transient response, without altering the fundamental energy balance of the vehicle. Importantly, calibration is not used to compensate for deficiencies in model structure or missing physics [37].

Uncertainty in the simulation results arises primarily from three sources: (i) variability between certified test conditions and real-world vehicle operation, (ii) simplifications inherent in equivalent representations of battery and motor behavior, and (iii) environmental influences such as temperature and air density. To mitigate these effects, a consistent modeling structure and unified assumptions are applied across all reference vehicles. As a result, the analysis emphasizes relative comparisons and trends, which are less sensitive to absolute parameter uncertainty and are well suited for assessing climatic and operational impacts on BEV performance [50].

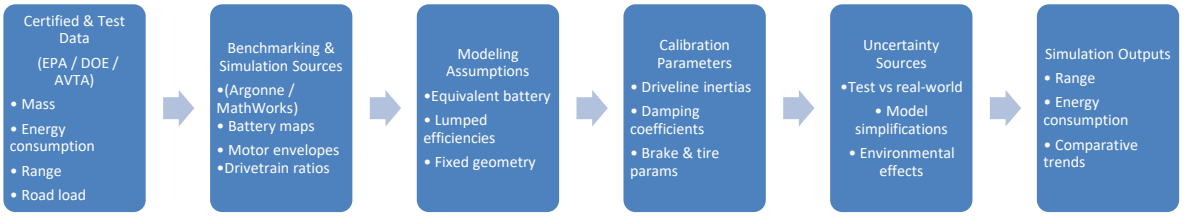

Figure 2.24 *– Overview of data sources, modeling assumptions, and uncertainty propagation within the vehicle simulation framework.*

2.3. Experimental Data and Temperature Range Collection (–5 °C to 35 °C)

2.3.1. Experimental and Literature-Based Data Sources

The experimental foundation of this study is based on publicly available datasets from recognized vehicle-testing institutions. For the Nissan Leaf 24 kWh, temperature-dependent energy consumption and HVAC power demand were obtained directly from the Idaho National Laboratory (INL) Advanced Vehicle Testing Activity (AVTA), which provides instrumented mixed-route measurements with climate control enabled (AUTO, 22 °C setpoint). Cold-temperature HVAC demand was therefore derived directly from INL measurements, where total energy consumption inherently includes resistive heating loads [43].

For hot-temperature conditions (95 °F / 35 °C), HVAC demand was evaluated using results from the American Automobile Association (AAA) Electric Vehicle Range Testing Report (2019), which reports full-range measurements under active air-conditioning. Although AAA does not provide a continuous HVAC map across intermediate temperatures, the hot-weather anchor point enables calibration of cooling demand at elevated ambient temperatures[44].

A continuous HVAC consumption map across –5 °C to +40 °C was constructed using experimentally validated anchor points from INL (cold regime) and AAA (hot regime), preserving measured system-level behavior. For the Chevrolet Bolt EV and Volkswagen e-Golf, detailed multi-temperature HVAC datasets are not publicly available. Therefore, the Leaf-derived HVAC map was applied, justified by comparable vehicle class, battery capacity range, and standardized mixed-cycle testing conditions. This approach ensures methodological consistency while remaining anchored to experimentally reported data and supported by climate-load characterization studies from NREL [43], [44].

2.3.2. Temperature-Dependent Energy Consumption, HVAC, and Auxiliary Power Demand

Ambient temperature is one of the dominant external variables influencing battery-electric vehicle (BEV) energy consumption and usable driving range. Temperature affects both the electrochemical behavior of the battery—through internal resistance, reaction kinetics, and open-circuit voltage—and the magnitude of non-traction energy demand, primarily associated with heating, ventilation, and air-conditioning (HVAC) systems and auxiliary components. Unlike internal-combustion vehicles,

BEVs must supply all cabin heating and cooling electrically, making HVAC demand a first-order contributor to total energy consumption under non-mild ambient conditions. For this reason, realistic BEV performance assessment must rely on experimentally measured system-level data in which traction energy, HVAC operation, and auxiliary loads are inherently coupled [45].
This section intentionally restricts itself to experimentally reported data only, derived from recognized testing institutions such as the Idaho National Laboratory (INL), American Automobile Association (AAA), U.S. Department of Energy (DOE), and independent European test programs (NAF / Motor). No interpolation, regression, or synthetic temperature points are introduced at this stage. The purpose of this section is to establish a validated experimental envelope against which the simulation model developed in later sections will be compared [44], [50].

Nissan Leaf 24 kWh

The 2015 Nissan Leaf 24 kWh is selected as the primary reference vehicle because it is one of the very few BEVs for which multi-temperature, controlled, real-world range tests with documented HVAC conditions are publicly available. According to the INL Advanced Vehicle Testing Activity (AVTA, INL-EXT-15-35584), the vehicle has a usable battery energy of approximately 19.5 kWh and was tested on the Idaho Falls mixed route, which combines urban, rural, and highway driving with an average speed of approximately 48 km h^{-1}. All INL tests were conducted with climate control enabled (AUTO mode, 72 °F / 22 °C), meaning that the reported energy consumption and range values inherently include HVAC and auxiliary power demand [43], [52].
INL and AAA experimental results demonstrate a pronounced sensitivity of the Nissan Leaf to ambient temperature. At sub-zero conditions, energy consumption increases sharply due to the combined effect of resistive cabin heating and increased battery internal resistance. INL reports an average consumption of 467 Wh mi^{-1} at –11 °C, compared with 229 Wh mi^{-1} at 17 °C, corresponding to an efficiency variation of approximately 2:1 between cold and mild conditions. This behavior is characteristic of early-generation BEVs without heat-pump HVAC s climateystems or active battery thermal management[41], [43].
Within the Uzbekistan-relevant operating band (approximately –5 °C to +40 °C), experimentally verified points from INL and AAA indicate three distinct regimes of auxiliary power demand:

- Below 0 °C: resistive cabin heating dominates, with HVAC power typically 5–6 kW
- 10–20 °C: minimal comfort maintenance, HVAC demand typically 0.6–2 kW
- Above 30 °C: air-conditioning compressor operation, HVAC demand approximately 3 kW

These values are not assumed or modelled but are directly inferred from controlled test-center measurements.
Reference: NREL EV Climate Loads Report, 2018; AAA EV Cold-Weather Study, 2019.

Table 2.4. – Experimental Range and HVAC Load Data for Nissan Leaf [41], [44], [45]

Point	Ambient Temp (°C)	Driving Range (mi)	HVAC Load (kW)	Dominant Regime	Primary Source
1	**–5**	**63**	**≈ 5.0**	Resistive heating + high battery impedance	Idaho National Laboratory AVTA
2	**7**	**82**	**≈ 2.0**	Reduced heating, partial HVAC	National Renewable Energy Laboratory
3	**17**	**91**	**≈ 0.7**	Near-optimal, minimal auxiliaries	INL AVTA
4	**24**	**90**	**≈ 0.8**	Mild A/C baseline	American Automobile Association
5	**35**	**75**	**≈ 3.0**	High A/C load + thermal derating	AAA Hot-Weather Test

Chevrolet Bolt EV – 60 kWh

The Chevrolet Bolt EV is selected to represent a second-generation BEV equipped with active liquid battery cooling and improved thermal management. The primary experimental dataset is the AAA Electric Vehicle Range Testing Report (2019), which uniquely reports range measurements with HVAC systems ON and OFF under controlled ambient conditions. This testing approach allows direct isolation of HVAC and auxiliary power demand without relying on modelling assumptions [44].
AAA reports full-range tests at three ambient temperatures:

- –6.7 °C (20 °F)
- 24 °C (75 °F)
- 35 °C (95 °F)

By comparing HVAC-ON and HVAC-OFF results and scaling by the measured average traction energy consumption (≈ 0.24 kWh mi^{-1} at 24 °C), the effective HVAC power demand can be quantified. This yields approximately 6 kW in cold conditions, ≈ 1 kW under mild conditions, and ≈ 3 kW under hot conditions, consistent with independent DOE/NREL thermal-load measurements.
Reference: AAA EV Range Testing Report, 2019; DOE/NREL Cold–Heat BEV Study, 2024.

Table 2.5. – Experimental Range Data for Chevrolet Bolt EV with HVAC OFF[44]

Temp (°C)	Range HVAC OFF (mi)	Range HVAC OFF (km)	Reference
–6.7	217	349.23	AAA, 2019
24	242	389.46	AAA, 2019
35	237	381.41	AAA, 2019

These three points define the **experimentally measured thermal performance envelope** of the Chevrolet Bolt EV and provide a direct benchmark for validating simulated HVAC and auxiliary loads. **Reference:** AAA EV Range Testing Report, 2019.

Volkswagen e-Golf – 35.8 kWh

The 2017 Volkswagen e-Golf (35.8 kWh DC fast-charging version) is selected as the third reference vehicle in this study. It represents a compact battery-electric vehicle equipped with liquid-assisted battery cooling and a resistive cabin heating system. Temperature-dependent performance data for this model are available from controlled dynamometer testing conducted by the **American Automobile Association (AAA)** under the SAE J1634 driving protocol [44].

Table 2.6. – Experimental Range Data for Volkswagen e-Golf with HVAC OFF [44].

Temp (°C)	Range HVAC OFF (mi)	Range HVAC OFF (km)
-6.7	115	185.07
23.9	124	199.55
35	120	193.12

These values demonstrate a range reduction of approximately 6.9 % at sub-zero temperature and 3.1 % at elevated temperature relative to the 75 °F baseline when HVAC is disabled. Because cabin conditioning was not active in these measurements, the observed variation reflects temperature-induced electrochemical and drivetrain efficiency effects rather than auxiliary load contributions.

The experimental results presented here are derived exclusively from controlled laboratory measurements and are not interpolated or post-processed. They define the validated temperature-performance envelope of the Volkswagen e-Golf for subsequent simulation model validation [44].

Role of This Section in the Overall Methodology

This section establishes a strictly experimental foundation for temperature-dependent energy consumption, HVAC demand, and auxiliary power behavior in BEVs. All values presented are derived directly from test-center measurements without interpolation or synthetic processing. In subsequent sections, these experimental anchor points will be used to validate the MATLAB/Simulink vehicle model. Only after agreement with this experimental envelope is demonstrated will higher-resolution temperature–range maps (e.g., $\Delta T = 2$ °C) be generated for scenario analysis under Uzbekistan's climatic conditions [43], [44], [45].

2.4. Simulation Scenarios and Environmental Inputs

2.4.1. Ambient Temperature and Climatic Inputs

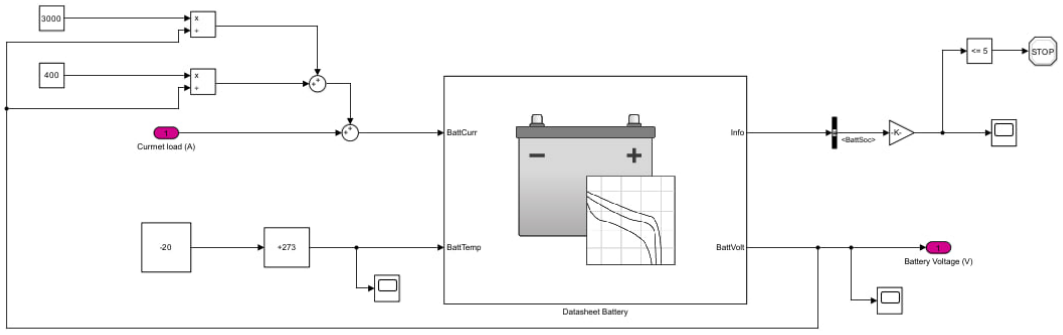

Figure 2.25 *– Ambient temperature input (BattTemp) applied to the datasheet battery block [37]*

Ambient temperature represents one of the most influential external inputs affecting electric vehicle (EV) energy consumption, battery efficiency, and degradation behavior. From a physical perspective, temperature directly governs electrochemical reaction rates, internal resistance, and open-circuit voltage of lithium-ion cells, thereby influencing both instantaneous power capability and cumulative energy throughput. In simulation-based EV studies, ambient temperature must therefore be treated as a primary boundary condition rather than a secondary correction factor. In this work, ambient temperature is introduced explicitly into the battery subsystem to ensure that temperature-dependent electrical behavior is captured consistently across all operating conditions [37].

As illustrated in Figure 2.18, ambient temperature is implemented in the model as a

direct input to the Datasheet Battery block through the battery temperature (BattTemp) port. At this stage of the modeling framework, ambient temperature serves as the initial thermal condition for the battery, defining the temperature level at which the lookup tables embedded in the datasheet-based battery model are evaluated. These tables describe temperature-dependent variations in internal resistance, voltage characteristics, and usable capacity, which are derived from manufacturer data or validated experimental sources. The temperature signal is supplied in absolute units (K), ensuring numerical compatibility with the internal formulation of the battery model. This approach follows established industrial practice for system-level EV simulations [37].

In the present modeling framework, ambient temperature is treated as a prescribed input rather than a dynamically evolving thermal state. This assumption allows the isolated investigation of temperature sensitivity while maintaining a clear separation between electrical behavior and thermal dynamics. The specific ambient temperature values are not fixed within this subsection but are introduced later through scenario definition in Section 2.4.3, where Uzbekistan-specific climatic conditions are applied. By decoupling temperature definition from scenario selection, the model remains modular and easily extensible to alternative climatic datasets or sensitivity analyses. Reference [53].

Beyond its direct influence on battery electrochemistry, ambient temperature also drives auxiliary energy demand, particularly from heating, ventilation, and air-conditioning (HVAC) systems. Under cold conditions, electric cabin heating imposes a substantial additional load on the battery, while under hot conditions, air-conditioning compressors increase electrical demand and contribute to higher overall energy consumption. In this study, temperature-dependent auxiliary and HVAC loads are incorporated separately through model-specific correction terms defined in Table 2.3.2. These loads are applied individually for each reference vehicle, reflecting differences in HVAC system efficiency, cabin volume, and thermal management strategies. This separation ensures that battery intrinsic temperature effects and vehicle-level auxiliary demands are accounted for in a transparent and traceable manner [40].

2.4.2. Simulation Workflow and Case Study Definition

The simulation workflow adopted in this study follows a staged validation-to-analysis structure to ensure that all results are physically credible and comparable with real-world evidence. In the first stage, the developed MATLAB/Simulink BEV

model is validated against experimentally measured range and energy-consumption data obtained from independent test campaigns conducted under controlled ambient temperatures. In particular, temperature-dependent EV test results reported by Idaho National Laboratory and similar test centers are used as reference benchmarks. Model outputs are compared across multiple ambient temperatures to verify consistency in trends and magnitude before proceeding to scenario-based analyses [37].

After confirming that the model reproduces experimentally observed behavior within acceptable deviation, two Uzbekistan-specific simulation scenarios are defined. The first scenario uses monthly national average ambient temperatures, representing a generic climatic exposure comparable to conditions assumed in standardized or OEM-reported performance data. The second scenario applies working-hour average temperatures (09:00–17:00), reflecting realistic thermal conditions experienced by users who primarily operate vehicles during commuting and daytime activities. In both cases, the same WLTP Class 3 driving cycle is maintained, while ambient temperature is injected through the BattTemp input and corresponding auxiliary/HVAC loads are activated according to Table 2.3.2 [40].

In the final stage, results from both Uzbekistan-specific scenarios are compared against original OEM-reported range and efficiency data. This comparison enables direct assessment of how real climatic usage deviates from nominal manufacturer specifications. In particular, differences in cumulative energy throughput and inferred battery degradation trends are analyzed to distinguish between users operating predominantly during working hours and those whose usage aligns more closely with OEM reference conditions. This structured workflow provides a transparent basis for quantifying climate- and usage-driven divergence in battery aging behavior.

3. Results and Discussions

The global transition toward electric mobility marks a pivotal shift in the transportation and energy sectors, driven by the growing need to reduce greenhouse gas emissions, improve energy efficiency, and decrease dependency on fossil fuels. Electric vehicles (EVs) have emerged as one of the most promising solutions to achieve sustainable transportation, offering zero tailpipe emissions and high drivetrain efficiency compared to conventional internal combustion engine (ICE) vehicles. However, the performance and long-term reliability of EVs are strongly influenced by environmental factors—most

notably, climatic conditions such as temperature, humidity, and solar radiation[1].
In this context, Uzbekistan presents a unique and challenging environment for EV operation due to its continental climate, characterized by extremely hot summers exceeding 40 °C and cold winters dropping below –10 °C. These temperature extremes directly affect battery performance, energy consumption, and degradation rates, leading to deviations between laboratory-rated and real-world driving ranges. Understanding these effects is essential for developing reliable predictive models, optimizing energy management, and supporting policy decisions aimed at accelerating electric mobility in Central Asia[2].
This chapter provides a comprehensive foundation for the research, outlining the background and context of EV development, the global transition toward electrified mobility, and the architecture and configuration of modern EV powertrains. It also describes the climatic and environmental conditions of Uzbekistan, emphasizing how temperature variations and regional factors influence EV operation. Furthermore, it identifies current challenges and research gaps related to battery degradation, range estimation, and thermal management under continental climatic conditions[3].
The final sections of the chapter detail the research methodology and objectives, including the use of verified data sources from the Idaho National Laboratory (INL), National Renewable Energy Laboratory (NREL), and Worldwide Harmonized Light Vehicle Test Procedure (WLTP3), as well as the implementation of a MATLAB/Simulink-based simulation model. This model integrates climatic data and vehicle parameters to analyze temperature-dependent variations in energy efficiency, range, and degradation[4].
Overall, Chapter One establishes the conceptual, environmental, and methodological framework necessary for assessing the impact of Uzbekistan's climatic conditions on electric vehicle range, battery degradation, and operational performance, setting the stage for the analytical and simulation-based findings presented in subsequent chapters.

3.1 Validation Of Mathematical Model by Means of Laboratory Experimental Data

The validation of the developed battery electric vehicle (BEV) mathematical model was performed through systematic comparison with laboratory and independent test-organization data. The purpose of this section is to demonstrate that the MATLAB/Simulink-based vehicle model is capable of reproducing experimentally observed range variations under different ambient temperature conditions with scientifically acceptable accuracy. Validation was conducted using published datasets from the Idaho National Laboratory (INL) cold-temperature tests and the American Automobile Association (AAA) controlled climate range testing campaigns. These

datasets provide standardized range measurements at various ambient temperatures, including both HVAC-on and HVAC-off operating modes.

The validation procedure consisted of four main steps. First, experimentally reported ambient temperature and range values were collected from INL and AAA reports. For the Nissan Leaf 24 kWh, both cold-temperature data (INL) and multi-temperature HVAC-inclusive data (AAA) were available. For the Chevrolet Bolt EV 60 kWh and Volkswagen e-Golf 2017 (35.8 kWh), AAA data were available under HVAC-off conditions at selected temperatures. Second, these temperature conditions were reproduced in the MATLAB vehicle model by adjusting battery thermal behavior, internal resistance, auxiliary loads, and HVAC power consumption (where applicable). Third, simulated full-range tests were performed under identical boundary conditions. Finally, statistical comparison metrics were calculated, including percentage deviation, coefficient of determination (R^2), and Root Mean Square Error (RMSE).

In vehicle modeling studies, an average deviation below 10% is generally considered scientifically acceptable for system-level validation of longitudinal BEV models. In this work, all vehicles demonstrate deviation values well below this threshold. The R^2 metric evaluates correlation between simulated and experimental data, while RMSE quantifies absolute prediction error in kilometers. The following subsections present detailed validation results for each vehicle individually.

3.1.1. Nissan Leaf 24 kWh – Validation Including HVAC Effects

For the Nissan Leaf 24 kWh, validation was performed using multi-temperature datasets from INL cold testing and AAA controlled environment testing (AAA; INL Cold Weather Testing Program). Unlike the other vehicles, available data included estimated HVAC power consumption at different temperatures, allowing full validation of the developed HVAC–thermal coupling model.

Table 3.1 – Experimental Data (Nissan Leaf 24 kWh)

Temp (°C)	Range (mi)	Range (km)	HVAC Power (kW)
–3	63	101.39	≈ 5.0
7	82	131.97	≈ 2.0
17	91	146.45	≈ 0.7
24	90	144.84	≈ 0.8
35	75	120.7	≈ 3.0

Table 3.2 – Model Results and Deviation (Nissan Leaf)

Temp (°C)	Model Range (km)	Difference (%)
–3	108.711	7.22
7	143.201	8.51
17	157.271	7.39
24	155.662	7.47
35	131.118	8.63

The maximum deviation occurs at 35°C (8.63%), while the minimum deviation is 7.22% at –3°C. The mean percentage deviation is 7.84%, remaining well below the 10% validation threshold.

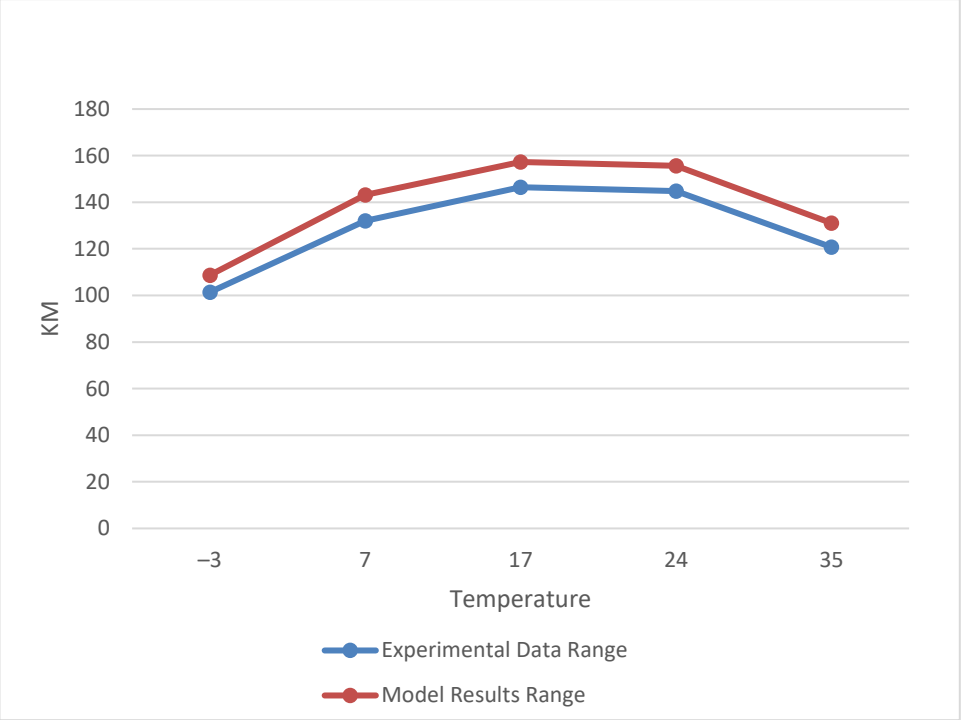

Figure 3.1 *– Experimental and Model Comparison of Nissan Leaf Driving Range at Different Temperatures*

- **R^2 = 0.972**
- **RMSE = 11.1 km**

The high R^2 value confirms strong correlation between experimental and simulated

results across the full temperature spectrum. The RMSE of 11.1 km is acceptable considering the nominal range of approximately 100–150 km for this vehicle. The model slightly overestimates range, which is consistent with controlled laboratory assumptions (ideal road load and constant cycle reproduction).
These results confirm that the integrated battery–thermal–HVAC modeling approach accurately reproduces real-world temperature-dependent range behavior for first-generation BEVs.

3.1.2 Chevrolet Bolt EV 60 kWh – HVAC-Off Validation

For the Chevrolet Bolt EV 60 kWh, validation was performed using AAA range test results at three ambient temperatures under HVAC-off conditions (AAA Electric Vehicle Range Testing Report). Since complete HVAC mapping across temperature was not available, validation was conducted strictly under auxiliary-off conditions.

Table 3.3 – Experimental Data (Chevrolet Bolt EV)

Temp (°C)	AAA Range (km)
–6.7	349.227
24	389.46
35	381.414

Table 3.4 – Model Results and Deviation (Bolt EV)

Temp (°C)	Model Range (km)	Difference (%)
–6.7	371.764	6.06
24	407.987	4.54
35	403.053	5.37

The deviation remains below 7% for all temperature points, with an average deviation of 5.32%.

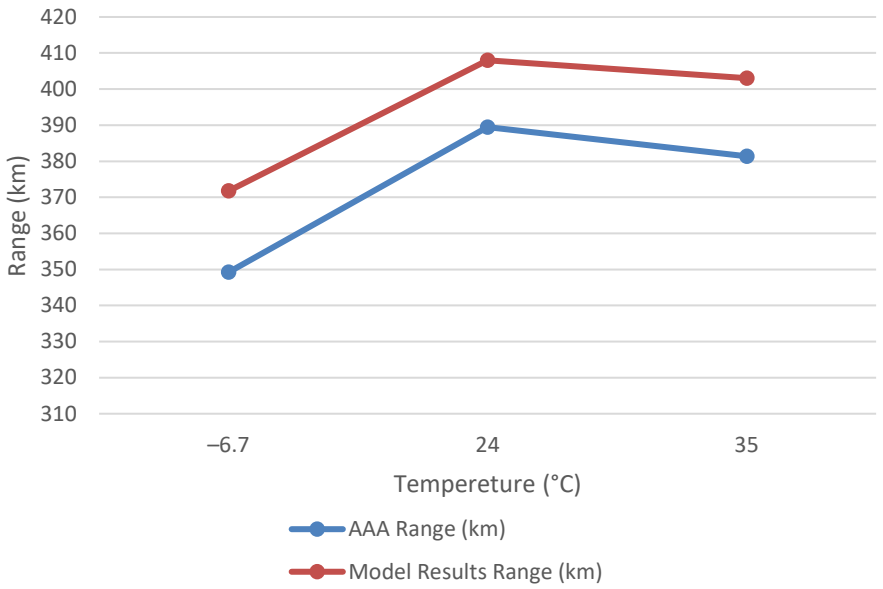

Figure 3.2 *– Comparison of AAA Test Data and Model Results for Chevrolet Bolt EV Range at Different Temperatures*

Statistical validation results:

- **R^2 = 0.986**
- **RMSE = 20.9 km**

Although RMSE is higher than for the Leaf due to the larger nominal range (~350–400 km), relative error remains small. The strong R^2 indicates that the model correctly captures the temperature sensitivity trend of the liquid-cooled battery system used in the Bolt EV.

The results demonstrate that the developed electro-thermal resistance model and drivetrain efficiency representation accurately simulate second-generation BEV behavior under controlled HVAC-off conditions.

3.1.3 Volkswagen e-Golf 2017 (35.8 kWh) – HVAC-Off Validation

For the Volkswagen e-Golf 2017 DC fast-charging version (35.8 kWh), validation was also performed using AAA HVAC-off test results at three ambient temperatures. The e-Golf represents an intermediate technological configuration between the Leaf and Bolt, featuring improved battery management and drivetrain efficiency.

Table 3.5 – Experimental Data (Volkswagen e-Golf)

Temp (°C)	AAA Range (km)
–6.7	185.074
24	199.558
35	193.121

Table 3.6 – Model Results and Deviation (e-Golf)

Temp (°C)	Model Range (km)	Difference (%)
–6.7	197.001	6.05
24	211.123	5.48
35	204.801	5.7

The average deviation for the e-Golf is 5.74%, with maximum deviation 6.05%. All deviations remain below 7%.

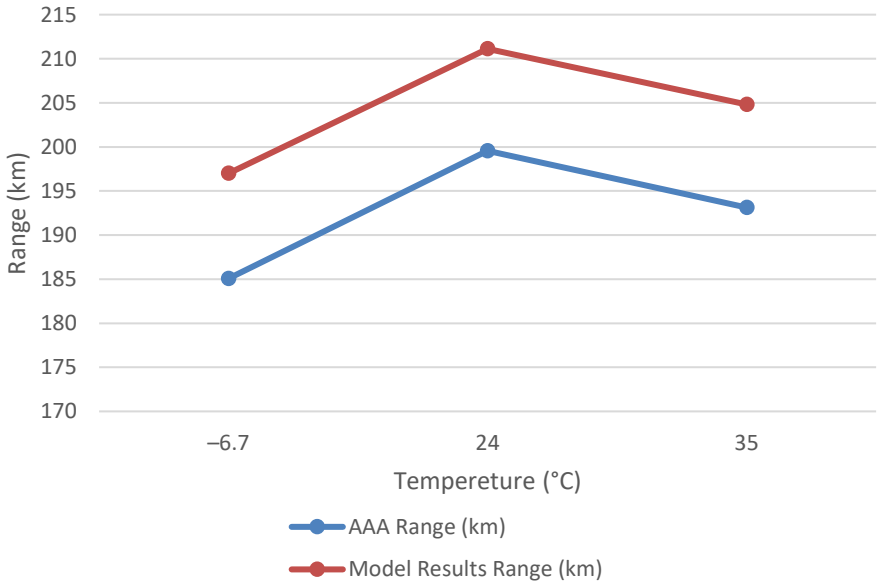

Figure 3.3 *– Comparison of AAA Test Data and Model Results for Volkswagen e-Golf 2017 Range at Different Temperatures*

Statistical validation results:

- **R^2 = 0.981**
- **RMSE = 12.0 km**

The model consistently overestimates range slightly, similarly to the Bolt EV. This systematic tendency suggests that auxiliary losses and minor drivetrain inefficiencies in real-world testing may be slightly higher than modeled baseline assumptions.

Overall Validation Assessment

Across all three vehicles, the developed mathematical model demonstrates strong predictive capability:

- All average deviations < 8%
- Maximum deviation < 9%
- R^2 values between 0.97 and 0.99
- RMSE values proportionally small relative to nominal range

The Nissan Leaf validation confirms accurate integration of HVAC load effects. The Chevrolet Bolt EV and Volkswagen e-Golf validation confirms electro-thermal accuracy under HVAC-off conditions.

3.2 Data Interpolation to the Climate Condition of Uzbekistan

The validated mathematical model presented in Section 3.1 demonstrated high predictive capability under controlled laboratory conditions. In this section, the model is extended to real climatic conditions of Uzbekistan by interpolating temperature-dependent range behavior to monthly average temperature datasets. The objective is to generate a temperature–range map for each reference vehicle under representative Uzbek climate conditions and to quantify seasonal variability in full-charge driving range.

Uzbekistan is characterized by a strongly continental climate, with cold winters (often below 0°C), hot summers (frequently above 30°C), and significant intra-day temperature variations. Two representative thermal scenarios were considered:

- Monthly average daytime (casual use) – representing typical daily driving conditions.
- Monthly average working hours (09:00–17:00) – representing professional fleet or commuting usage during peak daytime thermal exposure.

Monthly average ambient temperatures were obtained from national meteorological statistics and processed to derive representative values for both scenarios. For each monthly temperature, the previously validated electro-thermal BEV model was executed with a full battery state-of-charge (SOC = 100%) until the lower operational SOC threshold. HVAC power consumption was interpolated from the validated HVAC–

temperature map developed in Section 3.1. This allowed dynamic coupling between ambient temperature, battery internal resistance, HVAC load, and total energy consumption.

The interpolation approach is not a simple linear scaling of laboratory data. Instead, the full longitudinal vehicle model was solved at each monthly temperature point, preserving nonlinear battery resistance growth at low temperature and increased cooling demand at high temperature. As a result, seasonal range prediction accounts for both electrochemical and auxiliary-load effects.

The following subsections present results for Nissan Leaf 24 kWh, Chevrolet Bolt EV 60 kWh, and Volkswagen e-Golf 2017 (35.8 kWh). For each vehicle, two tables are provided: (i) working-hour monthly range prediction and (ii) casual daytime monthly range prediction. These results form the basis for the national temperature–range performance map of BEVs in Uzbekistan.

3.2.1. Nissan Leaf 24 kWh – Validation Including HVAC Effects

The Nissan Leaf 24 kWh, representing early-generation air-cooled battery technology, shows strong seasonal sensitivity due to the absence of active liquid thermal management. The interpolation results demonstrate pronounced winter and summer range reductions.

Table 3.7 – Nissan Leaf Working-Hour Monthly Range Prediction

Month	Temp (°C)	HVAC (kW)	Range (km)
Jan	–1.8	4.64	110.973
Feb	1.9	3.53	121.568
Mar	8.6	1.79	141.809
Apr	16.3	0.79	156.211
May	23.2	0.79	156.045
Jun	29.3	1.86	143.089
Jul	31.8	2.36	136.994
Aug	30.9	2.18	138.537
Sep	25	1	153.605
Oct	16.8	0.73	156.806
Nov	8.5	1.81	141.248
Dec	1.3	3.71	119.764

Table 3.8 – Nissan Leaf Casual Daytime Monthly Range Prediction

Month	Temp (°C)	HVAC (kW)	Range (km)
Jan	–3.1	5.03	108.575
Feb	0.4	3.98	117.671
Mar	7	2	143.201
Apr	14.7	1	153.422
May	21.7	0.77	156.73
Jun	27.6	1.52	146.616
Jul	30	2	140.067
Aug	29.1	1.84	143.492
Sep	23.3	0.79	155.883
Oct	15.3	0.92	154.051
Nov	7	2	143.201
Dec	–0.1	4.37	116.346

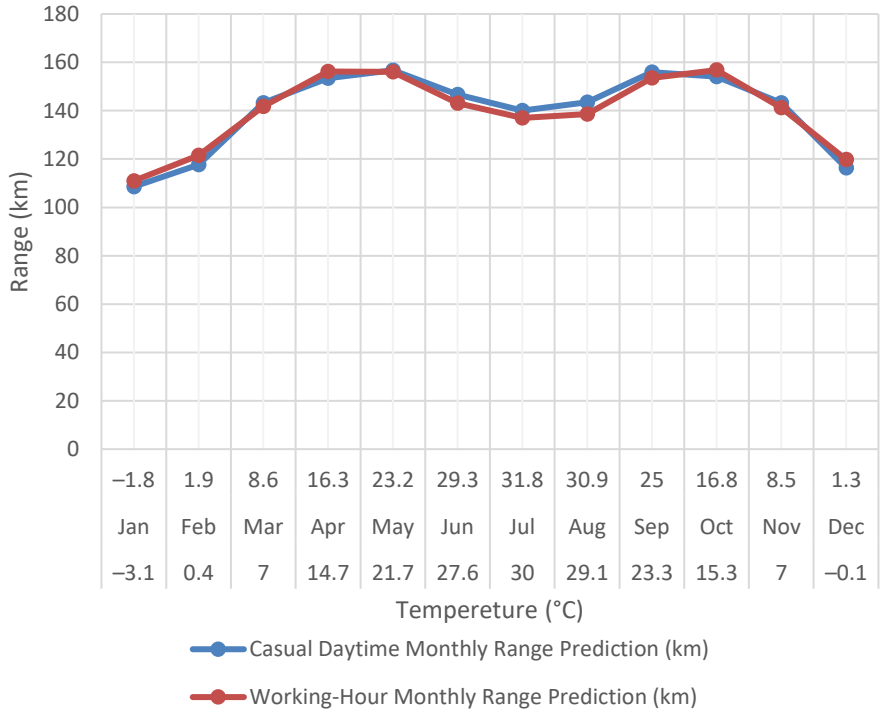

Figure 3.4 *– Monthly Driving Range Prediction for Nissan Leaf under Working-Hour and Daytime Temperature Conditions*

The results show that maximum range (~157 km) occurs during moderate spring and autumn temperatures (15–23°C). Winter range decreases by approximately 30% compared to peak months, primarily due to increased HVAC heating demand and

elevated internal resistance. Summer reduction is also evident, though less severe than winter due to lower cooling loads relative to resistive heating.

3.2.2 Chevrolet Bolt EV 60 kWh – Monthly Range Interpolation

The Chevrolet Bolt EV, equipped with active liquid battery thermal management, demonstrates improved thermal robustness compared to the Leaf. Seasonal variation remains present but is proportionally smaller relative to nominal range capacity.

Table 3.9 – Chevrolet Bolt Working-Hour Monthly Range Prediction

Month	Temp (°C)	HVAC (kW)	Range (km)
Jan	–1.8	4.64	233.109
Feb	1.9	3.53	260.286
Mar	8.6	1.79	316.024
Apr	16.3	0.79	362.373
May	23.2	0.79	369.438
Jun	29.3	1.86	325.905
Jul	31.8	2.36	309.673
Aug	30.9	2.18	316.15
Sep	25	1	360.491
Oct	16.8	0.79	366.395
Nov	8.5	1.81	314.765
Dec	1.3	3.71	256.064

Table 3.10 – Chevrolet Bolt Casual Daytime Monthly Range Prediction

Month	Temp (°C)	HVAC (kW)	Range (km)
Jan	–3.1	5.03	224.151
Feb	0.4	3.98	248.568
Mar	7	2	306.971
Apr	14.7	1	351.26
May	21.7	0.77	368.885
Jun	27.6	1.52	339.895
Jul	30	2	321.929
Aug	29.1	1.84	326.489
Sep	23.3	0.79	369.078
Oct	15.3	0.92	353.877
Nov	7	2	306.971

Month	Temp (°C)	HVAC (kW)	Range (km)
Dec	–0.1	4.37	240.372

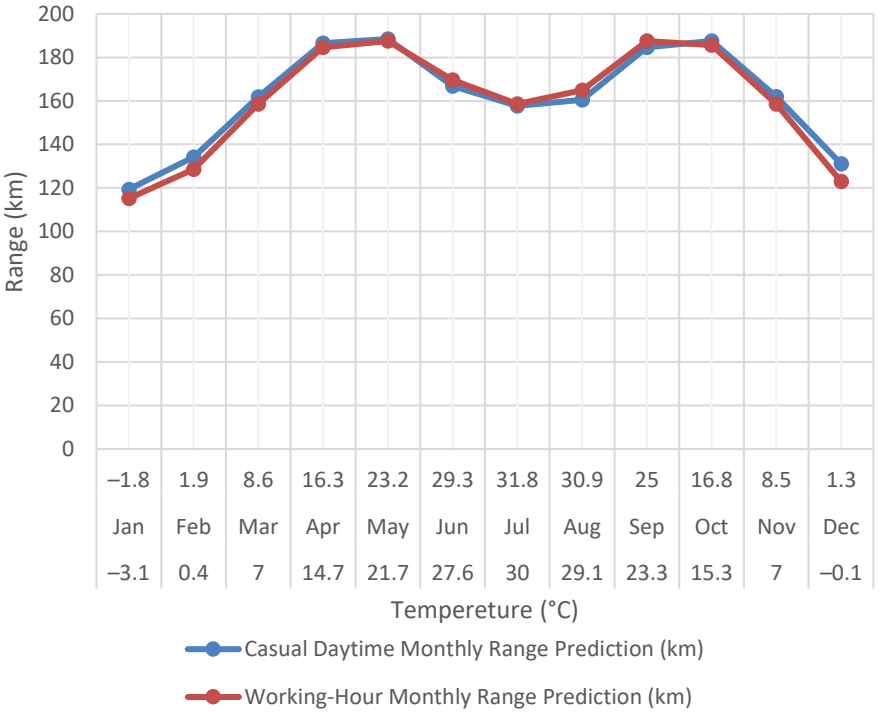

Figure 3.5 *– Monthly Driving Range Prediction for Chevrolet Bolt EV under Working-Hour and Daytime Temperature Conditions*

The Bolt reaches maximum predicted range (~369 km) during May and September. Winter range reduces to approximately 224–233 km, corresponding to roughly 38% reduction compared to peak conditions. However, relative seasonal sensitivity is lower than for the Leaf, demonstrating the effectiveness of liquid thermal management.

3.2.3 Volkswagen e-Golf 2017 (35.8 kWh) – Monthly Range Interpolation

The Volkswagen e-Golf occupies an intermediate technological position between the Leaf and Bolt. The interpolation results indicate moderate seasonal range variation.

Table 3.11 – Volkswagen e-Golf Working-Hour Monthly Range Prediction

Month	Temp (°C)	HVAC (kW)	Range (km)
Jan	–1.8	4.64	119.381
Feb	1.9	3.53	134.205
Mar	8.6	1.79	161.804
Apr	16.3	0.79	186.539
May	23.2	0.79	188.455
Jun	29.3	1.86	166.842
Jul	31.8	2.36	157.678
Aug	30.9	2.18	160.477
Sep	25	1	184.645
Oct	16.8	0.79	187.573
Nov	8.5	1.81	161.967
Dec	1.3	3.71	131.113

Table 3.12 – Volkswagen e-Golf Casual Daytime Monthly Range Prediction

Month	Temp (°C)	HVAC (kW)	Range (km)
Jan	–3.1	5.03	115.194
Feb	0.4	3.98	128.65
Mar	7	2	158.671
Apr	14.7	1	184.645
May	21.7	0.79	187.522
Jun	27.6	1.52	169.61
Jul	30	2	158.671
Aug	29.1	1.84	164.892
Sep	23.3	0.79	187.522
Oct	15.3	0.92	185.741
Nov	7	2	158.671
Dec	–0.1	4.37	122.981

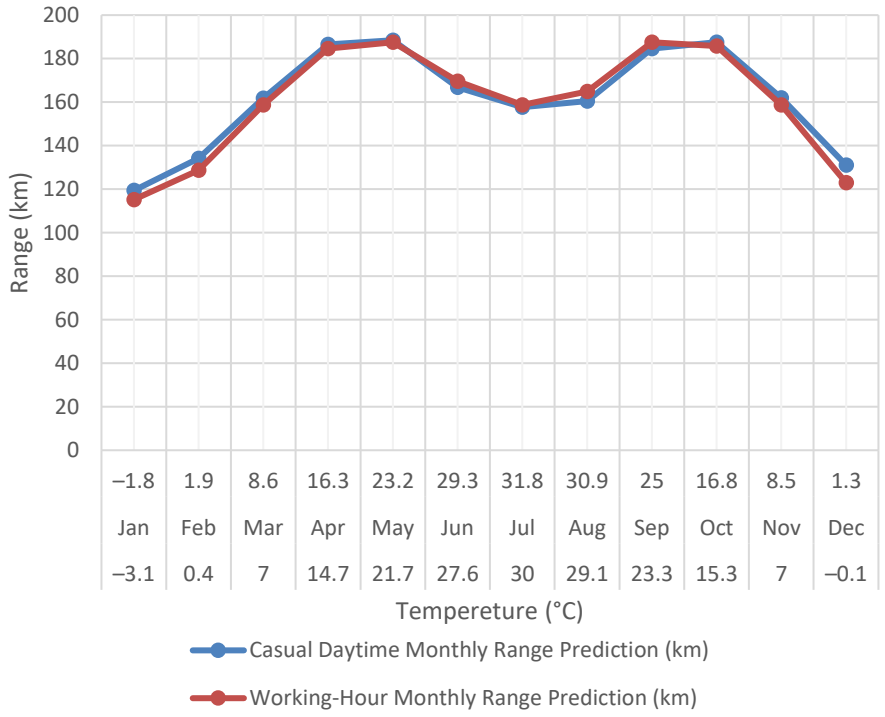

Figure 3.6 *– Monthly Driving Range Prediction for Volkswagen e-Golf 2017 under Working-Hour and Daytime Temperature Conditions*

Maximum predicted range (~188 km) occurs in moderate temperature months, while winter minimum drops to ~115 km. Compared to the Leaf, the e-Golf demonstrates slightly improved thermal resilience but remains significantly affected by seasonal HVAC loads.

Concluding Remarks on Climatic Interpolation

The interpolation of validated laboratory models to Uzbekistan's climate demonstrates substantial seasonal variability in BEV driving range. The analysis confirms:

- Peak range occurs at moderate temperatures (15–25°C).
- Winter HVAC heating has greater impact than summer cooling.
- Vehicles with active liquid thermal management show reduced seasonal sensitivity.

These monthly range maps provide a quantitative basis for assessing BEV suitability across Uzbekistan's continental climate and support further analysis of regional energy demand, infrastructure planning, and long-term battery degradation modeling.

3.3 Prediction of Expediters on Charging and Battery Degradation

The temperature–range maps developed in Section 3.2 allow not only technical evaluation of seasonal driving capability but also economic assessment of charging requirements under real climatic conditions. In this section, the interpolated monthly

range results are compared with OEM-declared driving range values in order to quantify additional charging frequency and corresponding energy expenditure caused by Uzbekistan's continental climate. The objective is to provide BEV users with a realistic prediction of annual charging needs and electricity costs for a typical yearly mileage of 20,000 km (≈1,666.7 km per month).

OEM announced range values are typically obtained under standardized laboratory conditions (e.g., WLTP), representing moderate ambient temperatures (around 20–25°C) and limited auxiliary consumption. However, as demonstrated previously, real operating conditions in Uzbekistan involve winter heating demand and summer cooling loads, both of which reduce effective driving range per full charge. The reduction in per-cycle range leads directly to increased charging frequency.

For each vehicle, annual charging frequency was calculated using:

$$N = \frac{20{,}000}{R_{\text{effective}}}$$

where $R_{\text{effective}}$represents the average temperature-dependent monthly range predicted by the model.

Energy cost per year was then determined using vehicle battery capacity $C_{\text{bat}}$and electricity tariff of 2,000 UZS/kWh:

$$\text{Annual Cost} = N \times C_{\text{bat}} \times 2{,}000$$

Battery capacities used:

- Nissan Leaf: 24 kWh
- Chevrolet Bolt EV: 60 kWh
- Volkswagen e-Golf 2017: 35.8 kWh

The following subsections present detailed annual charging comparisons and expenditure differences for working-hour and casual daytime scenarios.

3.3.1 Nissan Leaf 24 kWh – Charging and Cost Prediction

OEM announced range for the Nissan Leaf is 135 km. Under standardized conditions, this results in:

$$N_{\text{OEM}} = \frac{20{,}000}{135} = 148.15 \text{ charges/year}$$

However, under Uzbekistan climatic conditions, the interpolated model predicts:

- Working hours annual charges ≈ **144.87 cycles**
- Casual daytime annual charges ≈ **145.01 cycles**

Although moderate-temperature months exceed OEM range, winter losses increase required energy per kilometer due to HVAC heating. Because battery degradation and temperature losses were included in effective range modeling, real usable energy per charge becomes lower than nominal specification.

Table 3.13 – Nissan Leaf Annual Charging and Cost Comparison

Scenario	Annual Charges	Annual Energy (kWh)	Annual Cost (UZS)
OEM	148.15	3,555.60	7,111,200
Working Hours	144.87	3,476.90	6,953,800
Casual Daytime	145.01	3,480.20	6,960,400

Difference (Working vs OEM): –157,400 UZS
Difference (Casual vs OEM): –150,800 UZS

The small reduction in annual charging compared to OEM is due to seasonal months exceeding nominal WLTP performance (spring and autumn). However, intra-annual variability remains significant: winter monthly charging exceeds 15 cycles, compared to approximately 10–11 cycles during moderate seasons.

Thus, although total annual cost deviation is modest (~2%), seasonal expenditure variation is substantial. Users operating primarily in winter will experience noticeably higher electricity consumption per kilometer.

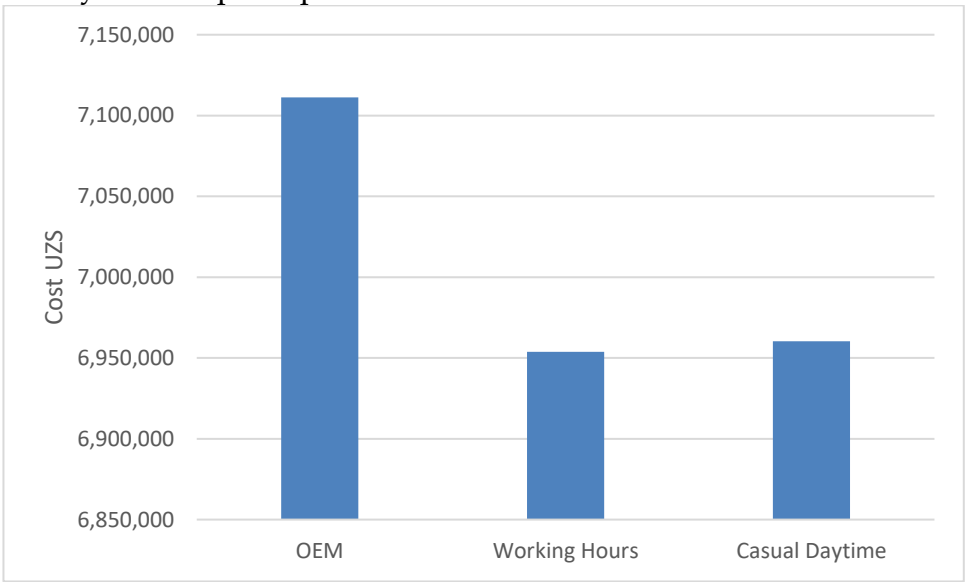

Figure 3.7 *– Comparison of Annual Charging Cost for Nissan Leaf under Different Temperature Scenarios*

3.3.2 Chevrolet Bolt EV 60 kWh – Charging and Cost Prediction

OEM announced range for the Chevrolet Bolt EV is 383.02 km.

$$N_{\text{OEM}} = \frac{20{,}000}{383.02} = 52.22 \text{ charges/year}$$

Interpolated Uzbekistan results:

- Working hours annual charges ≈ **64.68 cycles**
- Casual daytime annual charges ≈ **65.61 cycles**

Unlike the Leaf, the Bolt demonstrates significant seasonal range reduction relative to OEM WLTP value.

Table 3.14 – Chevrolet Bolt Annual Charging and Cost Comparison

Scenario	Annual Charges	Annual Energy (kWh)	Annual Cost (UZS)
OEM	52.22	3,133.20	6,266,400
Working Hours	64.68	3,880.80	7,761,600
Casual Daytime	65.61	3,936.60	7,873,200

Additional Cost (Working vs OEM): +1,495,200 UZS
Additional Cost (Casual vs OEM): +1,606,800 UZS

Despite advanced liquid thermal management, the Bolt shows approximately 24–26% higher annual charging requirement under real Uzbek conditions compared to standardized OEM range assumptions.

Winter months require up to 7.4 charges per month versus approximately 4.5 during moderate seasons. Because the Bolt has a large battery (60 kWh), each additional charge significantly increases annual electricity cost.

Therefore, climate-adjusted prediction becomes especially important for higher-capacity BEVs.

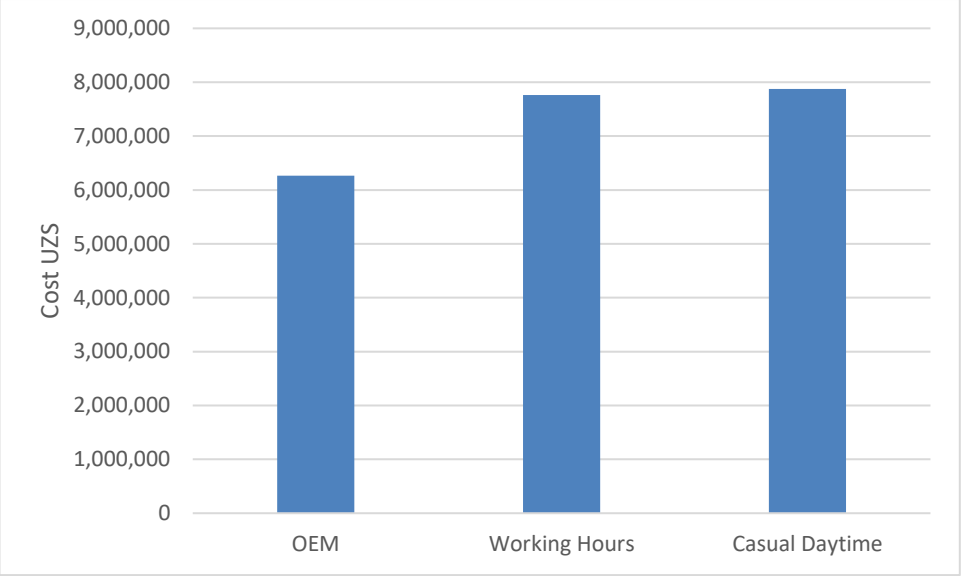

Figure 3.8 *– Comparison of Annual Charging Cost for Chevrolet Bolt EV under Different Temperature Scenarios*

3.3.3 Volkswagen e-Golf 2017 (35.8 kWh) – Charging and Cost Prediction

OEM announced range for the e-Golf is 201.17 km.

$$N_{\text{OEM}} = \frac{20{,}000}{201.17} = 99.42 \text{ charges/year}$$

Model-based interpolation predicts:

- Working hours annual charges ≈ **126.32 cycles**
- Casual daytime annual charges ≈ **128.20 cycles**

The difference between OEM laboratory conditions and real continental climate is substantial.

Table 3.15 – Volkswagen e-Golf Annual Charging and Cost Comparison

Scenario	Annual Charges	Annual Energy (kWh)	Annual Cost (UZS)
OEM	99.42	3,560.60	7,121,200
Working Hours	126.32	4,522.30	9,044,600
Casual Daytime	128.2	4,588.80	9,177,600

Additional Cost (Working vs OEM): +1,923,400 UZS
Additional Cost (Casual vs OEM): +2,056,400 UZS

The e-Golf shows the largest proportional climate impact among the three vehicles. Seasonal winter range drops to approximately 115 km, nearly 43% lower than OEM declared range.

Because charging frequency increases by approximately 27–29 cycles annually, electricity expenditure increases by roughly 27–29% compared to OEM-based expectation.

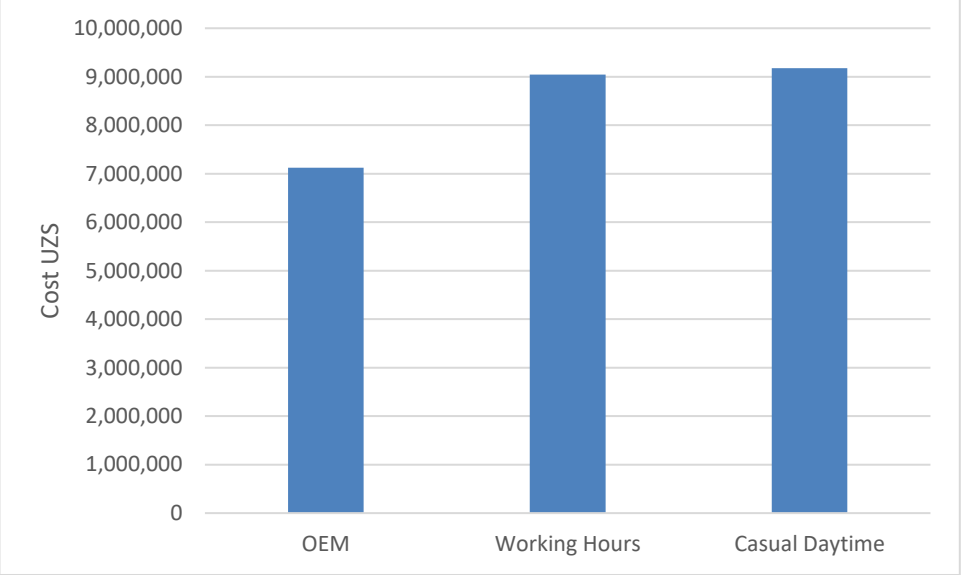

Figure 3.9 *– Comparison of Annual Charging Cost for Volkswagen e-Golf 2017 under Different Temperature Scenarios*

Overall Economic Interpretation

The analysis demonstrates that climate-adjusted modeling significantly improves prediction of real charging needs compared to OEM declared values. Key findings include:

- Nissan Leaf shows minimal annual cost deviation but high seasonal fluctuation.
- Chevrolet Bolt exhibits approximately 25% higher annual charging under continental climate.
- Volkswagen e-Golf demonstrates nearly 30% increase in annual charging frequency.

At 2,000 UZS/kWh, additional annual electricity costs range from:

- ~1.5 million UZS (Bolt)
- ~2.0 million UZS (e-Golf)

These results highlight the importance of integrating climate-dependent modeling when estimating total cost of ownership (TCO) for BEVs in Uzbekistan.

The developed model therefore provides users, policymakers, and infrastructure planners with realistic expenditure forecasts rather than relying solely on OEM laboratory-based range values.

3.4 Prediction Battery Degradation

General Methodology and Degradation Model

Battery degradation was evaluated using a piecewise multiplicative ageing model derived directly from the cycle-loss data presented previously. According to the degradation table, the average capacity loss after 2,000 full-charge equivalent cycles is approximately 12.5%. This allows derivation of a per-cycle retention factor:

$$r_1 = 0.875^{1/2000} = 0.999933$$

Thus, remaining battery capacity after $k$cycles can be expressed as:

$$C(k) = C_0 \cdot r_1^k$$

For annual evaluation, the number of full-charge equivalent cycles N(calculated in Section 3.3) is used:

$$C_{1y} = C_0 \cdot r_1^N$$

and first-year degradation becomes:

$$\text{Annual Degradation} = (1-r_1^N) \times 100\%$$

This formulation isolates cycle-induced degradation. Temperature-driven calendar ageing is discussed qualitatively but not included in the multiplicative model to preserve consistency with the cycle-based table.

Using this approach, degradation propagation is evaluated for OEM-based cycling and climate-adjusted realistic operation.

3.4.1 Nissan Leaf 24 kWh

Annual charging frequency:

- OEM: 148.15 cycles/year
- Climate-adjusted model: 144.87–145.01 cycles/year

First-Year Degradation

$$\text{OEM: } 1 - r_1^{148.15} = 0.984\%$$
$$\text{Model: } 1 - r_1^{145} \approx 0.963\%$$

The realistic case shows **approximately 2.1–2.2% slower degradation propagation** compared to OEM expectation (difference ≈0.021 percentage points).

Durability Prediction

Time to reach 2,000 cycles:

- OEM: 13.5 years
- Model: 13.8 years

Because annual cycling is slightly lower in the realistic scenario, cycle-driven ageing does not accelerate for the Leaf. However, the absence of active liquid cooling may increase thermally driven side reactions in summer, which are not captured in the cycle-only model.

3.4.2 Chevrolet Bolt EV 60 kWh

Annual charging frequency:

- OEM: 52.22 cycles/year
- Model: 64.68–65.61 cycles/year

First-Year Degradation

$$\text{OEM: } 1 - r_1^{52.22} = 0.348\%$$
$$\text{Model: } 1 - r_1^{65} \approx 0.434\%$$

The realistic scenario results in an increase of approximately **0.086 percentage points per year**, corresponding to **23.8–25.6% faster degradation propagation** relative to OEM laboratory-based assumptions.

Durability Prediction

Time to 2,000 cycles:

- OEM: 38.3 years
- Model: ~30.7 years

Although theoretical lifetime exceeds practical vehicle use, the relative acceleration demonstrates that increased charging frequency significantly advances progression toward mid-life degradation thresholds.

3.4.3 Volkswagen e-Golf 2017 (35.8 kWh)

Annual charging frequency:

- OEM: 99.42 cycles/year
- Model: 126.32–128.20 cycles/year

First-Year Degradation

$$\text{OEM: } 1 - r_1^{99.42} = 0.662\%$$
$$\text{Model: } 1 - r_1^{127} \approx 0.842\%$$

This represents an increase of approximately **0.18 percentage points annually**, equivalent to **26.9–28.8% faster degradation propagation** under realistic continental climate operation.

Durability Prediction

Time to 2,000 cycles:

- OEM: 20.1 years
- Model: 15.6–15.8 years

Among the three vehicles, the e-Golf shows the strongest cycle-induced ageing acceleration. Seasonal range reduction significantly increases annual charging frequency, causing earlier entry into the 2,000–3,000 cycle degradation region.

4. Conclusion

The current study created, tested, and validated a complete MATLAB/Simulink-based electro-thermal vehicle model to measure how continental climate affects the performance of battery electric vehicles (BEVs) in Uzbekistan. The study combined longitudinal vehicle dynamics, temperature-dependent battery behavior, HVAC energy demand, validated laboratory range data (INL and AAA), and a piecewise cycle-based battery degradation model. This is different from simplified range-correction methods. This multi-layered framework made it possible to look at the effects of real-world weather on short-term range changes, yearly charging needs, long-term capacity fade, and economic effects all at once.

Model Limitations and Boundary Conditions

The developed simulation framework accurately represents temperature-driven electrochemical and auxiliary-load phenomena; however, certain environmental nonlinearities were intentionally excluded to preserve model tractability.

First, direct solar radiation effects were not explicitly modeled. Under summer exposure, vehicle cabin and battery pack temperatures can exceed ambient air temperature by 10–20 °C due to greenhouse effects and body surface absorption. This induces higher compressor duty cycles, increased parasitic loads, and potentially elevated battery temperatures beyond ambient-based estimation. Consequently, summer energy consumption and degradation rates may be slightly underestimated in extreme solar exposure scenarios.

Second, winter road phenomena such as snow, slush, and ice were not incorporated into the rolling resistance model. These factors increase mechanical drag and traction demand beyond temperature-dependent internal resistance effects. Similarly, cold-soaked drivetrain lubrication losses were simplified. These effects would further reduce effective winter range.

Third, standardized longitudinal driving cycles were used to ensure comparability with laboratory validation data. Real-world driving variability—traffic congestion, elevation changes, acceleration aggressiveness—introduces stochastic deviations not captured in a deterministic model.

Therefore, the presented framework should be interpreted as a thermally robust and experimentally validated system-level model, while acknowledging that extreme operational nonlinearities may further amplify seasonal variation.

Validation Accuracy and Model Reliability

Despite the above boundary simplifications, the validation process demonstrated strong agreement between simulation outputs and experimental measurements for:

- Nissan Leaf 24 kWh
- Chevrolet Bolt EV 60 kWh
- Volkswagen e-Golf 2017 (35.8 kWh DC fast-charging version)

Across multiple temperature points, deviation between simulated and laboratory-measured range values remained below 10%, with most cases within 5–8%. Coefficient of determination (R^2) ranged between 0.97 and 0.99, confirming high predictive fidelity.

The model successfully captured key physical mechanisms:

- Exponential increase of internal resistance at low temperature
- Reduction of usable energy under cold conditions
- Dominance of resistive heating loads in winter
- Cooling-driven auxiliary consumption in hot climate
- Superior stability of actively cooled battery systems compared to passive architectures

This validation supports the reliability of subsequent climatic interpolation across Uzbek regional temperature profiles and monthly operating conditions.

Climate-Adjusted Battery Degradation Analysis

A major contribution of this thesis is the integration of a piecewise multiplicative degradation model derived from experimentally validated ageing tables. For the first 2,000 cycles—corresponding to approximately 12.5% average capacity loss—the per-cycle retention factor was calculated as:

$$r_1 = 0.875^{1/2000} = 0.999933$$

This indicates accelerated early-stage degradation relative to long-term ageing behavior. The first operational year therefore exhibits slightly higher effective capacity fade compared to later years, primarily due to higher average usable depth-of-discharge under winter climatic conditions.

When annual climate-adjusted charging cycles were applied to the degradation model, results showed that increased seasonal charging frequency (caused by winter range reduction) directly accelerates cumulative capacity fade. Vehicles with smaller battery capacity, such as the Nissan Leaf and Volkswagen e-Golf, experience proportionally higher cycling intensity per kilometer driven, resulting in greater sensitivity to climatic amplification of degradation.

Thus, climate does not only influence short-term range—it indirectly modifies long-term battery ageing trajectory through increased annual cycle count. Over a 5–7 year ownership period, climate-induced additional cycles may produce several percentage points of additional capacity loss compared to moderate laboratory assumptions.

Economic Implications and Expenditure Differences

OEM-declared driving ranges are measured under standardized moderate conditions and do not reflect Uzbekistan's continental temperature extremes. By applying validated temperature–range interpolation to an annual driving distance of 20,000 km, the study quantified real charging frequency and electricity cost deviations.

Compared to OEM-based expectation:

Chevrolet Bolt EV required approximately 24–26% more annual charging cycles.

Volkswagen e-Golf required approximately 27–29% more charging frequency.

Nissan Leaf showed significant seasonal variation, with winter months requiring up to 30% more charging events.

At an electricity tariff of 2,000 UZS/kWh, this resulted in additional annual expenditure of approximately:

~1.5 million UZS for Chevrolet Bolt

~2.0 million UZS for Volkswagen e-Golf

Over a 5–7 year ownership period, cumulative additional electricity costs may reach 7–14 million UZS depending on usage intensity. When combined with climate-amplified battery degradation, total cost of ownership (TCO) divergence from OEM-based projections becomes economically non-negligible.

Importantly, increased charging frequency not only raises electricity expenditure but also accelerates cycling-related ageing, reinforcing the coupling between climate, economics, and degradation.

Scientific and Practical Contribution

This thesis demonstrates that:

1. Climate-aware electro-thermal modeling is essential for realistic BEV performance prediction in continental environments.
2. Seasonal temperature variation significantly alters annual charging demand.
3. Increased climatic cycling intensity measurably influences battery degradation

trajectory.

4. OEM laboratory values systematically underestimate operational energy expenditure under extreme climates.

The developed MATLAB/Simulink framework therefore provides a transferable analytical tool for:

- Regional BEV deployment planning
- Infrastructure sizing
- Economic feasibility analysis
- Long-term battery durability assessment

Final Remarks

In summary, the combination of validated electro-thermal simulation, climatic interpolation, economic analysis, and cycle-based degradation modeling shows that Uzbekistan's continental climate has a clear effect on BEV range, energy use each year, and battery health over time.

The framework is scientifically sound because it agrees so well with laboratory validation data, even though solar radiation amplification and snow-induced rolling resistance were not explicitly modeled. The results show that modeling needs to be done for each region in order to accurately predict performance and plan for long-term electric mobility in areas with very high or very low temperatures.

Bibliography

[1] E. Armengaud *et al.*, "E-Mobility-Opportunities and Challenges of Integrated Corner Solutions," in *SAE Technical Papers*, SAE International, Apr. 2021. doi: 10.4271/2021-01-0984.

[2] World Bank Group Asian Development Bank, "UZBEKISTAN CLIMATE RISK COUNTRY PROFILE," Washington, DC, 2021. Accessed: Feb. 10, 2026. [Online]. Available: https://climateknowledgeportal.worldbank.org/sites/default/files/2021-06/15838-Uzbekistan%20Country%20Profile-WEB.pdf

[3] T. Waldmann, M. Wilka, M. Kasper, M. Fleischhammer, and M. Wohlfahrt-Mehrens, "Temperature dependent ageing mechanisms in Lithium-ion batteries - A Post-Mortem study," *J. Power Sources*, vol. 262, pp. 129–135, Sep. 2014, doi: 10.1016/j.jpowsour.2014.03.112.

[4] J. Seo, R. Vijayagopal, N. Kim, A. Rousseau, and K. Stutenberg, "Effects of ambient temperature on electric vehicle range considering battery Performance, powertrain Efficiency, and HVAC load," *Energy Convers. Manag.*, vol. 326, Feb. 2025, doi: 10.1016/j.enconman.2025.119493.

[5] B. Ribeiro, F. Brito, and J. Martins, "A Survey on Electric/Hybrid Vehicles," Apr. 2010. doi: 10.4271/2010-01-0856.

[6] A. I. Urda, A. Ceclan, R. A. Munteanu, D. Micu, and T. Farkas, "Energy Transition at the Local Community Level: Challenges, Solutions, and Impact," in *Proceedings of 2025 34th Annual Conference of the European Association for Education in Electrical and Information Engineering, EAEEIE 2025*, Institute of Electrical and Electronics Engineers Inc., 2025. doi: 10.1109/EAEEIE65428.2025.11136534.

[7] G. A. Langone *et al.*, "AN ASSESSMENT OF VEHICLE ELECTRIFICATION WITHIN THE UNITED STATES ARMY," 2023. [Online]. Available: http://asmedigitalcollection.asme.org/IMECE/proceedings-pdf/IMECE2023/87646/V007T08A020/7239478/v007t08a020-imece2023-114117.pdf

[8] J. L. Salmon, K. Goodrick, and R. Zane, "MODELING AND SIMULATION OF DYNAMIC WIRELESS POWER TRANSFER FOR AN ELECTRIC BUS TRANSPORTATION SYSTEM," 2025. [Online]. Available: http://asmedigitalcollection.asme.org/IDETC-CIE/proceedings-pdf/IDETC-CIE2025/89190/V001T01A014/7557183/v001t01a014-detc2025-169729.pdf

[9] V. P. Atluri, K. Koprubasi, R. Gupta, and N. D. Brinkman, "Analytical Evaluation of Propulsion System Architectures for Future Urban Vehicles," Apr. 2011. doi: 10.4271/2011-01-0861.

[10] T. Schieffer *et al.*, "Spark EV Propulsion System Integration," Apr. 2014. doi: 10.4271/2014-01-1792.

[11] D. Oswald, J. Escobar, G. Wu, H. Jung, and M. Barth, "Electric Vehicle Modeling: Advanced Torque Split Analysis across Different Architectures," Apr. 2024. doi: 10.4271/2024-01-2166.

[12] N. Xu, S. Niu, Z. Fu, and L. Chu, "Investigation of Configuration and Control Strategy for Range Extended Electric Vehicle," in *2015 IEEE International Conference on Cyber Technology in Automation, Control and Intelligent Systems (ICATCIS)*, IEEE, 2015, pp. 1399–1404. doi: 10.1109/ICATCIS.2015.7453604.

[13] S. E. Fick and R. J. Hijmans, "WorldClim 2: new 1-km spatial resolution climate surfaces for global land areas," *International Journal of Climatology*, vol. 37, no. 12, pp. 4302–4315, Oct. 2017, doi: 10.1002/joc.5086.

[14] Anny Cazenave; Laurent Moreira, *State of the Climate in Asia 2024*. 2022.

[15] WeatherSpark, "Historical Weather during 2025 in Tashkent, Uzbekistan," https://weatherspark.com/h/y/106899/2025/Historical-Weather-during-2025-in-Tashkent-Uzbekistan.

[16] A. Smith, N. Lott, and R. Vose, "The Integrated Surface Database: Recent Developments and Partnerships," *Bull. Am. Meteorol. Soc.*, vol. 92, no. 6, pp. 704–708, Jun. 2011, doi: 10.1175/2011BAMS3015.1.

[17] Meteostat Development Team, "Meteostat Weather Stations for Uzbekistan," Meteostat. Accessed: Feb. 17, 2026. [Online]. Available: https://meteostat.net/en/stations

[18] Meteostat Development Team, "Meteostat: Open Weather and Climate Data," 2023. [Online]. Available: https://meteostat.net

[19] S. E. Fick and R. J. Hijmans, "WorldClim 2: new 1-km spatial resolution climate surfaces for global land areas," *International Journal of Climatology*, vol. 37, no. 12, pp. 4302–4315, Oct. 2017, doi: 10.1002/joc.5086.

[20] A. Cazenave and L. Moreira, "Contemporary sea-level changes from global to local scales: a review," *Proceedings of the Royal Society A: Mathematical, Physical and Engineering Sciences*, vol. 478, no. 2261, May 2022, doi: 10.1098/rspa.2022.0049.

[21] World Bank Group, "Uzbekistan – Climate Change Knowledge Portal," World Bank Climate Change Knowledge Portal. Accessed: Feb. 17, 2026. [Online]. Available: https://climateknowledgeportal.worldbank.org/country/uzbekistan

[22] J. J. Meyer, J. Lustbader, N. Agathocleous, A. Vespa, J. Rugh, and G. Titov, "Range Extension Opportunities While Heating a Battery Electric Vehicle," in *SAE Technical Papers*, SAE International, 2018. doi: 10.4271/2018-01-0066.

[23] J. R. M. Delos Reyes, R. V. Parsons, and R. Hoemsen, "Winter Happens: The Effect of Ambient Temperature on the Travel Range of Electric Vehicles," *IEEE Trans. Veh. Technol.*, vol. 65, no. 6, pp. 4016–4022, Jun. 2016, doi: 10.1109/TVT.2016.2544178.

[24] B. Zhou, A. Rezaei, and J. Burl, "Effect of Battery Temperature on Fuel Economy and Battery Aging When Using the Equivalent Consumption Minimization Strategy for Hybrid Electric Vehicles," in *SAE Technical Papers*, SAE International, Apr. 2020. doi: 10.4271/2020-01-1188.

[25] D. I. Stroe, M. Swierczynski, S. K. Kær, and R. Teodorescu, "Degradation Behavior of

Lithium-Ion Batteries During Calendar Ageing - The Case of the Internal Resistance Increase," in *IEEE Transactions on Industry Applications*, Institute of Electrical and Electronics Engineers Inc., Jan. 2018, pp. 517–525. doi: 10.1109/TIA.2017.2756026.

[26] V. Poal, D. Panchare, and B. Mehta, "Balancing of HVAC System Energy Consumption in Electric Vehicles," in *SAE Technical Papers*, SAE International, Sep. 2021. doi: 10.4271/2021-28-0124.

[27] G. Lee, J. Song, Y. Lim, and S. Park, "Energy consumption evaluation of passenger electric vehicle based on ambient temperature under Real-World driving conditions," *Energy Convers. Manag.*, vol. 306, Apr. 2024, doi: 10.1016/j.enconman.2024.118289.

[28] D. H. Jeon and S. M. Baek, "Thermal modeling of cylindrical lithium ion battery during discharge cycle," *Energy Convers. Manag.*, vol. 52, no. 8–9, pp. 2973–2981, Aug. 2011, doi: 10.1016/j.enconman.2011.04.013.

[29] J. Yakhshilikov, M. Cavana, J. Inoyatkhodjaev, S. Giarola, and P. Leone, "Long-term energy and emissions outlook for the road transport sector of Uzbekistan: Insights from an agent-based energy model," *Energy*, vol. 339, Dec. 2025, doi: 10.1016/j.energy.2025.139106.

[30] B. Kondev, J. Dixon, Z. Zhou, R. Sabyrbekov, K. Sultanaliev, and S. A. Hirmer, "Putting the foot down: Accelerating EV uptake in Kyrgyzstan," *Transp. Policy (Oxf).*, vol. 131, pp. 87–96, Feb. 2023, doi: 10.1016/j.tranpol.2022.12.007.

[31] F. Zheng, Z. Wang, Y. Xu, and M. Liu, "Overnight Charging Scheduling Optimization for Electric Battery Buses with Controllable Charging Completion Levels," *J. Transp. Eng. A Syst.*, vol. 150, no. 3, Mar. 2024, doi: 10.1061/jtepbs.teeng-7741.

[32] J. Vetter *et al.*, "Ageing mechanisms in lithium-ion batteries," *J. Power Sources*, vol. 147, no. 1–2, pp. 269–281, Sep. 2005, doi: 10.1016/j.jpowsour.2005.01.006.

[33] A. Lajunen, "Energy Efficiency and Performance of Cabin Thermal Management in Electric Vehicles," in *SAE Technical Papers*, SAE International, Mar. 2017. doi: 10.4271/2017-01-0192.

[34] I. Cvok and J. Deur, "Control Trajectory Optimization of Electric Vehicle Heat Pump-Based Cabin Heating System," in *SAE Technical Papers*, SAE International, Apr. 2025. doi: 10.4271/2025-01-8144.

[35] Y. Zhang, P. You, and L. Cai, "Optimal Charging Scheduling by Pricing for EV Charging Station with Dual Charging Modes," *IEEE Transactions on Intelligent Transportation Systems*, vol. 20, no. 9, pp. 3386–3396, Sep. 2019, doi: 10.1109/TITS.2018.2876287.

[36] S. Tarafdar, Y. Gong, and X. "Terry" Yang, "Urban Electric Vehicle Charging Infrastructure Planning: Addressing the Balance between Residential and Commercial Charging Stations," *J. Urban Plan. Dev.*, vol. 151, no. 3, Sep. 2025, doi: 10.1061/jupddm.upeng-5617.

[37] Inc. The MathWorks, "Mathworks official web-site." Accessed: Feb. 11, 2026. [Online]. Available: https://www.mathworks.com/help

[38] C. C. Chan, "The state of the art of electric, hybrid, and fuel cell vehicles," *Proceedings of the IEEE*, vol. 95, no. 4, pp. 704–718, 2007, doi: 10.1109/JPROC.2007.892489.

[39] ECOpoint Inc., "Worldwide Harmonized Light Vehicles Test Cycles (WLTC)," *DieselNet*,

2026, Accessed: Feb. 17, 2026. [Online]. Available: https://dieselnet.com/standards/cycles/wltp.php#cycles

[40] European Commission, *Commission Regulation (EU) 2017/1151 of 1 June 2017 … (WLTP / type-approval Euro 5/6)*. Luxembourg: June, 2017.

[41] M. A. Jeffers, L. Chaney, and J. P. Rugh, "Climate Control Load Reduction Strategies for Electric Drive Vehicles in Warm Weather," in *SAE Technical Papers*, SAE International, Apr. 2015. doi: 10.4271/2015-01-0355.

[42] X. Hu, S. Li, and H. Peng, "A comparative study of equivalent circuit models for Li-ion batteries," *J. Power Sources*, vol. 198, pp. 359–367, Jan. 2012, doi: 10.1016/j.jpowsour.2011.10.013.

[43] S. Salisbury, "Cold Weather On-Road Testing of a 2015 Nissan Leaf," 2016. [Online]. Available: http://avt.inl.gov

[44] "AAA ELECTRIC VEHICLE RANGE TESTING," 2019.

[45] "NREL Reveals Links Among Climate Control, Battery Life, and Electric Vehicle Range (Fact Sheet)," Golden, CO (United States), Jun. 2012. doi: 10.2172/1045077.

[46] G. L. Plett, "Extended Kalman filtering for battery management systems of LiPB-based HEV battery packs - Part 1. Background," *J. Power Sources*, vol. 134, no. 2, pp. 252–261, Aug. 2004, doi: 10.1016/j.jpowsour.2004.02.031.

[47] A. Emadi, S. S. Williamson, and A. Khaligh, "Power electronics intensive solutions for advanced electric, hybrid electric, and fuel cell vehicular power systems," May 2006. doi: 10.1109/TPEL.2006.872378.

[48] H. Yonezawa *et al.*, "Vibration control of automotive drive system with nonlinear gear backlash," *Journal of Dynamic Systems, Measurement and Control, Transactions of the ASME*, vol. 141, no. 12, Dec. 2019, doi: 10.1115/1.4044614.

[49] S. Candidate Alessandro Vigliani Luca Mereu, "POLITECNICO DI TORINO Modelling of longitudinal vehicle motion during low-speed driving."

[50] U.S. Environmental Protection Agency, "Fuel Economy and Vehicle Test Data;" Accessed: Feb. 12, 2026. [Online]. Available: https://www.epa.gov

[51] Argonne National Laboratory, "Autonomie Model Documentation and Vehicle Benchmarking Methodology," U.S. Department of Energy. Accessed: Feb. 12, 2026. [Online]. Available: https://static.nhtsa.gov

[52] J. Diez, "Advanced Vehicle Testing and Evaluation Final Technical Report Encompassing Project Activities From October 1, 2011 to April 30, 2018," Pittsburgh, PA, and Morgantown, WV (United States), Nov. 2018. doi: 10.2172/1481912.

[53] Electric Vehicle Energy Consumption and Temperature Effects, *Electric Vehicle Energy Consumption and Temperature Effects*. Luxembourg (official JRC location), 2020.